DISSERTATION

Dynamics of noise-induced neurodegeneration and neuroplasticity in the central nervous system

Dynamik der lärminduzierten Neurodegeneration und Neuroplastizität im zentralen Nervensystem

zur Erlangung des akademischen Grades Doctor rerum medicinalium (Dr. rer. medic.)

vorgelegt der Medizinischen Fakultät
Charité – Universitätsmedizin Berlin

von

Víctor Giménez Esbrí

Erstbetreuung: PD Dr. Dietmar Basta

Datum der Promotion: 29.11.2024

TABLE OF CONTENTS

LIST OF ABBREVIATIONS

1d: 1 day post-exposure
1H MRS: Proton Magnetic Resonance Spectroscopy
56d: 56 days post-exposure
7d: 7 days post-exposure
84d: 84 days post-exposure
ABR: Auditory Brainstem Recording
AC: Auditory Cortex
AMPA: α-amino-3-hydroxy-5-methyl-4-isoxazolepropionic acid
ANF: Auditory nerve fibers
ARHL: Age-related hearing Loss
BA: Bland-Altman
BDNF: Brain-derived neurotrophic factor
BIC: Brachium of the Inferior Colliculus
BM: Basilar Membrane
CIC: Central Inferior Colliculus
CN: Cochlear Nucleus
CNS: Central Nervous System
CTCF: Corrected Total Cell Fluorescence
D1: Staining Day 1
D2: Staining Day 2
DAPI: 4′,6-diamidino-2-phenylindole
dB: Decibels
DCIC: Dorsal Cortex Inferior Colliculus
DCN: Dorsal Cochlear Nucleus
DFG: Deutschen Forschungsgemeinschaft
DTI: Diffusion Tensor Imaging
ECIC: External Cortex of the Inferior Colliculus
FI: Fluorescence Intensity
FIHC: Fluorescence Immunohistochemistry
FG: Fluorogold
FOV: Field of View
G: Ground electrode
GABA: Gamma-aminobutyric acid
GAD: Glutamic acid decarboxylase
GLAST: Glutamate Aspartate Transporter
HC: Hair Cell
HT: Hearing Threshold
IC: Inferior Colliculus
IHC: Inner Hair Cell
LL: Lateral Lemniscus
LTD: Long-term depression

LTP: Long-term potentiation
MGB: Medial Geniculate Body of the Thalamus
MGD: Dorsal subnucleus of the Ventral Geniculate Body of the thalamus
MGM: Medial subnucleus of the Ventral Geniculate Body of the thalamus
MGV: Ventral subnucleus of the Ventral Geniculate Body of the thalamus
NeuN: Neuronal Nuclear Protein
NIHL: Noise-Induced Hearing Loss
NMDA: N-metil-D-aspartate
NT-3: Neurotrophin-3
NWFZ: Neurowissenschaftliches Forschungszentrum
OAE: Otoacoustic Emission
OC: Organ of Corti
OHC: Outer Hair Cell
OSF: Open Science Framework
PC: Pearson Correlation
PFA: Paraformaldehyde
PV-IN: Parvalbumin-positive interneurons
RC: Recording electrode
RF: Reference electrode
ROI: Region of Interest
ROS: Reactive Oxygen Species
SC: Support cell
SD: Standard Deviation
SE: Standard Error
SGN: Spiral Ganglion Neurons
SOC: Superior Olivary Complex
SPL: Sound Pressure Level
T2w: T2-weighted
TM: Tectorial Membrane
TUNEL: Terminal deoxynucleotidyl transferase dUTP nick end labeling
VBM: Voxel-Based Morphometry
VCN: Ventral Cochlear Nucleus
VGAT: Vesicular GABA transporter
VGLUT1: Vesicular glutamate transporter 1
VGLUT2: Vesicular glutamate transporter 2
VGLUT3: Vesicular glutamate transporter 3
VNTT: Vesicular Neurotransmitter transporters
WHO: World Health Organisation

LIST OF FIGURES

LIST OF TABLES

ABSTRACT

ENGLISH

Noise-induced hearing loss is the sensorineural deafness caused by noise exposure. Besides peripheral consequences, noise exposure might lead to changes in the central nervous system (CNS). The present study investigates how cell density, axonal density and glutamatergic and GABAergic synaptic plasticity are affected as a consequence of noise exposure in the central inferior colliculus (CIC) and the ventral medial geniculate body of the thalamus (MGV). Mice were exposed under anesthesia for 3 h to broadband white noise (5–20 kHz) at high (115 dB SPL) and moderate (90 dB SPL) noise exposure. Unexposed mice were used as controls (Ctrl). Different mice were separately investigated at different time points after noise exposure: 1 day (115 dB: n=8; 90 dB: n=8; Ctrl: n=7), 7 days (115 dB: n=8; 90 dB: n=8; Ctrl: n=8), 56 days (115 dB: n=8; 90 dB: n=8; Ctrl: n=8) and 84 days (115 dB: n=8; 90 dB: n=8; Ctrl: n=8). Magnetic Resonance Imaging (MRI) techniques were performed at the corresponding time point. Auditory brainstem responses (ABR) were recorded at different frequencies (4, 6, 18 and 32 kHz) to examine auditory thresholds 1 week before noise exposure (pre-ABR), and before corresponding MRI measurements (post-ABR). Fluorescence immunohistochemistry (FIHC) against NeuN and DAPI was used to label neuronal and cell nuclei. Automated cell counting was used to assess total neuronal and cell density. FIHC against neurofilament (SMI312), and glutamatergic (VGLUT1 and VGLUT2) and GABAergic (VGAT) vesicular transporter markers was used. Then, mean fluorescence intensity was quantified in order to study neuroconnectivity and neurotransmission imbalances. Auditory threshold shifts were significantly elevated at all tested frequencies and investigated time points between the 115 dB and both the 90 dB and Ctrl groups ($p \leq 0.001$), whereas no changes were observed between the 90 dB and Ctrl groups ($p \geq 0.05$). 1d after noise exposure, significant increases in neurofilament density were observed in the CIC in 115 dB-exposed mice when compared to Ctrls, but no significant changes were detected between the 115 dB and 90 dB groups. Significant differences in the 115 dB group when compared to both the 90 dB and Ctrl groups were found in the MGV. Nevertheless, no significant differences in neurofilament density were detected between any experimental groups at later time points after noise exposure (7d, 56d and 84d). Moreover, no significant changes in neuronal and cell density and/or VGLUT1, VGLUT2 and VGAT expression were found at any time point after noise exposure. Therefore, increases in neurofilament density could not be correlated with cell loss or glutamatergic and GABAergic imbalances. The present findings should help clinicians to better understand and detect complex psychoacoustic phenomena underlying NIHL-induced CNS pathophysiologies. Funding was provided by the Deutsche Forschungsgemeinschaft (DFG, Research Foundation). The present study was pre-registered in the Open Science Framework (osf.io).

DEUTSCH

Lärmschwerhörigkeit ist die sensorineurale Taubheit, die durch Lärmbelastung verursacht wird. Neben den peripheren Folgen kann Lärmbelastung auch zu Veränderungen im zentralen Nervensystem (ZNS) führen, Die vorliegende Studie untersucht, wie die Zelldichte, die axonale Dichte und die glutamaterge und GABAerge synaptische Plastizität als Folge von Lärmbelastung im zentralen inferioren Colliculus (CIC) und dem ventralen medialen Kniehöcker des Thalamus (MGV) beeinflusst werden. Mäuse wurden unter Narkose für 3 Stunden einem breitbandigen weißen Rauschen (5-20 kHz) hoher (115dB SPL) und moderater (90dB SPL) Intensität exponiert. Nicht exponierte Mäuse wurden als Kontrollen (Ctrl) verwendet. 1 Tag (115dB: n=8; 90dB: n=8; Ctrl: n=7), 7 Tage (115dB: n=8; 90dB: n=8; Ctrl: n=8), 56 Tage (115dB: n=8; 90dB: n=8; Ctrl: n=8) und 84 Tage (115dB: n=8; 90dB: n=8; Ctrl: n=8) nach Lärmexposition wurden jeweils Gruppen von Mäusen mittels Magnetresonanztomographie-Verfahren (MRT) untersucht. Auditorische Hirnstammantworten (ABR) wurden bei verschiedenen Frequenzen (4, 6, 18 und 32 kHz) aufgezeichnet, um die Hörschwellen 1 Woche vor der Lärmexposition (pre-ABR) und vor den entsprechenden MRT-Messungen (post-ABR) zu untersuchen. Fluoreszenz-Immunhistochemie (FIHC) gegen NeuN und DAPI wurde verwendet, um neuronale und nichtneuronale Zellkerne zu markieren. Die gesamte Neuronen- und Zelldichte wurde durch automatisierte Zellzählung ermittelt. FIHC gegen Neurofilament (SMI312) und glutamaterge (VGLUT1 und VGLUT2) und GABAerge (VGAT) vesikuläre Transportermarker wurden verwendet. Anschließend wurde die mittlere Fluoreszenzintensität quantifiziert, um die Neurokonnektivität und Ungleichgewichte in der Neurotransmission zu untersuchen. Die Hörschwellenverschiebungen waren bei allen getesteten Frequenzen und untersuchten Zeitpunkten zwischen den 115 dB- und den 90 dB- sowie Ctrl-Gruppen signifikant erhöht ($p<0,001$), während zwischen den 90dB- und Ctrl-Gruppen keine Veränderungen beobachtet wurden ($p>0,05$). 1d nach der Lärmexposition wurden signifikante Erhöhungen der Neurofilament-Dichte im CIC bei 115dB-exponierten Mäusen im Vergleich zu den Ctrl-Gruppen beobachtet, aber es wurden keine signifikanten Veränderungen zwischen den 115dB- und 90dB-Gruppen festgestellt. Signifikante Unterschiede in der 115dB-Gruppe im Vergleich zu den 90dB- und Ctrl-Gruppen wurden im MGV gefunden. Dennoch wurden zu späteren Zeitpunkten nach der Lärmbelastung (7d, 56d und 84d) keine signifikanten Unterschiede in der Neurofilament-Dichte zwischen den einzelnen Versuchsgruppen festgestellt. Darüber hinaus wurden zu keinem Zeitpunkt nach der Lärmexposition signifikante Veränderungen in der Neuronen- und Zelldichte und/oder der Expression von VGLUT1, VGLUT2 und VGAT gefunden. Daher konnten Erhöhungen der Neurofilament-Dichte nicht mit Zellverlusten oder glutamatergen und GABAergen Ungleichgewichten korreliert werden. Die vorliegenden Ergebnisse tragen zu einem besseren Verständnis und Diagnose komplexer psychoakustischer Phänomene bei, denen NIHL-indurierten ZNS-Pathophysiologien zu Grunde liegen. Die Studie wurde von der Deutschen Forschungsgemeinschaft (DFG) gefördert und ist beim Open Science Framework (osf.io) vorregistriert.

01 INTRODUCTION

1.1. NOISE-INDUCED HEARING LOSS: A MODERN EPIDEMIC

Noise-induced hearing loss (NIHL) is defined as the sensorineural deafness caused by prolonged and repetitive exposure to loud noise (Ding et al., 2019). NIHL is the second most common cause of acquired hearing loss after presbyacusis, representing a serious cause of deafness and hearing impairment (Lein et al., 2007; Natarajan et al., 2023). Industrialization of society has severely increased the risk of exposure to harmful noise and noise pollution. It has been estimated that 10% of the global population is affected by hearing loss, and 50% of these cases could be attributed to some form of NIHL (Daniel, 2007; Ding et al., 2019; Mao & Chen, 2021). The World Health Organization (WHO) estimates that approximately 466 million people worldwide suffer from hearing loss, which is expected to almost double by 2050 (Basner et al., 2014; WHO, 2021). Furthermore, the National Institute on Deafness estimates that 33% of people over the age of 65 have significant hearing impairment at a great economic cost and detriment to the quality of life of those affected (Oishi & Schacht, 2011; Sliwinska-Kowalska & Davis, 2012; WHO, 2011).

NIHL is one of the main causes of occupational hearing loss, being an urgent concern in many industries such as manufacturing, construction, mining, and agriculture. Nowadays, it is estimated that 7 to 21% of hearing loss in the workplace is produced by prolonged exposure to loud noises, having an especially profound impact in developing countries (Dawes, 2015; Gopinath et al., 2021; Lie et al., 2016; Miao et al., 2023; Themann & Masterson, 2019). Although the consequences of NIHL are frequently not life-threatening, they could have a significant impact on people's quality of life due to the crucial role of hearing in communication, speech, language development, and learning (American Speech Language-Hearing Association, 2022; Centers for Disease Control and Prevention, 2021; Sliwinska-Kowalska & Zaborowski, 2017; Theodoroff et al., 2015). These noise-induced alterations can profoundly limit an individual's ability to communicate, issues that could lead to increased social stress, depression, embarrassment, poor self-esteem and/or relationship difficulties. NIHL can also cause sleep disturbances, work impairment, psychiatric distress and poor word recognition in noisy environments (Alberti, 1992; Dawes, 2015; Dobie, 2003; Eggermont & Roberts, 2004; Kohrman et al., 2020; Resnik & Polley, 2021; Wu et al., 2021). In addition, there is a reasonable body of evidence suggesting that there is an increased risk for cognitive decline and dementia associated with hearing loss, despite this having been mainly associated with age-related hearing loss (ARHL) (Chern & Golub, 2019; Jafari et al., 2019; Knipper et al., 2022; Loughrey et al., 2018).

Furthermore, although exposure to harmful noise can happen at any age, the younger population is right now at a high risk of suffering from NIHL. This problematic arises as a consequence of the increase of new damaging hearing behaviors that involve exposure to intense loud noise, such as the unappropriated use of portable hearing devices or attending to live music events at bars, restaurants, or fitness clubs (Fligor et al., 2014; Henderson et al., 2011) (see Figure 1). Currently, it is estimated that 1.1 million teenagers and young adults worldwide are suffering from NIHL due to problematic listening behaviors. Moreover, it is estimated that by 2050 over 700 million people, or one in every ten people, will have disabling hearing loss, and over 1 billion young adults are at risk of permanent and avoidable hearing loss due to unsafe listening practices (WHO, 2021). Thus, environmental noise should be considered as a serious public concern in terms of environmental health for the younger populations (Imam & Alam Hannan, 2017; Neitzel & Fligor, 2019; Pienkowski, 2021; Sułkowski et al., 2017; Wang et al., 2020).

Additionally, although some management strategies could be applied in order to alleviate the symptoms and improve communication abilities, there is no standard treatment for people suffering from acute NIHL, as the damage produced is usually irreversible. However, up to 60% of cases are preventable (Daniel, 2007; Neitzel & Fligor, 2019; Ryan, 2000). For this reason, the development of new preventive strategies such us reduced exposure to loud noise, use of hearing protection, and education and awareness programs can help prevent or reduce the severity of NIHL. At the same time, growing awareness and new policy development play a crucial role in NIHL prevention, promoting healthy and safe hearing practices (WHO, 2011). Nevertheless, there is a need for additional diagnostic tools to identify the consequences of NIHL in its early stages.

Figure 1. Sound intensity across different human activities. Exposure to loud noise has been extensively increased due to the industrialization of society. Nowadays, many extensive damaging auditory behaviors can contribute to the development of noise-induced hearing loss (NIHL). Sound intensity is shown in decibels (dB). *Source: Varela-Nieto et al., 2020. Copyright (2020) Taylor & Francis Group.*

Researchers are exploring new diagnostic tools that could help to identify NIHL and facilitate earlier intervention and treatment (Mao & Chen, 2021).

1.2. NOISE-INDUCED HEARING LOSS PATHOGENESIS: CURRENT INSIGHTS

NIHL is a multifactorial and complex disorder caused by the interaction of genetic and environmental factors, but is primarily determined by the degree of biological injury caused by noise exposure (Le et al., 2017). This disorder can be produced either by a single one-time exposure to a loud noise, such as an explosion or gunshot, or by continuous exposure over time, such as working in noisy environments, attending loud events, or using loud personal hearing devices (Ding et al., 2019). In both cases, current evidence supports that excessive noise exposure can have profound effects on the entire auditory system, both in the inner ear as well as in the ascending auditory structures of the central nervous system (CNS).

1.2.1. NOISE-INDUCED CONSEQUENCES ON THE PERIPHERAL AUDITORY SYSTEM: PERMANENT AND TEMPORARY THRESHOLD SHIFT

In the peripheral auditory system, NIHL has a dramatic impact on the homeostasis and physiology of the primary sensory receptor cells, the hair cells (HC) (Ding et al., 2019; Le et al., 2017). The HC are the sensory receptors responsible for transducing sound vibrations in the inner ear. They are highly sensitive to mechanical stimulation, which allows them to convert sound vibrations into electrical signals thanks to their mechanosensing organelles, the stereocilia (McPherson, 2018). Loud noise exposure can produce excessive vibration of the middle ear ossicles and a violent movement of the endolymph and perilymph inside the cochlea. With sufficient intensity and duration, this aggressive movement can overstimulate the stereocilia and produce profound damages in its intrinsic structure which disrupt metabolic pathways implicated in synaptic transmission (Ding et al., 2019; Hong et al., 2013; Liberman, 2017; Park et al., 2013). In addition, powerful vibration of the endolymphatic liquid can produce mechanical damage, oxidative stress, and extensive inflammatory processes that could damage the HC and related structures of the Organ of Corti (OC), such as the basilar membrane (BM), the tectorial membrane (TM) or the support cells (SC). All these effects can lead to dramatic death of HC and/or a reduction of the number of ribbon synapses, the glutamatergic contacts between them, the spiral ganglion neurons (SGN) and the auditory nerve fibers (ANF). In the long term, these effects induce the degeneration of the SGN and the deafferentation of the ANF, elements playing a crucial role in the transmission of sound signals from the cochlea to the brain. Therefore, synaptic transmission

in the cochlea may become impaired after aggressive noise trauma, producing a decreased auditory output to higher auditory structures that can lead to extensive neural pathological changes (Fetoni et al., 2015; Honkura et al., 2016; Kujawa & Liberman, 2017, 2015; Sliwinska-Kowalska & Davis, 2012; Tuerdi et al., 2017; Willott & Lu, 1982; Zhang et al., 2022) (see Figure 2).

The magnitude of damage produced by noise exposure is frequently assessed through the pure tone auditory hearing threshold (HT). The HT refers to the minimum sound intensity or volume level that an individual can detect or hear in a specific frequency range, and it is expressed in decibels (dB). Nonetheless, exceeding the noise level thresholds above 90dB for a prolonged time could have serious pathological consequences in the entire auditory system. These consequences might produce an elevation of the HT, and evoke what is called an auditory threshold shift (Ding et al., 2019; Kujawa & Liberman, 2009). After prolonged acute noise exposure, two different phases can be observed depending on the nature of the auditory threshold shift: Temporary Threshold Shift (TTS), in which pure-tone thresholds return to pre-exposure levels in a time-period manner due to transient and reversible auditory damage; and Permanent Threshold Shift (PTS), where exposure to loud noise induces a permanent change in HT due to profound and non-recoverable damage. There is robust evidence to suggest that those different sound exposure paradigms could cause different consequences in hearing function and signal transmission through all the ascending auditory pathways (Daniel, 2007; Gröschel et al., 2010; Le et al., 2017; Liberman, 2016; Oxenham, 2016; Singer et al., 2020).

Hearing is frequently restored within 24 - 48 h after a TTS, probably as a result of transient mechanical damage of the outer hair cells (OHC) and/or inner hair cells (IHC) and their stereocilia right after noise exposure (Nordmann et al., 2000; Shi et al., 2015). Moreover, homeostatic compensatory processes in the CNS like elevations in neural activity found in the CN or IC could mitigate the detrimental the effects of prolonged noise exposure in the inner ear (Knipper et al., 2013; Kraus et al., 2009; Salvi et al., 2000). For this reason, this temporary hearing impairment is extremely important from a clinical perspective, and there have been extensive efforts in order to develop preventive therapeutic strategies directed to prevent further damage that could develop in a non-recoverable PTS (Gröschel et al., 2010). However, the degree of recovery might be limited, and its extent depends on the pathological consequences produced by excessive acoustic overstimulation (Ding-Pfennigdorff et al., 1998). Even when there is a recovery of auditory pure tone thresholds, normal audiograms are measured, and no direct evident signs of HC loss are observed, there could be considerable damage present in the ribbon synapses associated with

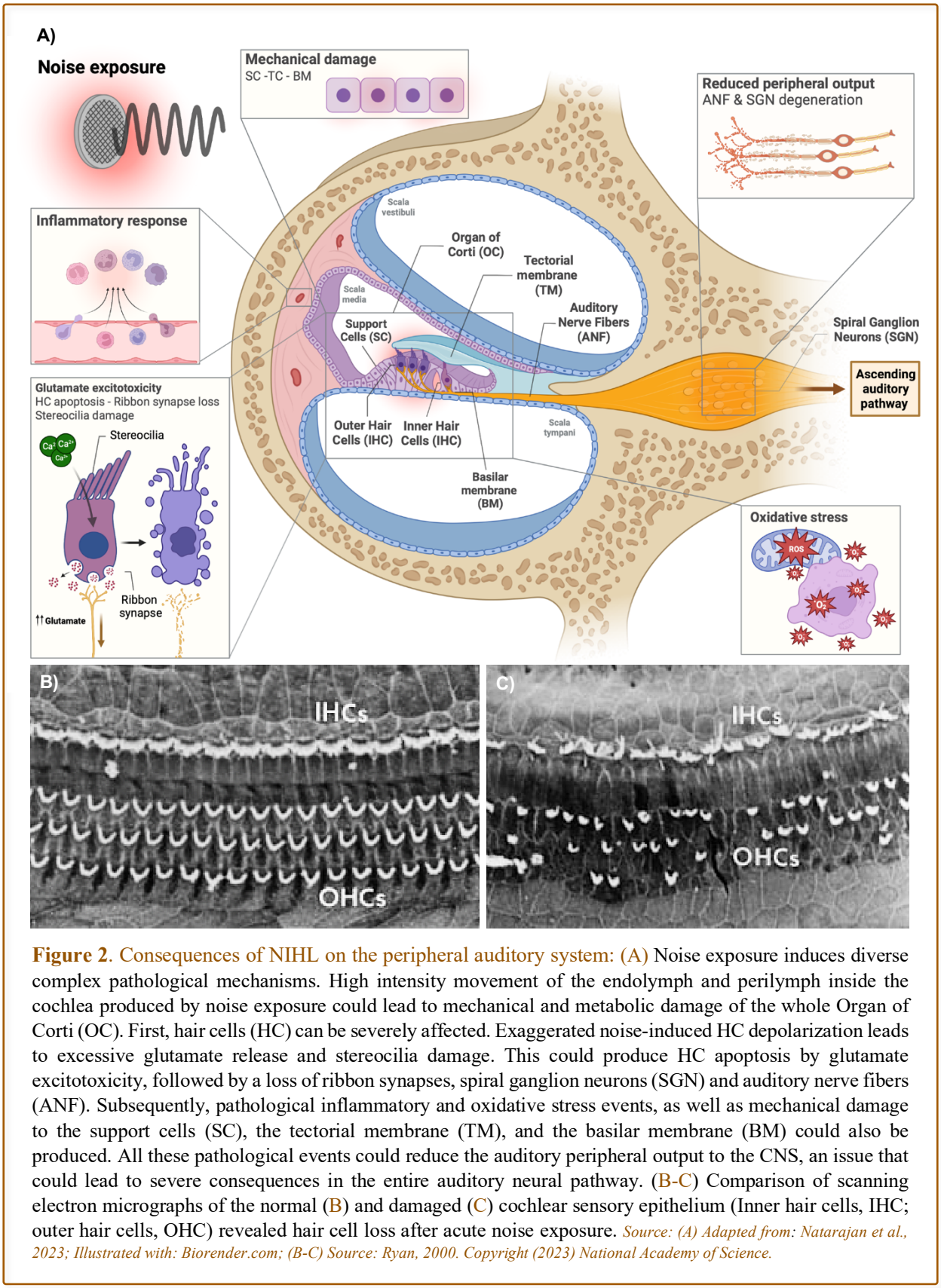

Figure 2. Consequences of NIHL on the peripheral auditory system: (A) Noise exposure induces diverse complex pathological mechanisms. High intensity movement of the endolymph and perilymph inside the cochlea produced by noise exposure could lead to mechanical and metabolic damage of the whole Organ of Corti (OC). First, hair cells (HC) can be severely affected. Exaggerated noise-induced HC depolarization leads to excessive glutamate release and stereocilia damage. This could produce HC apoptosis by glutamate excitotoxicity, followed by a loss of ribbon synapses, spiral ganglion neurons (SGN) and auditory nerve fibers (ANF). Subsequently, pathological inflammatory and oxidative stress events, as well as mechanical damage to the support cells (SC), the tectorial membrane (TM), and the basilar membrane (BM) could also be produced. All these pathological events could reduce the auditory peripheral output to the CNS, an issue that could lead to severe consequences in the entire auditory neural pathway. (B-C) Comparison of scanning electron micrographs of the normal (B) and damaged (C) cochlear sensory epithelium (Inner hair cells, IHC; outer hair cells, OHC) revealed hair cell loss after acute noise exposure. *Source: (A) Adapted from: Natarajan et al., 2023; Illustrated with: Biorender.com; (B-C) Source: Ryan, 2000. Copyright (2023) National Academy of Science.*

cochlear degeneration, which has been termed cochlear synaptopathy (Kujawa & Liberman, 2015). This damage can hide behind a normal audiogram and produce perceptual difficulties in understanding speech in noisy environments, as well as the emergence of tinnitus (defined as a

psychoacoustic phenomenon caused by the perception of sound in the absence of external stimuli) and/or hyperacusis (defined as an increased sensitivity to sound and a low tolerance for environmental noise) (Alberti, 1992; Baguley, 2003; Hesse & Kastellis, 2019; Hickman et al., 2020; Hickox & Liberman, 2014; Kohrman et al., 2020; Plack et al., 2014). This phenomenon is defined as Hidden Hearing Loss (HHL), and it represents a major problem in the early detection and prevention of NIHL consequences (Valderrama et al., 2022). Indeed, it is estimated that there are many more individuals suffering from noise-induced pathology and dysfunction than are currently diagnosed (Dewey et al., 2018; Hesse & Kastellis, 2019; Le Prell et al., 2020). This could happen because ABR or OAE techniques may not be sensitive enough to detect slight changes in hearing function caused by NIHL.

Alternatively, there is no evidence of recovery from dramatic noise-induced trauma during the PTS phase (Le et al., 2017). Intense stimulation typically ends in dramatic HC death or damage, as well as to several metabolic imbalances on the cellular level. First, generation of reactive oxidative species (ROS) have been shown to be a contributor to cell damage, as well as to the rise of inflammatory processes occurring in the cochlea after noise exposure like swelling of the ANF. At the same time, an elevation of intracellular calcium mediated activity due to a massive influx of Ca^{+2} into the HC has been demonstrated. This elevation is especially harmful for HC, as it could produce an intracytoplasmic accumulation of ROS and trigger apoptotic and necrotic mechanisms, eventually leading to cell death. In addition, this Ca^{+2} overload can produce an excessive release of glutamate by HC synaptic terminals, an issue that can disrupt synaptic transmission and contribute to cell death due to glutamate excitotoxicity. Simultaneously, mechanical damage can lead to profound alterations of the entire OC (TM, BM and SC) (Ding et al., 2019; Kurabi et al., 2017; Mao & Chen, 2021; Orrenius et al., 2003; Y. Wang et al., 2002). Thus, when HC and ribbon synapse transmission loss reaches a particular threshold, a severe and permanent hearing loss is produced due to a complete disruption of the auditory signal transduction into the central auditory system. Unfortunately, these effects cannot be reversed, primarily because mammalian sensory cells do not have the capacity to regenerate over time (Ding-Pfennigdorff et al., 1998; Mao & Chen, 2021). Therefore, due to these consequences, hearing loss can become irreversible (Daniel, 2007; Liberman, 2016). Since none of those pathological processes perfectly explain the occurrence of noise-induced hearing loss on their own, an interplay between different noise-induced pathological mechanisms is expected. Moreover, further mechanisms could be contributing to the final NIHL pathology (Imam & Alam Hannan, 2017; Mao & Chen, 2021; Oishi & Schacht, 2011; Varela-Nieto et al., 2020; Wang et al., 2019). Therefore, many studies have put

extensive efforts into investigating the role of the central auditory system in order to expand the knowledge of NIHL biological mechanisms.

1.2.2. NOISE-INDUCED HEARING LOSS: CONSEQUENCES IN THE CENTRAL NERVOUS SYSTEM

Excessive loud noise exposure can produce pathological effects that can extend from the cochlea to the entire auditory neural pathway, affecting several CNS structures (Ding et al., 2019; Gröschel et al., 2018; Salvi et al., 2000; Shore & Wu, 2019; Sliwinska-Kowalska & Davis, 2012; Willott & Lu, 1982; Willott & Turner, 2000). In these auditory areas, several neurodegenerative and neuroplastic changes have been observed. Those changes involve the elevation of HT, the activation of apoptotic and cell death pathways, increases in neural activity, changes in neural connectivity, tonotopic synaptic reorganization or imbalances in the excitatory and inhibitory activity. Taken together, they could exert a severe impact in NIHL pathology, contributing to the generation of several audiological symptoms such as tinnitus, hyperacusis, loudness misperceptions, reduced speech intelligibility, difficulties isolating important sounds in a background, cognitive decline and working memory or mood disorders (Basta et al., 2017; Basta et al., 2005; Dallos & Harris, 1978; Kim et al., 2004; Knipper et al., 2022; Kraus & Canlon, 2012; Salvi et al., 2000; Syka, 2002). These effects cannot be solely explained by cochlear damage.

Therefore, there is a clear implication of the central auditory system in NIHL pathophysiology. However, the biological consequences of acute noise exposure on the CNS are still largely unexplored. This issue adds further complexity when trying to analyse which detailed mechanism causes hearing impairment after acoustic overstimulation. In several cases, It can be difficult to understand the underlying mechanisms of NIHL because it can be unclear whether the pathological effects affect the cochlea, the ascending neural pathways, or both (Henry, 2013; Saunders et al., 1991). In addition, there is a lack of consensus when trying to understand how different auditory brain areas can be affected by noise exposure and how these consequences can specifically contribute in the generation of noise-induced pathological processes (Gröschel et al., 2018; Säljö et al., 2002).

Therefore, one of the biggest challenges in the field is undoubtedly to identify the specific role of the CNS auditory structures in the NIHL pathology. Although some crucial advances have been made, the general mechanisms by which noise exposure damages the inner ear and how this relates to noise-induced CNS alterations remain not well understood. For these reasons, an

extensive characterization of different neurodegenerative and neuroplastic events happening in the CNS after loud noise exposure will be extensively investigated in the present study.

1.2.2.1. The ascending auditory pathway: Noise-induced changes in the Inferior Colliculus and the Medial Geniculate Body of the thalamus

After auditory information is processed by the inner ear, auditory signals travel to different intracranial neural structures through the ascending auditory pathway. Although complex auditory interactions make it challenging to establish a concrete physiological role for each auditory neural area, a basic approach can be given (Peterson et al., 2022; Pickles, 2015). First, auditory signals leave the inner ear through the ANF until reaching the ipsilateral Cochlear Nucleus (CN), the first auditory brainstem structure responsible for transducing auditory signals from the inner ear into the brain. The ANF enters the CN in a tonotopical manner, preserving the spatial arrangements arising from the cochlea across the entire ascending auditory neural pathway (Pickles, 2015). Then, ascending information leaves the CN to the second major relay in the auditory brainstem, the Superior Olivary Complex (SOC). The SOC is a complex of different nuclei involved in important hearing functions such as the accurate spatial localization of sounds by integrating binaural information from both ears (Reuss, 2000).

Subsequently, ascending fibers travel bilaterally through the Lateral Lemniscus (LL) to the Inferior Colliculus (IC), one of the most important anatomical locations of the ascending auditory neural pathway. Notably, different imbalances in the IC have been involved with NIHL, which contribute to the development of tinnitus and hyperacusis (Basta & Ernst, 2004; Gröschel et al., 2010, 2014; Palmer & Berger, 2018; Szczepaniak & Møller, 1996). The IC is an auditory CNS area located in the posterior portion of the roof of the midbrain, which is mainly responsible for sound localization, pitch and rhythm discrimination, and orienting the body toward a relevant stimuli (Ito & Oliver, 2012; Ma et al., 2020). The IC can be divided into three different subdivisions: the central nucleus (CIC), the dorsal cortex (DCIC), and the external or lateral cortex (ECIC) of the inferior colliculus (see Figure 3) (Morest & Oliver, 1984). Together, the DCIC and ECIC can also be described as the IC shell, whereas the CIC is also known as the IC core. Each of these subdivisions play different roles in auditory processing due to their underlying circuitry, and can be affected in different ways after acoustic damage. The DCIC and ECIC mainly integrate descending fibers from higher auditory structures, whereas the CIC receives major tonotopic afferent inputs from the CN, SOC and LL, regions thought to be primarily affected after loud noise exposure. Furthermore, the CIC is the neural region where primary ascending afferent outputs to

higher auditory structures arise, thus being an essential region for auditory neural processing (Huffman & Henson, 1990; Palmer & Berger, 2018; Ito, 2016). Furthermore, many alterations have been described in the CIC after different kinds of peripheral acoustic trauma, such as increases of central neural activity or apoptotic and cell death mechanisms (Fröhlich et al., 2018; Gröschel et al., 2010; Palmer & Berger, 2018).

Ascending projections leave the CIC by way of the brachium of the inferior colliculus (BIC) to ascend to the next auditory neural station, the Medial Geniculate Body of the thalamus (MGB) (Izquierdo et al., 2008; Mellott et al., 2014; Palmer & Berger, 2018; Ito, 2016; Yin et al., 2008). The MGB plays a decisive role in auditory processing, being a crucial relay for ascending auditory signals before they reach the Auditory Cortex (AC) (Winer et al., 2005; Mellot et al., 2014). It is responsible for different important hearing functions, such as auditory discrimination, auditory attention or auditory memory. The MGB is a complex of thalamic nuclei that can be divided into three subdivisions: the ventral subnucleus of the medial geniculate body of the thalamus (MGV), the dorsal subnucleus of the medial geniculate body of the thalamus (MGD), and the medial subnucleus of the medial geniculate body of the thalamus (MGM) (see Figure 3). As is the case in the IC, these different subnuclei comprise diverse neural organizations with distinct functional differences. The MGV is a prominent tonotopically organized region that constitutes the main source of ascending auditory inputs coming from the CIC through the BIC (Fujimoto et al., 2021). Furthermore, it sends ascending projections to relevant areas of the AC. The MGD and MGM receive inputs mainly from the IC shell, and from different non-auditory areas. Therefore, although some studies have questioned this assertion, the MGV constitutes a part of the primary or lemniscal auditory pathway, whereas the MGD and the MGM are considered a part of the secondary or non-lemniscal auditory pathway (Anderson & Linden, 2011; Pickles, 2015). Additionally, contrary to the MGV, the MGD and MGM are poorly responsive to most sounds, and tonotopy is not a remarkable feature (Brugge & Howard, 2002). Moreover, the MGV has been proposed as one of the major areas involving changes after acoustic trauma and tinnitus, as pathological increases in spontaneous activity, neuronal cell death pathways and/or tonotopic reorganizations have been detected (Almasabi et al., 2022; Basta et al., 2005; Brinkmann et al., 2021; Cook et al., 2021; Kalappa et al., 2014; Kamke et al., 2003; Shore & Wu, 2019). Moreover, the MGB presents a complex interaction with neural areas of the limbic system such as the amygdala or the hippocampus. It has been hypothesized, that alterations of these neural circuits

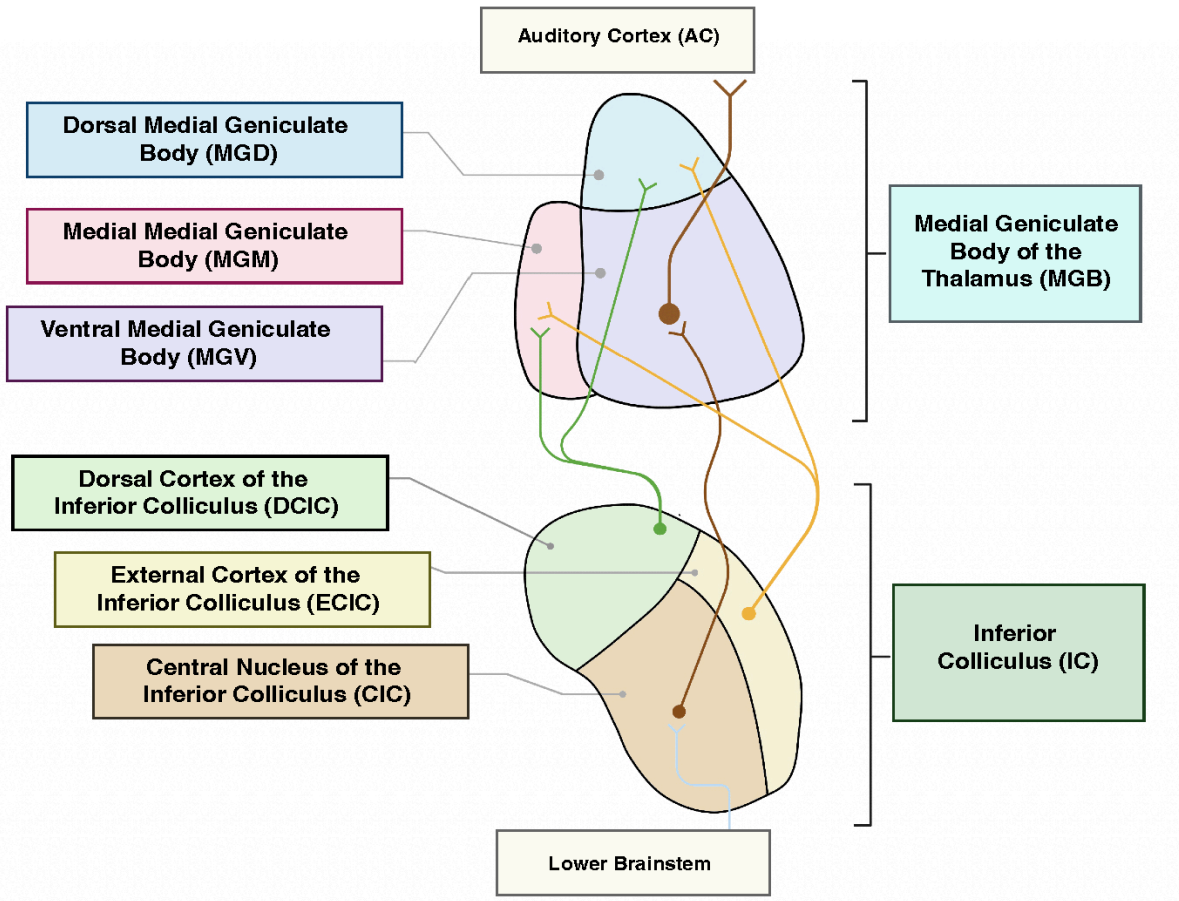

Figure 3. Simplified neuroanatomic connections between the mouse Inferior Colliculus (IC) and Medial Geniculate Body of the thalamus (MGB). The IC is anatomically distributed into three different subnuclei: The Dorsal Cortex of the Inferior Colliculus (DCIC), the external Cortex of the Inferior Colliculus (ECIC) and the Central nucleus of the Inferior Colliculus (CIC). The MGB has three distinct major subthalamic nuclei: the ventral subnucleus of the medial geniculate body of the thalamus (MGV), the dorsal subnucleus of the medial geniculate body of the thalamus (MGD) and the medial subnucleus of the medial geniculate body of the thalamus (MGM). The CIC receives auditory inputs from brainstem nuclei (cochlear nucleus (CN), superior olivary complex (SOC) or lateral lemniscus (LL)), and sends ascending projections to the MGV through the brachium of the Inferior Colliculus (BIC) (lemniscal or primary auditory pathway). The MGV connects with relevant areas of the auditory cortex (AC). The MGD and MGM receive ascending inputs from the DCIC and ECIC (non-lemniscal or secondary auditory pathway). Diverse alterations have been described in the CIC and the MGV after acoustic trauma. In the present study, neuroplastic and neurodegenerative changes as a consequence of NIHL will be investigated in the CIC and MGV. *Illustrated with: www.biorender.com.*

might be related to several tinnitus and NIHL associated symptoms, like cognitive decline or working memory and mood disorders (Basta et al., 2005; Brinkmann et al., 2021; Clopton & Spelman, 2003; Cook et al., 2021; Fröhlich et al., 2017; Gröschel et al., 2018; Janssen & Jahanshahi, 2022; Keifer et al., 2015).

Finally, ascending auditory projections leave the MGV and reach the AC (see Figure 3). The AC is critical for different higher auditory functions, such as sound localization, auditory

memory, or sound and speech processing. Furthermore, it is the auditory station where auditory perception occurs (Pickles, 2015).

In this context, due to the previously discussed relevance of the MGV and CIC within the ascending auditory neural pathway, and due to its described involvement in NIHL and/or tinnitus, these auditory neural regions will represent the main target areas of study during the present work.

1.2.2.2. Noise-induced neurodegeneration in the ascending auditory pathway: cell death in higher auditory structures

Some studies suggest that neurodegenerative processes can extend through the whole auditory CNS after peripheral noise-induced trauma. Thus, besides the impact of acute noise exposure on dramatic HC loss in the cochlea, cell death mechanisms can also be observed in higher central auditory structures such as the CN, SOC, IC, MGB or AC after prolonged loud noise exposure. Therefore, a relationship between noise exposure, peripheral damage, and cell death in the central auditory pathway has been reported, moving beyond the conventional focus on inner ear changes following NIHL (Basta et al., 2005; Coordes et al., 2012; Frohlich et al., 2017; Gröschel et al., 2010). Nevertheless, how exactly NIHL can lead to neurodegenerative events in the CNS is a major unanswered question with enormous clinical implications.

In order to understand the fundamental mechanisms of noise-induced neurodegeneration, apoptosis has been suggested as one of the major pathological mechanisms behind noise-induced cell loss in central auditory structures (Aarnisalo et al., 2000; Coordes et al., 2012; Fröhlich et al., 2017). HC death produced as a result of excessive acoustic overstimulation can lead to subsequent degeneration of the ribbon synapses, the SGN, or the auditory nerve (see Figure 2). These noise-induced pathological mechanisms are responsible for the activation of further apoptotic cascades in higher auditory structures like the CN, IC, MGB, or AC. Those apoptotic pathways may be activated due to a prominent Ca^{+2} influx happening in neuronal populations of the auditory CNS due to acoustic overstimulation. In addition, an increase in intracellular Ca^{+2} may be accompanied by a massive release of glutamate into the synaptic cleft, leading to excessive neuronal excitation followed by excitotoxic mechanisms. Moreover, auditory nerve deafferentation has been related to a decrease in the number of axonal projections in the CN. Thus, although the exact mechanisms are not well understood, these effects could explain the sudden loss of cell density, axon degeneration, and/or tissue shrinkage in central structures (Basta et al., 2005; Gröschel et al., 2010, 2011; Kujawa & Liberman, 2009). At the same time, cell loss observed in the CNS could have

potential relationships with different symptoms associated with NIHL, such as reduction in speech discrimination rates, tinnitus or hyperacusis. Moreover, there is growing evidence to support that central neurodegeneration may play a role in permanent hearing impairment (Gröschel et al., 2018; Kujawa & Liberman, 2015). As is the case with the HC, neurons in the adult CNS do not have the capacity to regenerate over time (Kurabi et al., 2017). Due to that reason, as is the case in other neurodegenerative diseases, when those clinical symptoms start to appear, neuronal death rates could already be elevated and auditory function might be permanently compromised. Thus, it is critical to understand the biological pathways by which cell death occurs as a consequence of NIHL when trying to develop preventive, diagnostic, and therapeutic strategies.

Following this line of evidence, our research group demonstrated that a significant noise trauma can change the neuronal cytoarchitecture and induce significant cell density reductions in the MGB and in the layers IV-VI of the AC 1 week after noise exposure (Basta et al., 2005). In subsequent studies, similar decreases in cell density were also observed 7 days post-exposure in the CN, IC, MGB and AC, consistently with previous described results (Gröschel et al., 2010) (see Figure 4). In addition, it was shown that different neurodegeneration mechanisms could be observed depending on the sort of noise trauma being induced (PTS or TTS), suggesting how different noise-exposure paradigms can cause different pathological mechanisms in the CNS (Gröschel et al., 2010). Subsequently, terminal deoxynucleotidyl transferase dUTP nick end labelling assay or TUNEL assay techniques were used with the aim to identify if apoptotic processes are hidden behind cell loss events in the CNS after NIHL. This was performed due to the ability of the TUNEL assay to detect DNA fragmentation by labelling the free 3'-OH ends of fragmented DNA with fluorescent or chromogenic dUTP (deoxyuridine triphosphate) probes (Kyrylkova et al., 2012). A significant increase in the number of apoptotic or TUNEL-positive ($TUNEL^+$) cells in the VCN, DCN and IC between 6h and 24h post-exposure was detected by our research group. These effects were followed by a significant $TUNEL^+$ cell decrease 7 days post-exposure in some of those brain regions (Coordes et al., 2012). These findings were consistent with studies made by Karnes et al., (2009) in which an increase in Caspase-3 and a detection of $TUNEL^+$ cells was found in the VCN between 24h and 7 days after unilateral cochlear removal. Accordingly, Mostafapour et al., (2000) detected $TUNEL^+$ cells 12h and 48h after cochlear removal, but no $TUNEL^+$ cells were found 3 weeks post-exposure.

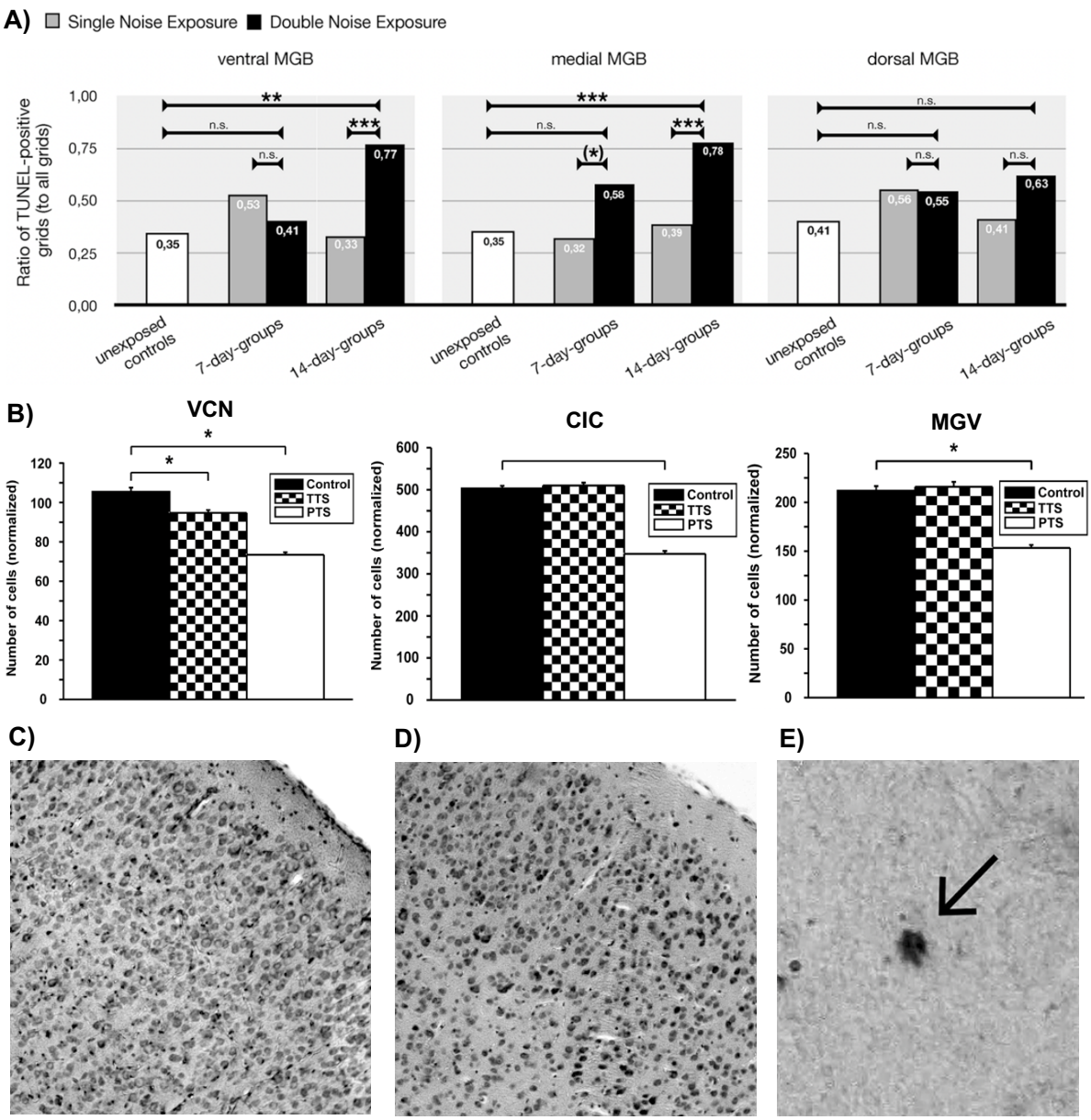

Figure 4. Neurodegenerative consequences in the CNS after noise-induced trauma: A) An increase in the number of TUNEL-positive cells was observed in the ventral and medial MGB after repeated noise exposure in noise-exposed animals when compared to controls (Mean ± Standard Error), showing evidence of increased apoptotic mechanisms after noise overstimulation; B) A significant decrease in the number of cells was observed in different brain auditory areas (VCN, CIC, MGV) after a single acute noise exposure (Mean ± Standard Error); C-D) Detailed Kluever-Barrera (KB) staining microphotographs of the AC acquired from noise-exposed (C) and control (D) animals, showing structural cell density differences as a consequence of noise trauma. E) An example of an apoptotic TUNEL- positive cell in the MGB observed after long-term noise exposure. *Source: (C, D) Basta et al., 2005, Copyright (2005) Elsevier B.V., All rights reserved; (A, E) Fröhlich et al., 2017, Copyright (2017) Springer-Verlag GmbH; Gröschel et al., 2010, Copyright (2010) Mary Ann Liebert, Inc.*

Adding further complexity, our group investigated if repeated exposure to loud noises could produce an increase in the number of $TUNEL^+$ cells 7 days and 14 days post-exposure (Fröhlich et al., 2017, 2018). 7 days after noise exposure, a significant increase in $TUNEL^+$ cells

between mice exposed once to intense noise and mice exposed twice was detected in the MGM, but not in the MGV and MGD. These effects were not seen between unexposed and both single and double-exposed mice. 14 days after noise exposure, increases in $TUNEL^+$ cells were found in the MGV and MGM in double-exposed mice, but not in the MGD (Fröhlich et al., 2017) (see Figure 4). However, these increases were not detected either in the IC or CN (Fröhlich et al., 2018). Similarly, Aarnisalo et al., (2000) showed that degeneration of SGN in guinea pigs after noise exposure could be correlated with an increased number of apoptotic cell nuclei in the ipsilateral CN and the SOC. Interestingly, this study found an increase in apoptotic cells without evident signs of cell loss. The previously listed findings were consistent with results described after performing protein and gene expression studies of different pro-apoptotic and anti-apoptotic markers after acute noise exposure (Gröschel et al., 2018). Furthermore, it was also described that the number of apoptotic cells could be reduced after intracochlear application of different neurotrophic factors such as brain-derived neurotrophic factor (BDNF) and neurotrophin-3 (NT-3), evidence that was in line with studies made by Suneja et al., 2005. It is well known that neurotrophic factors are crucial elements for the development and survival of neurons in both developmental and adult CNS. A proper BDNF function is critical for the homeostatic development of the auditory system, as well as for maintaining elements that modulate central noise-induced neuroplasticity, like the central activity modulation exerted by Parvalbumin-positive interneurons (PV-IN) found in the AC (Knipper et al., 2022). Therefore, studies like those performed by Aarnisalo et al., (2000) and Suneja et al., (2005) suggested that a decreased release or an impaired function of such neurotrophic factors after noise exposure may also lie behind the observed cell death and apoptotic mechanisms. These studies revealed that noise exposure induced gene and protein expression imbalances in different apoptotic markers, suggesting apoptotic signaling pathways that might be affected during the pathological course of NIHL.

However, it is important to highlight that histological studies present some limitations when they are transferred them into clinical practice. Concretely, they cannot be performed during *in vivo* conditions and the current knowledge generated from them comes mostly from studies made in animal models such as mouse, rat, chinchilla or guinea pig. Thus, they currently provide limited knowledge about how NIHL affects ascending auditory areas, particularly in human models. It is also challenging to differentiate the contributions of hearing loss and NIHL in a specific way using these techniques (Muca, 2018). Nonetheless, there is no available powerful diagnostic tool that could detect, prevent and predict NIHL neurodegenerative consequences on the neuronal level during *in vivo* conditions in a time-dependent manner. Hence, as mentioned

previously, developing new clinical strategies for assessing noise-induced neurodegeneration might become a powerful new preventive and therapeutic perspective.

1.2.2.3. Noise-induced neuroplastic changes in the central nervous system

In addition to neurodegenerative events, diverse neuroplastic mechanisms have been observed in the central auditory system in response to intense acoustic overstimulation. The changes mainly involve increases in central neural activity and synaptic connectivity reorganizations, which could be potentially produced by complex changes in the excitatory and inhibitory balance. It is well known that these imbalances are produced by changes in glutamate and γ-aminobutyric acid (GABA) synaptic neurotransmission. Glutamate is considered as the main excitatory neurotransmitter in the CNS, whereas GABA constitutes the major inhibitory neurotransmitter. Both neurotransmitters play a crucial role in shaping responses to both simple and complex acoustic stimuli in the whole auditory system. Therefore, any imbalance or disturbance of the homeostasis of both neurotransmission mechanisms can lead to significant physiological implications in some neurological disorders (Sears & Hewett, 2021). These effects can lead to important changes in neural connectivity through the entire auditory pathway, affecting auditory function (Cai et al., 2014; Eggermont & Roberts, 2004; Lee & Godfrey, 2014; Ma et al., 2020; Milbrandt et al., 2000; Sears & Hewett, 2021; Ito, 2011).

1.2.2.3.1. Compensatory mechanisms after acoustic overstimulation

In this regard, the described noise-induced neuroplastic mechanisms primarily arise in different CNS auditory structures in order to counteract peripheral auditory damage and reduced auditory output. Under homeostatic circumstances, central neuroplasticity plays relevant roles in partially restoring hearing function and preventing further auditory damage. However, during prolonged and repeated noise exposure, the auditory CNS may fail to recover from the damage produced in the inner ear. This occurs because early compensatory mechanisms could be excessively sustained over time, producing extensive central pathological consequences. These detrimental neuroplastic events may produce changes in neural activity and synaptic connectivity promoting excitotoxic mechanisms, conditions which are associated with permanent hearing damage. Nevertheless, it is poorly understood which conditions lead to this maintained neural activity and how exactly these could be translated into traumatic effects in the CNS or into clinical symptoms (Durham et al., 2000; Eggermont, 2006; Hickman et al., 2020; Jean-Baptiste & Morest, 1975; Kaltenbach et al., 1992; Morest & Bohne, 1983; Persic et al., 2020; Salvi et al., 2000;

Schrode et al., 2018; Xia et al., 2019). Expanding our knowledge in this regard is especially critical for assessing how noise exposure can shape the central auditory response.

1.2.2.3.2. Noise-induced hyperactivity in the CNS

One of the main mechanisms arising in the CNS with the aim to compensate for diminished neural output is a pronounced hyperactivity of different structures of the ascending auditory pathway, such as the IC and the CN (Knipper et al., 2013; Manzoor et al., 2012a; Salvi et al., 2000). The strongest current hypothesis suggests that an elevation of excitatory influences by an increase in glutamatergic neurotransmission is responsible for the observed hyperactivity in the CNS. This increase might be produced due to a decreased influence of inhibitory GABAergic neurotransmission (Berger & Coomber, 2015; Sturm et al., 2017). If this increase in neural activity is maintained over time due to prolonged acute noise exposure, the excitatory and inhibitory balance may become permanently disrupted. This disruption may occur due to a pronounced Ca^{+2} influx into the presynaptic terminals due to excessive stimulation, causing an excessive release of glutamate into the synaptic cleft. This excessive release could trigger similar neurotoxic effects as have been described in the inner ear, such as apoptotic pathway activation, synaptic or axonal plasticity changes, oxidative stress, and/or inflammatory mechanisms (Gunes et al., 2021; Caspary et al., 2008; Greenwood & Connolly, 2007; Puel, 1999). Nevertheless, the detailed synaptic mechanisms behind these alterations are poorly understood, as a large variety of complex effects have been found in animal studies for different kinds of neurotransmitter-related imbalances (Browne et al., 2012; Chang et al., 2002; Godfrey et al., 2012; Lee & Godfrey, 2014; Muly et al., 2004; Noreña & Eggermont, 2003).

First, a correlation between NIHL and an alteration of neuronal spontaneous firing rates (SFRs) in CNS auditory structures such as the IC or the AC has been observed. Altered SFRs constitute evidence of elevated neural activity in the CNS after noise exposure and/or peripheral damage, and might be linked to hearing impairment. For that reason, many studies have made remarkable efforts to characterize those increases. However, there is still an ongoing debate about the intrinsic nature of the changes (Basta & Ernst, 2004; Brozoski et al., 2002; Eggermont, 2006; Imam & Alam Hannan, 2017; Kaltenbach et al., 1992; Salvi et al., 1990; Seki & Eggermont, 2003).

Sun et al. (2012) observed that an increased AC response could affect sound sensitivity, inducing hyperacusis-related behaviors. But interestingly, noise trauma induced a decrease in the spontaneous activity in the IC. Accordingly, Basta & Ernst (2004) reported similar decreases in

spontaneous activity in the IC after noise exposure. Nonetheless, studies made by Ma et al. (2020) showed that the firing rate of glutamatergic neurons in the IC is increased post-exposure *in vivo*, contrary to the *in vitro* results presented by Sun et al. (2012) and Basta & Ernst (2004) in brain slices. Similarly, Mulders & Robertson (2013) and Wang et al. (2002) detected significant increases in the activity of the CIC within 12 and 24 hours after noise exposure. Additionally, studies made by Kaltenbach et al. (1998) and Kaltenbach & Afman (2000) demonstrated that increases in spontaneous activity after noise exposure could also be observed in the CN 30 days after noise exposure. Hickox & Liberman (2014) found that elevated behavioral hyperresponsiveness to sound and enhanced central auditory activity within the first and the second week post-exposure could be observed after loud noise exposure. Those effects were associated with a reduction in the amplitude of ABR Wave I and an increase in the amplitude of ABR Wave IV/V, which is thought to be correlated with reduced auditory nerve response and enhanced central neural activity in order to compensate for further inner ear deficits (Heeringa & van Dijk, 2014; Kujawa & Liberman, 2009; Lin et al., 2011; Singer et al., 2020). These controversial findings may perhaps be explained by complex noise-induced interactions between various central auditory structures and/or by variations in methodological approaches.

Therefore, it seems that peripheral damage can change neural homeostasis in the CNS, and this might correlate with some noise-induced related disorders like tinnitus or hyperacusis. Nonetheless, there is still a need for finding a detailed biological explanation of what is behind those phenomena. As described before, excitatory and inhibitory imbalances which can be accompanied by synaptic connectivity reorganizations or cell death may lie behind those effects. For that reason, several studies investigated functional and structural alterations of specific synaptic pathways in order to understand how noise exposure could lead to enhanced neural activity.

1.2.2.3.3. Synaptic changes in central glutamatergic and GABAergic neurotransmission

Therefore, it has been suggested that noise-induced hyperactivity may arise as a consequence of changes in presynaptic and postsynaptic elements crucial for regulating glutamatergic and GABAergic neurotransmission (Heeringa et al., 2016; Browne et al., 2012; Hakuba et al., 2000; Ma et al., 2021; Muly et al., 2002; Park et al., 2020; Schrode et al., 2018; Singer et al., 2020). In this context, some studies tried to describe noise-induced excitatory/inhibitory imbalances focusing on the expression of Vesicular Glutamate Transporter 1 (VGLUT1), Vesicular Glutamate Transporter 2 (VGLUT2), and Vesicular GABA transporter

(VGAT). VGLUT1 and VGLUT2 are presynaptic proteins responsible for loading glutamate into presynaptic vesicles, whereas VGAT is accountable for loading GABA into presynaptic vesicles. These presynaptic transporters are found in the nerve terminals of neurons in the CNS and are critical for proper neurotransmission (Eriksen et al., 2021). Together, they are currently the best markers for glutamatergic nerve terminals and GABAergic synapses (Ito, 2011; Hackett, 2011; Zhou, 2007). Therefore, changes in the expression of those vesicular neurotransmitter transporters (VNTTs) may produce an inappropriate release of glutamate and GABA into the synaptic cleft. A permanent disruption of these neurotransmission mechanisms might be a potential reason behind the noise-induced overexcitation in the auditory pathway. These effects may have a relationship with an elevation of HT and loss of auditory function, increases in apoptotic events, excitotoxicity, or tinnitus and hyperacusis.

In this context, some studies detected an increase in VGLUT2 and a decrease in VGLUT1 in the CN after noise trauma (Heeringa et al., 2016; Barker et al., 2012; Kurioka et al., 2016; Zeng et al., 2009). It is thought that this could be related to the differential expression patterns of VGLUT2 and VGLUT1. While VGLUT2 is mostly associated to somatosensory projections, VGLUT1 is mostly expressed in type I ANF (Ito & Oliver, 2012; Zeng et al., 2009; Zhou, 2007). Thus, a downregulation of VGLUT1 is often linked to reduced peripheral input due to auditory nerve deafferentation, whereas increases in VGLUT2 may imply compensatory reinnervation of the CN by projecting somatosensory inputs (Heeringa et al., 2016). In addition, Fyk-Kolodziej et al. **(**2011) and Heeringa et al. **(**2018) provided evidence of synaptic reorganization of glutamatergic terminals containing VGLUT1 and VGLUT2 in the CN due to hearing loss or tinnitus. Furthermore, Park et al. **(**2020) also detected changes in VGLUT1 and VGLUT2 in the AC and in the IC 30 days after repeated acute noise trauma was induced. Moreover, Zhang et al. **(**2021) found an increase in VGLUT1 in distinct hippocampal regions of noise-exposed guinea pigs. Those results suggest a possible relationship of impaired glutamatergic neurotransmission even in higher cortical areas of the limbic system, and might explain changes in emotional stress, cognitive decline, or depression symptoms observed in patients suffering from chronic tinnitus (Kraus & Canlon, 2012; Manohar et al., 2022).

In addition, little and contradictory information is available on the role of VGAT during noise-induced neuroplasticity. Park et al., 2020 were not able to detect changes in VGAT between noise and control groups either in the AC or IC. However, Bledsoe (1995) detected that GABA release *in vivo* in the CIC was significantly reduced in deafened animals when compared to controls. Similarly, Milbrandt et al. (2000) detected a significant decrease in glutamic acid

decarboxylase (GAD) (an enzyme responsible for catalyzing the conversion of glutamate into GABA) in the IC right after noise exposure, which had completely recovered by 30 days post-noise exposure. Moreover, Zhang et al. (2021) showed a decline in VGAT expression in the hippocampus. Hence, GABA release could be also impaired as a consequence of excessive noise-induced excitation, and alterations in VGAT might constitute a potential reason. Nonetheless, the role of VGAT in regulating GABAergic neurotransmission must be fully elucidated.

Therefore, it seems that changes in VNTT expression may constitute a crucial neuroplastic factor behind altered glutamatergic and GABAergic neurotransmission after noise exposure. However, few studies have addressed this question, and the role of VNTTs in auditory CNS areas like the IC or the MGB in this regard is poorly understood. Furthermore, it is not clear which molecular pathway could be implicated in VNTT abnormal expression after noise exposure. For these reasons, VGLUT1, VGLUT2 and VGAT were selected to undergo extensive investigation during the present study.

Furthermore, some studies investigated additional pre- and postsynaptic alterations, suggesting an enhancement of release together with a decreased uptake ability for glutamate and GABA after noise exposure. Muly et al. (2004) showed that 7 days post-exposure, before the cochlear nerve axons degenerated, an increase in glutamatergic release in the CN after noise exposure was observed, whereas uptake was depressed. Accordingly, Ma et al. (2021) detected a disruption in the expression of vesicular glutamate transporter 3 (VGLUT3) in the cochlea after noise-induced trauma without detecting hair cell damage, whereas the glutamate/aspartate transporter (GLAST) expression gradually increased 2h and up to 7 days post-exposure. Those results were consistent with the observations of Hakuba et al. (2000), in which GLAST-deficient mice showed increased accumulation of glutamate after acoustic overexposure. Additionally, Szczepaniak & Moller (1995) and Basta & Ernst (2004) showed how the firing rate of neurons increase in the IC in combination with the $GABA_A$ receptor antagonist, Bicuculline. Subsequently, Llano et al. (2012) showed that an increase in cortical activation was accompanied by a diminished sensitivity to GABAergic blockade. However, Kapolowicz & Thompson (2016) did not find any changes in GAD expression in the AC, amygdala, and hippocampus right after noise exposure. Subsequently, several studies reported noise-induced changes in the hydroxy-5-methylisoxazole-4-propionic (AMPA) and N-methyl-D-aspartate receptor (NMDA) glutamate receptors (Chen et al., 2004; Duan et al., 2006; Hu et al., 2020). Finally, Browne et al. (2012) reported fluctuations in the protein expression patterns of different excitatory and inhibitory neurotransmission-related

proteins for at least a month following acute noise exposure, but it was difficult to assign an exact role to each change in the final excitatory and inhibitory alteration.

The listed evidences show how changes in presynaptic and postsynaptic elements may play a role in neural hyperactivity, disrupting the homeostatic neurotransmission balance in the CNS. However, these changes are still not extensively understood. Furthermore, these effects have a potential relationship with cell loss and connectome rearrangement events within neural structures of the central auditory pathway.

1.2.2.3.4. Noise-induced connectivity reorganizations in the central auditory pathway

In this context, increased activity produced as a consequence of excitatory and inhibitory imbalances might also stimulate complex axonal connectivity changes in order to adapt to excessive noise exposure. This shown by the fact that following primary peripheral lesion and auditory deafferentation in experimental animals, nerve degeneration and synaptic rearrangements were observed in the CN and the SOC (Benson et al., 1997; Bilak et al., 1997, 1997; Hildebrandt et al., 2011; Illing et al., 1997; Izquierdo et al., 2008; Jean-Baptiste & Morest, 1975; Kraus et al., 2009; Muly et al., 2002). It has been hypothesized that these connectivity reorganizations could be related to the previously described increases in central activity in the ascending auditory pathway. The reason for this is that under prolonged and pathological noise exposure, excessive excitation and diminished inhibition may result in different alterations in synaptic connectivity (mainly through changes in the expression of different neurotransmission-related elements such as the VNTTs, or the AMPA and/or NMDA receptors), which in turn could lead to changes in synaptic function (Çakır et al., 2015; Chen et al., 2004; Duan et al., 2006; Hu et al., 2020; Kurioka et al., 2016; Tagoe et al., 2017). These events might be translated into functional changes in the intrinsic physiology of higher auditory areas, and may contribute to abnormal hearing function, producing tinnitus and/or hyperacusis (Brinkmann et al., 2021; Çakır et al., 2015; Knipper et al., 2013; Kujawa & Liberman, 2009; Luan et al., 2021; Zhang et al., 2021).

Following this line, some studies showed that extensive nerve degeneration can be observed in some higher auditory structures within the first moments after noise trauma. However, a certain degree of recovery in terms of axonal growth and synaptogenesis is possible several weeks or months after noise exposure (Jean-Baptiste & Morest, 1975; Kraus et al., 2009; Manohar et al., 2019). Jean-Baptiste & Morest (1975) observed primary auditory nerve degeneration right after acute cochlear ablation, but a new growth of axons and a recovery of their normal appearance was observed at up to seven months in the medial trapezoid nucleus (MTN), a distinct nucleus of

the SOC. Similarly, Morest et al. (1997) and Bilak et al. (1997) described signs of terminal degeneration in the CN immediately following cochlear lesions. However, 8 months after trauma, an increase in the number of synaptic endings could be observed. Subsequently, Kim et al. (2004) detected significant loss of axons and synaptic terminals in the CN of chinchillas 1 week after noise trauma, which progressed for 16 to 24 weeks. Nevertheless, a resurgence in the axonal growth and an increased number of synaptic terminals within these structures was detected after 24-32 weeks of noise exposure. In addition, Manohar et al. (2020) showed that changes at the gene expression level occurred more frequently 28 days post-exposure versus 2 days post-exposure.

Equally, some studies tried to observe if synaptic activity could be affected within the ascending auditory pathway as a consequence of acute noise exposure. First, Illing et al. (1997, 2005, 1995) and Kraus et al. (2009) detected an upregulation of the growth-associated protein GAP-43 (a presynaptic protein expressed in growth cones during axonal changes) several days after cochlear ablation in the CN of guinea pigs after noise exposure, but not in the first moments (see Figure 5). Second, some studies addressed this question by studying synaptophysin expression, an integral membrane Ca^{+2} binding glycoprotein present in presynaptic vesicles of neurons, which provides an indirect measure of synaptic activity (Gil-Loyzaga, 1998; Bartolomé et al, 1993). Benson et al. (1997) observed decreased synaptophysin immunolabelling in the CN 7 days after cochlear removal in adult guinea pigs, although, at later times, immunolabelling density recovered up to normal levels. Correspondingly, Muly et al. (2002) showed how axonal degeneration was clearly evident in light microscopic preparations following noise exposure (see Figure 5). Nevertheless, following degeneration, a new increase of growing synaptic terminals was observed together with changes in synaptophysin expression and synaptic vesicle accumulation over time.

Additionally, cross-modal plasticity and connectivity reorganization have also been reported in neural structures not frequently associated with the auditory central nervous system, suggesting that neuroplastic changes after acoustic trauma could even affect different nervous system structures which are not directly related to the auditory system. These alterations might be crucial in order to explain different symptoms associated with tinnitus, hyperacusis, or NIHL as described before (Aldhafeeri et al., 2012; Chen et al., 2016; Kraus & Canlon, 2012; Leaver et al., 2011; Lockwood et al., 1998; Luan et al., 2021; Manohar et al., 2022; Morest al., 1998; Oluwole et al., 2022; Schormans et al., 2017; Wieczerzak et al., 2021; Wolak et al., 2016).

All previously listed evidences suggest that these axonal density changes observed in the

CNS may be linked with increases in neural activity and excitatory imbalances (Hickman et al., 2020; Hickox & Liberman, 2014; Knipper et al., 2013; Manzoor et al., 2012a; Niu et al., 2013; Singer et al., 2020). Nevertheless, the biological relationship between all those neuroplastic changes and how connectivity reorganizations fluctuate during the time course of NIHL in different areas of the ascending auditory pathway are still poorly investigated. Therefore, understanding how axonal changes occur might give answers about how acoustic overstimulation can remodel the neural circuitry of the central auditory system. In addition, it might constitute a potential indicator for the existence of early NIHL neuroplasticity and/or neurodegeneration events in the CNS, which may be critical from a therapeutic perspective.

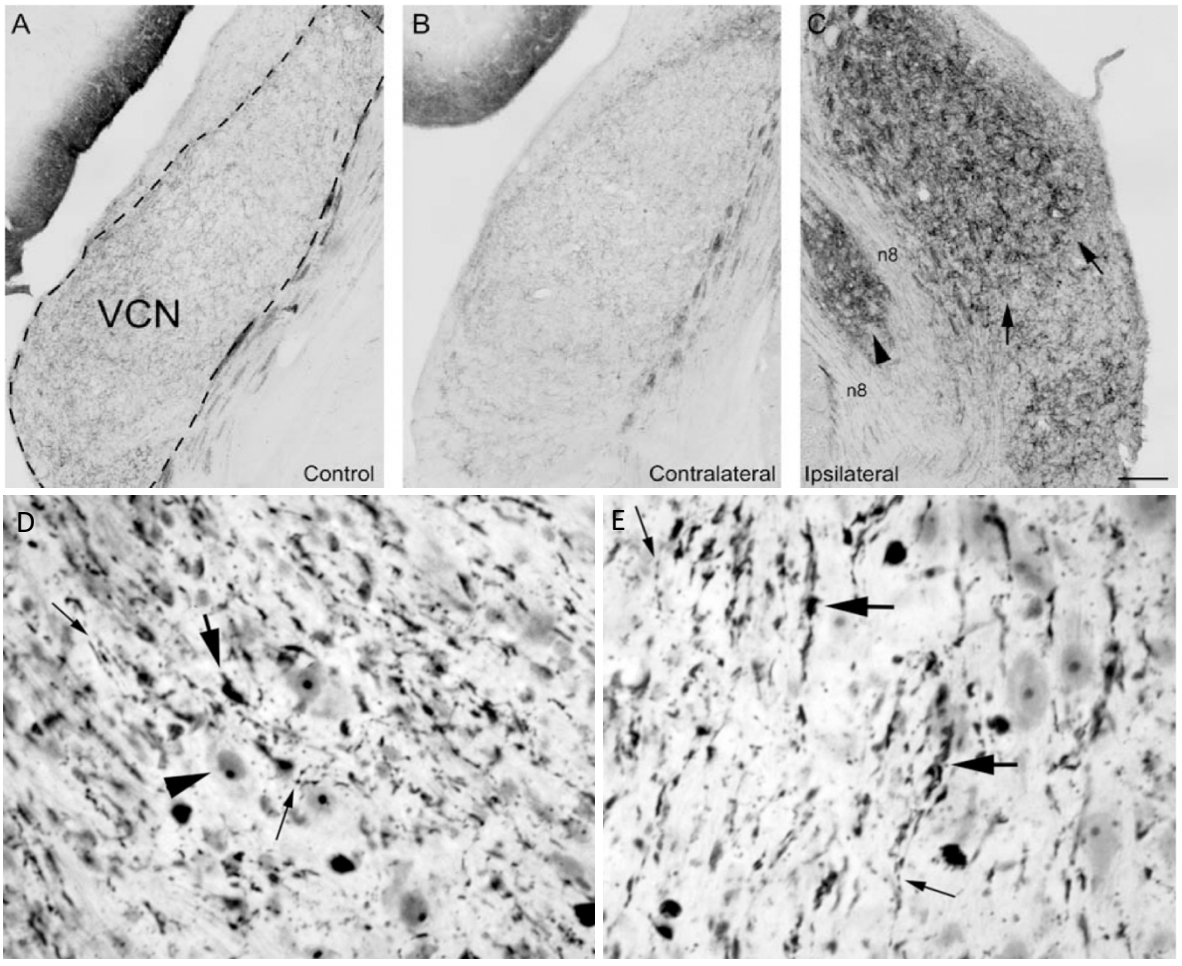

Figure 5. Synaptic reorganization after noise trauma: (A-C) GAP-43 immunoreactivity observed in the VCN of normal hearing or control animals (A) compared to immunoreactivity observed in experimental animals following unilateral cochlear ablation in both contralateral (B) and ipsilateral sites (C). In the experimental animal, GAP-43 was upregulated in the ipsilateral VCN after treatment, whereas expression was moderately lower in the control animal as well as in the untreated control side in the experimental animal. These results indicate that cochlear ablation could led to neuroplastic remodeling in the CNS. (D-E) Signs of axonal degeneration detected in the ipsilateral VCN after noise exposure. Degenerating axons can be seen as beaded black deposits with irregular shapes. The degeneration may affect thick neural fibers (thick arrows) as well as thin axonal tracks (thin arrows). Neuronal soma are indicated by large black arrowheads. *Source: (A-C) Kraus et al., 2009; Copyright (2009) Elsevier B.V, all rights reserved; (D-E) Muly et al., 2002; Copyright (2002) Elsevier Science (USA), all rights reserved.*

1.3. MAIN OBJECTIVES

For the reasons listed above, understanding how neurodegenerative and neuroplastic events can occur in the auditory neural pathway as a result of acute noise exposure might be a critical step in order to understand the underlying mechanisms of NIHL. Therefore, it is crucial to investigate how cell density changes, connectivity reorganizations or glutamatergic and GABAergic imbalances can happen during the time course of NIHL. Equally, it is remarkably important to highlight that neurodegeneration and neuroplasticity events might be not independent of each other. Thus, finding the relationship between these phenomena could be essential. Furthermore, there is still a lack of knowledge when trying to understand the time course of the pathological progression of NIHL after acute noise trauma. This is strongly needed in order to observe the pathological consequences of NIHL with a more widespread view. Additionally, it might constitute a critical step in the field in order to develop precise clinical strategies to prevent, diagnose and treat NIHL consequences.

Therefore, the aim of the present study was to understand the dynamics of cell density, axonal density, and glutamatergic and GABAergic neurotransmission imbalances in the CNS as a consequence of NIHL. To achieve this goal, three different analyses were carried out to tackle the following hypotheses:

1. Neurodegeneration analysis (Experiment 1): NIHL leads to a decrease in cell density in the CIC and/or MGV.
2. Neuroconnectivity analysis (Experiment 2): NIHL results in neurofilament density changes between the CIC and/or MGV.
3. Neurotransmission analysis (Experiment 3): NIHL leads to changes in glutamate and GABAergic influences in the CIC and/or MGV.

02 MATERIALS AND METHODS

2.1. PRE-REGISTRATION

This project was pre-registered in the Open Science Framework (osf.io) (https://osf.io/2aknq/).

2.2. RANDOMIZATION

For randomization, each individual was equally assigned to each experimental group. Mice were picked randomly by hand for the factor affiliation and were tested in parallel cohorts per time point.

2.3. BLINDING

Noise exposure and subsequent measurements pre- and post- noise exposure were performed under blinded conditions. Personnel who analysed the data collected from the study were not aware of the treatment applied to any given group.

2.4. ANIMALS

Normal hearing mice (NMRI strain) purchased from Charles River Inc. were used for measurements in an adult state (aged 8-10 weeks at noise exposure) to guarantee a fully developed auditory system. Mice did not exceed the age of 6 months to prevent age-related hearing disorders which might interfere with proper data collection. During our experiments, mice received the same treatment sex-independently. Every mouse was caged in groups of no more than six mice. Each cage included a resting area as well as enrichment elements (plastic tunnels and nesting materials). The animals were kept in a 12/12h dark/light cycle and had constant access to food and water. All mice were divided among the experimental groups so that no animal remained. ABR recordings, noise exposure, MRI, and tissue perfusion experiments were performed in the Neurowissenschaftliches Forschungszentrum (NWFZ) (Campus Charité Mitte). The governmental Ethics Commission for Animal Welfare (LaGeSo Berlin, Germany) gave their seal of approval to the experimental protocol (approval code: G0256/19). The EU Directive 2010/63/EU on the protection of animals used for scientific purposes was followed in the conduct of this study.

2.5. NOISE EXPOSURE PARADIGM

Three different experimental groups were established:

1. 115 dB (High noise exposure) (n = 8): In this group, mice were binaurally exposed to an intense white noise (5-20 kHz) at 115 dB SPL inside a sound-proof chamber for 3h in an anesthetized state in order to create a profound threshold shift.

2. 90 dB (Moderate noise exposure) (n = 8): In this group, mice were binaurally exposed to a moderate white noise (5-20 kHz) at 90 dB SPL inside a sound-proof chamber for 3h in an anesthetized state in order to induce an acoustic overstimulation without a permanent threshold shift.

3. Normal hearing control (n = 8): In this group, mice were not noise-exposed but anesthetized for 3h in order to show physiological homeostatic changes.

The chosen noise exposure paradigm was based on earlier studies on neuronal degeneration and cell death mechanism detection after noise exposure in order to ensure similar experimental conditions, and taking into account the hearing range of mice (≥1Hz and ≤100 kHz) (Basta et al., 2005; Fröhlich et al., 2017; Gröschel et al., 2010). The noise was delivered binaurally by a speaker (HTC 11.19; Visaton, Haan, Germany). The speaker was connected to an audio amplifier (Tangent AMP-50; Aulum, Denmark) that was placed right above the position of the animal's head using a wooden bar holder. SPL levels were adjusted with our audio amplifier and calibrated until the desired levels using a sound level meter (Voltcraft 329; Conrad Electronic, Hirschau, Germany) placed right at the animal's head position. Afterwards, the temperature inside the chamber was measured with a temperature controller (GTH 1200A Digital thermometer, Greisinger Electronic GmbH, Germany) and a heating pad (Thermolux Wärmeunterlagen, Witte & Sutor GmbH, Germany) in order to ensure proper temperature conditions (36 °C) before starting the experiments. Then, noise exposure experiments were conducted.

During the performance of a noise exposure experiment, three different animals received an intraperitoneal injection of a mixture of different anesthetics (4 mg/kg xylazine and 100 mg/kg ketamine). Subsequently, animals were placed inside a heating chamber (MediaHeat TM, Peco Services Ltd, UK) heated at 36 °C, and toe-spread and eyelid reflexes were continuously checked until no reaction was visible before starting the next procedures. Then, all the animals were properly weighed and two out of three animals were selected randomly to undergo noise exposure treatment (115 dB or 90 dB SPL). The remaining animal was established as the control group, and

did not receive any noise exposure treatment. The control animals were equally anesthetized and kept in the heating chamber at 36 °C, but were not exposed to noise.

The experimental subjects were placed inside a soundproof chamber kept at 36 °C using a heating pad (Thermolux Wärmeunterlagen, Witte & Sutor GmbH, Germany) and a temperature controller (GTH 1200A Digital thermometer, Greisinger Electronic GmbH, Germany), and eye gel (Pan-Opthal Gel, Dr. Winzer Pharma GmbH, Germany) was applied to the eyes in order avoid eye damage. Subsequently, two different catheters connected to two different syringes containing the same anesthetic mixture as described before (4 mg/kg xylazine and 100 mg/kg ketamine) were subcutaneously inserted into the animal's neck in order to apply 30% of the initial anesthesia dose approximately every 30 minutes during noise exposure treatment. This was performed with the aim of maintaining the anesthetized status of the animals during the whole noise exposure procedure. These two syringes were placed outside the soundproof chamber in order to apply anesthetics during the experiments through the catheters when the soundproof chamber was closed in order to avoid external sound disturbances. Then, it was ensured that animal respiration rate was clearly visible and could be controlled using a video camera (Logilink UA0072A, Logitech Inc., Switzerland) connected to a laptop, and the temperature was constantly monitored until the end of the experiment.

Subsequently, noise exposure was performed for 3h to broadband white noise (5-20 kHz) (115 dB or 90 dB) in accordance with earlier studies by our group (Coordes et al., 2012; Gröschel et al., 2010). The experiment was interrupted if the animals awoke during the noise exposure procedure. In that case, 30% of the initial anesthesia dose was subcutaneously injected, and the animals were kept in a heating chamber (MediaHeat TM, Peco Services Ltd, UK) at 36 °C. Then, toe-spread and eyelid reflexes were continuously checked until no reaction was visible before continuing with the procedure. Afterwards, the animals were again introduced into the soundproof chamber, the previously used catheters were inserted subcutaneously and experiments continued until reaching the 3h time-frame. In the end, catheters were removed from the subjects and animals were placed into the heating chamber kept at 36 °C until the anesthetic state completely disappeared. Finally, the animals were placed in the same cages as they were before the start of the experiments and were kept in the animal facility with continuous access to food and water until subsequent measurements were performed. An explanation of all noise exposure procedures performed can be seen in Figure 6.

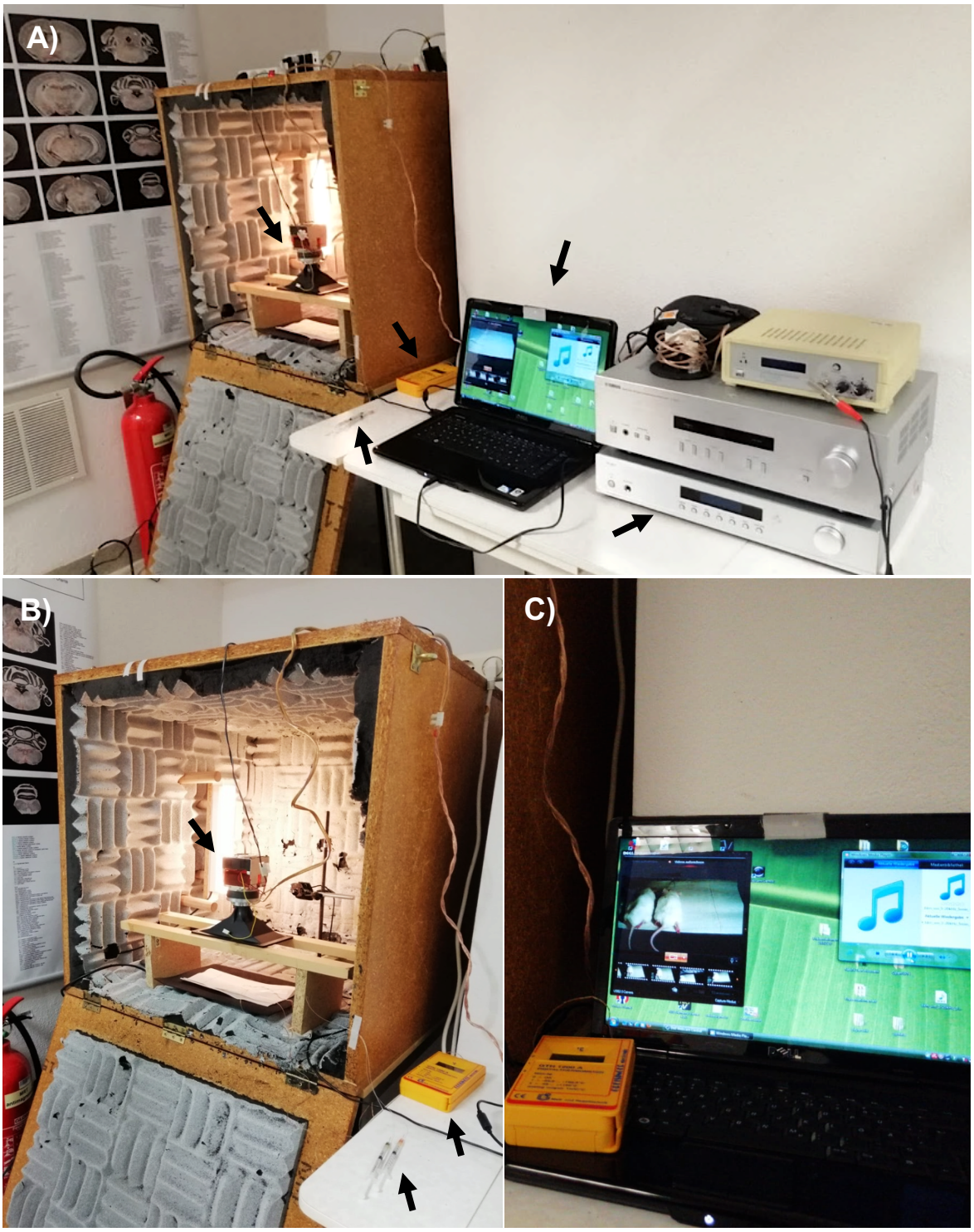

Figure 6. Noise exposure paradigm. (A-B) Noise exposure setup: animals were noise exposed to broadband white noise (5-20kHz) at different intensities (115 dB or 90 dB SPL) for 3h inside a soundproof chamber. Noise was delivered binaurally by a speaker connected to an audio amplifier and a DVD player. The speaker was placed right above the animal's head, held by wooden bars. The loud noise speaker was cooled down using a ventilator placed above the speaker. The temperature inside the chamber was constantly monitored using a temperature probe and kept between 38-36 °C. Two syringes connected to two catheters were placed outside the chamber in order to deliver 30% of the original anesthetic every 30 minutes in order to keep the anesthetized state of the animals. The catheters were correctly labelled and placed subdermally. SPL levels were adjusted with our audio amplifier and calibrated until the desired levels using a sound level meter. (C) The activity of the animals was constantly monitored using a video camera that allowed the observation of breathing respiration patterns.

Finally, to explore the noise-induced time course of cell density, axonal density, and glutamatergic and GABAergic imbalances after NIHL, the effects of each of the three treatments described above were studied at 4 different experimental time points after the noise trauma. The four experimental time points selected were:

1. 1-day (1d) group (n =23; 115 dB: n = 8; 90 dB: n = 8; Ctrl: n = 7)): In this group, animals were investigated 1 day after noise exposure.
2. 7-day (7d) group (n=24; 115 dB: n = 8; 90 dB: n = 8; Ctrl: n = 8)): In this group, animals were investigated 7 days after noise exposure.
3. 54-day (54d) group (n=24; 115 dB: n = 8; 90 dB: n = 8; Ctrl: n = 8)): In this group, animals were investigated 56 days after noise exposure.
4. 84-day (84d) group (n=24; 115 dB: n = 8; 90 dB: n = 8; Ctrl: n = 8)): In this group, animals were investigated 84 days after noise exposure.

Auditory Brainstem Response (ABR) measurements were performed before (pre-ABR) and after (post-ABR) noise. Magnetic Resonance Imaging (MRI) was acquired at the time points listed above. Animals were prepared for Fluorescence immunohistochemistry (FIHC) and image analysis techniques directly after MRI scanning. A detailed timeline of all techniques performed in the present study can be seen in Figure 7.

2.6. MAGNETIC RESONANCE IMAGING (MRI)

During the time course of the present study, different Magnetic Resonance (MR) techniques were performed. The measurements were acquired using a 7 T animal scanner (BioSpec 70/20 USR) with a cryogenically cooled transmit/receive mouse head surface coil and Paravision 6.0.1 software (Bruker, Ettlingen, Germany). The protocol consisted of T2-weighted (T2w) MRI for voxel-based morphometry analyses (VBM) of gray matter density, diffusion tensor imaging (DTI) for connectome reconstruction, and 1H MR spectroscopy (1H MRS) for neurotransmitter quantification. These procedures were carried out as part of a complementary project in order to assess the effectiveness of MRI techniques in the early study of NIHL pathophysiology.

MRI measurements and MRI-derived data analysis were entirely performed by personnel from the 7T experimental MRI Core Facility of the Charité Universitätsmedizin Berlin at the respective experimental time points. At the beginning, MRI measurements were transferred immediately after post-ABR measurements. Mice were carried out in an anesthetized state (100

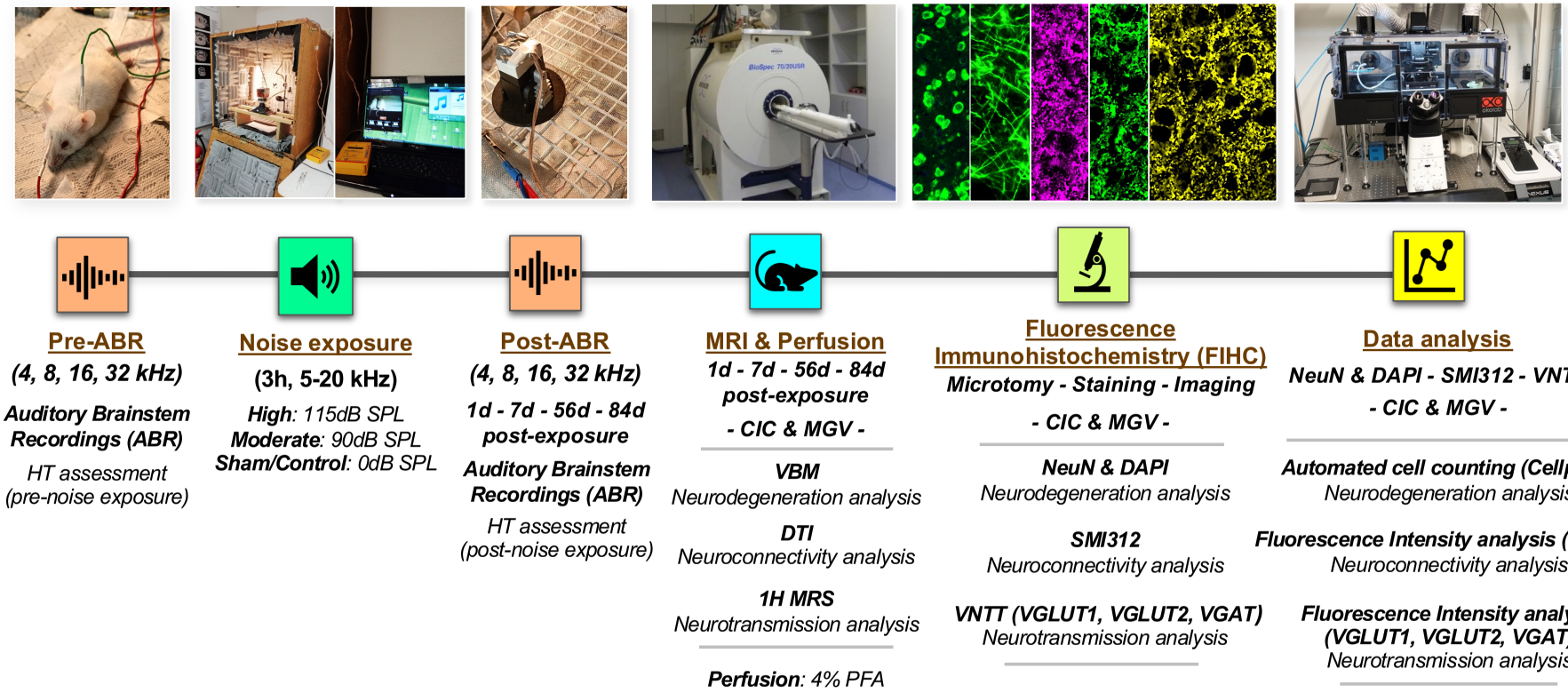

Figure 7. Study plan overview Figure 7. Study plan overview. First, Auditory Brainstem recordings (ABR) were recorded prior to noise exposure (pre-ABR) in order to assess the Hearing Threshold (HT) of the experimental subjects prior to acute noise trauma. Subsequently, different noise exposure treatments (High noise: 115 dB SPL; Moderate noise: 90 dB SPL; Control (Ctrl): 0dB SPL) were applied for 3h (5-20kHz). Additionally, ABR recordings were also performed after noise exposure (post-ABR) for assessing HT after noise trauma. Afterwards, Voxel-Based Morphometry (VBM), Diffusion Tensor Imaging (DTI) and Proton magnetic Resonance Spectroscopy (1H MRS) MRI-based techniques were performed in order to study neurodegenerative (neurodegeneration analysis), neuroconnectivity (neuroconnectivity analysis) and neurotransmission (neurotransmission analysis) changes in the Central Inferior Colliculus (CIC) and the Ventral subnucleus of the Medial Geniculate Body of the thalamus (MGV). These changes were assessed at different experimental time points after noise exposure: 1 day (1d) (n = 23: 115 dB, n = 8; 90 dB, n = 8; Ctrl, n = 7), 7 days (7d) (n = 24: 115 dB, n = 8; 90 dB, n = 8; Ctrl, n = 8), 56 days (56d) (n = 24: 115 dB, n = 8; 90 dB, n = 8; Ctrl, n = 8) and 84 days (n = 24: 115 dB, n = 8; 90 dB, n = 8; Ctrl, n = 8). Within each experimental time point, the previously listed noise exposure treatments (115 dB, 90 dB, Ctrl) were analysed in different subjects. Thus, different experimental subjects were included within different time points and experimental groups. Mice were sacrificed and perfused immediately after MRI measurements (4% PFA). Brains were embedded and sectioned in paraffin blocks (microtomy). Fluorescence Immunohistochemistry (FIHC) stainings were performed in the ICC and MGV using: NeuN & DAPI labelling as a neuronal and cell marker in order to assess neuronal and cell density changes (neurodegeneration analysis); anti-neurofilament marker SMI312 labelling in order to study neurofilament density changes (neuroconnectivity analysis); and vesicular transporter glutamate 1 (VGLUT1) and 2 (VGLUT2) labelling in order to analyse glutamatergic imbalances, and vesicular GABA transporter (VGAT) labelling in order to assess GABAergic imbalances (neurotransmission analysis) as a consequence of NIHL. Fluorescence microscopy imaging procedures were performed. Finally, automated cell counting and fluorescence intensity analysis were performed in order to analyse histological data. The main contribution of the present doctoral dissertation is included in the noise exposure, electrophysiological (ABR) and FIHC (data collection & data analysis) part of the present study.

mg/kg ketamine, 4 mg/kg xylazine) and properly heated directly to the MRI scanner. Then, mice were placed on an animal holder with ear and tooth bar fixation and were anesthetized during the entire MRI measurements using isoflurane (1.5%) in a 70%/30% N2O/O2 mixture. Mice were sacrificed immediately after the acquisition of MRI measurements according to the study plan. During all MRI measurements, animal temperature and respiration rates were continuously monitored using a rectal probe and a pressure sensitive pad under the thorax. Nevertheless, too many animals were lost during the time course of the present study due to the mixture of ketamine, xylazine and isoflurane, in particular with male subjects. Therefore, a post-ABR procedure immediately before MRI measurements was avoided and a gap was introduced. Then, all MRI measurements were performed either one or two days after post-ABR measurements were recorded in order to avoid the mixture of anesthetics. Moreover, it was assumed that HT did not change inside the selected time-frame. During this procedure, animals were directly carried out from the animal facility into the MRI scanner and were anesthetized only using only isoflurane (1.5%) in a 70%/30% N2O/O2 mixture as described before. This protocol shift increased the animal survival rate during MRI measurements, following the principles of the 3Rs animal welfare regulations.

It is important to highlight that the main contributions of the doctoral candidate were performed in the data acquisition and data analysis of the electrophysiological and the histological part of the present study. Data collection as well as data analysis of the electrophysiological and histological experiments included in the present study were performed by the doctoral candidate (excluding the development of Image J automated analysis macros for histological analysis). Those parts will constitute the core contribution of the present monograph and will be described in following sections.

2.7. AUDITORY BRAINSTEM RESPONSE (ABR)

During this study, Auditory Brainstem Response (ABR) techniques were performed to assess hearing impairment after noise exposure. ABR audiometry is defined as a neurophysiological test to assess the hearing threshold (HT) in response to characterized auditory stimuli that generate electrical impulses in the auditory neural pathway, which can be recorded by different electrodes. This technique was first described by Jewett & Williston (1971), and it is considered as a strong tool to identify the magnitude of hearing loss, as it provides information mainly about the function and integrity of the auditory brainstem structures, as well as for the inner ear (Habib & Habib, 2021). Using the mouse as an animal model, ABR recordings reflected the

electrical responses from both cochlear ganglion neurons and different nuclei of the central ascending auditory pathway to sound stimulation via electrodes placed on the scalp of an anesthetized animal. HT refers to the lowest SPL that can generate identifiable electrical response waves (Akil et al., 2016; Eggermont, 2019; Habib & Habib, 2021; Radeloff et al., 2014). Up to 5 prominent waves that occur during the first 10 ms after presentation of a transient sound stimulus can be identified. These waves are labeled by Roman numerals (I-V), and despite there being some controversy, each of the waves can be assigned to the electrical response of different auditory areas from the ascending auditory pathway. In this way, wave I is generated by the auditory nerve (AN), wave II by the cochlear nucleus (CN), wave III by the superior olivary complex (SOC), wave IV by the lateral lemniscus (LL), and wave V by the inferior colliculus (IC). However, it is important to take into account that some studies suggest that waves might have contributions from more than one anatomical structure of the ascending auditory pathways (Akil et al., 2016; Xie et al., 2018) (see Figure 8). The test itself is considered as an objective measure that can properly detect auditory brainstem responses and assess the HT of the experimental subjects. Nevertheless, proper interpretation of the records might be subjective, as the identification of the different waves needs to be done by visual inspection by a trained investigator. Moreover, in this study, ABR recordings were also performed due to their potential for identifying the HT of our experimental model without extracting any behavioral information (Brookhouser et al., 1990; Jerger, 1978).

ABR recordings were performed during two different time points under anesthetic conditions (100 mg/kg ketamine, 4 mg/kg xylazine). ABR recordings were carried out 1 week prior to provoking noise-induced trauma (pre-ABR measurements) in order to assess the HT before noise exposure. Secondly, ABR recordings were performed again in a time frame that varied from two days to moments immediately before starting MRI measurements on the subsequent experimental days (post-ABR measurements) in order to assess the HT of the subjects after noise induced trauma. Anesthesia was injected intraperitoneally between 10-15 minutes before the recordings started, and animals were placed into a heating chamber at 35 °C (MediaHeat TM, Peco Services Ltd, UK) until reaching an anesthetized state. Toe-spread and eyelid reflexes were continuously checked until no reaction was visible before starting the next procedures. Mice were weighed using a scaled balance (MC1 Laboratory LC 4200, Sartorius GmbH, Germany) and immediately placed inside a soundproof chamber (80 cm × 80 cm × 80 cm, minimal attenuation 60 dB). Eye gel solution was placed on the eyes in order to avoid ocular damage (Pan-Opthal Gel, Dr. Winzer Pharma GmbH, Germany) and body temperature was constantly monitored to be between 37 °C and 36 °C using a temperature probe (GTH 1200A Digital thermometer, Greisinger Electronic GmbH, Germany)

and a heating pad (Thermolux Wärmeunterlagen, Witte & Sutor GmbH, Germany), both placed right below the mice. Afterwards, subdermal needle electrodes (Neuro.Dart SD57-426-M, Spes Medica Inc., Italy) were positioned on the forehead (reference), mastoid (active), and at one foot (ground) (see Figure 8). In order to prevent interference with the electrical signal, a metal cage was positioned above the animals. Subsequently, tones were presented binaurally at various sound pressure levels (SPL) using a high-frequency loudspeaker (HTC 11.19; Visaton, Germany) placed right above the animals in order to ensure equally binaural distribution of the sound waves. The presented tones were adjusted using a sine-wave generator (FG 250 D, H-Tronic, Germany) connected to an audio amplifier (Yamaha A-S 201, Yamaha Corp., Japan) and maintained at 0.2 VAC using a voltmeter (EX330, Extech instruments, USA).

ABR waveforms were collected from the output of EEG software (MC_Rack, Multichannel Systems, Harvard Bioscience Inc.) and a recording amplifier (USB-ME16-FAI-System, Multi-Channel Systems, Germany). ABR specific responses were recorded at four different frequencies (4, 8, 16, and 32 kHz). Sound stimuli were initially presented at 90 dB or 60 dB for each tested frequency. Then, sequential decreasing steps of 10 dB and/or 5 dB SPL were chosen and frequency-specific recordings were performed for each loudness step until there was no discernible ABR wave. The hearing threshold (HT) was determined to be at this point. Before beginning the ABR recordings, researchers were unaware of the treatment given to each animal. The HT for each frequency was always estimated by visually inspecting the series of recordings. Finally, the soundproof chamber was opened and the metal cage and the loudspeaker were removed. After the pre-ABR recording, the subdermal needle electrodes were removed, and the animal was transferred to the heating chamber, keeping the temperature constant at 36 °C until no anesthetic effects were visible. Mice were returned to the same cages and kept in the animal facility until the respective experimental day. Subsequently, post-ABR measurements were carried out under the same experimental conditions either one or two days before performing MRI measurements, or immediately before them due to the previously described reasons. In the last case, animals were transported immediately in an anesthetized state in order to proceed with the subsequent MRI measurements. The whole ABR procedure is summarized in Figure 8.

From ABR recording data, threshold differences between pre-ABR and post-ABR recordings were calculated for assessing the mean threshold shift (dB) for each investigated frequency and for each investigated subject (Mean Threshold Shift = Threshold $\text{Mean}_{\text{post-ABR}}$ − Threshold $\text{Mean}_{\text{pre-ABR}}$). Then, results from individual animals were averaged over the respective experimental group and experimental time point, and mean threshold shifts (Mean (dB) ± Standard

Deviation) were calculated relative to the hearing threshold of the control animals. This technique was also described in previous publications from our group (Basta & Ernst, 2004; Coordes et al., 2012; Gröschel et al., 2018). Finally, only animal subjects that exhibited a normal hearing function were included in this study.

Moreover, it is crucially important to highlight that post-ABR recordings were not performed in the 1d post-exposure group. Firstly, this procedure was carried out in order to minimize the stress of our experimental subjects and avoid animal death. Secondly, previous experiments showed that it was difficult to detect any ABR response 1 day after acute noise exposure. Furthermore, the observed elevated threshold shifts in the 115 dB groups of the 7d, 56d and 84d groups confirmed the efficiency of the noise exposure treatment. Due to those reasons, the performance of ABR measurements in the 1d group was avoided.

2.8. TISSUE FIXATION

After proceeding with the MRI measurements described before, animals were perfused via the left heart chamber with 4% paraformaldehyde (PFA, pH 7.4, Sigma Aldrich, Germany) using a perfusion pump (Reglo CIC, Avantor Inc., USA). In this way, animals were deeply anesthetized, doubling the dose from Section 2.5. to prevent awakening. The efficacy of anesthesia was checked using reflex tests pinching the feet of the animals. Posterior procedures were carried out when no reflexes were observed. Then, the animals were restrained in a plastic holder, lying on their backs with pins inserted on the front and hind legs. The abdominal cavity was opened on both sides by lifting and incising the epidermis and underlying tissue at the lower edge of the sternum. Subsequently, the diaphragm was cut and respiration immediately collapsed. The costal arches and overlying tissues were now transected on both flanks of the animal and the thorax was lifted and fixed with another pin into the plastic holder, exposing the still beating heart, and the surrounding pericardium was removed using microscissors to facilitate further processes. Then, a perfusion cannula was carefully inserted into the left main chamber of the heart, and the pericardium was sectioned and opened using microscissors. Afterwards, several perfusion solutions were applied in a time dependent manner. First, NaCl (0.9%) solution was flushed into the circuit using a pressure pump (9 ml/min, 2 min, RT) in order to flush the blood from the circulatory system of the animal. After a few minutes, the liver became bright and the exuding fluid became clear. Subsequently, it was possible to continue with 4% PFA solution as a fixative for 9 min in sequential steps of different pump pressure rates: 9ml/min during 1 min; 7.7ml/min for 1 min; 7 l/min for 1 min; 6ml/min for 1 min; 5.7ml/min for 4 min. In total, 52.5 ml of PFA

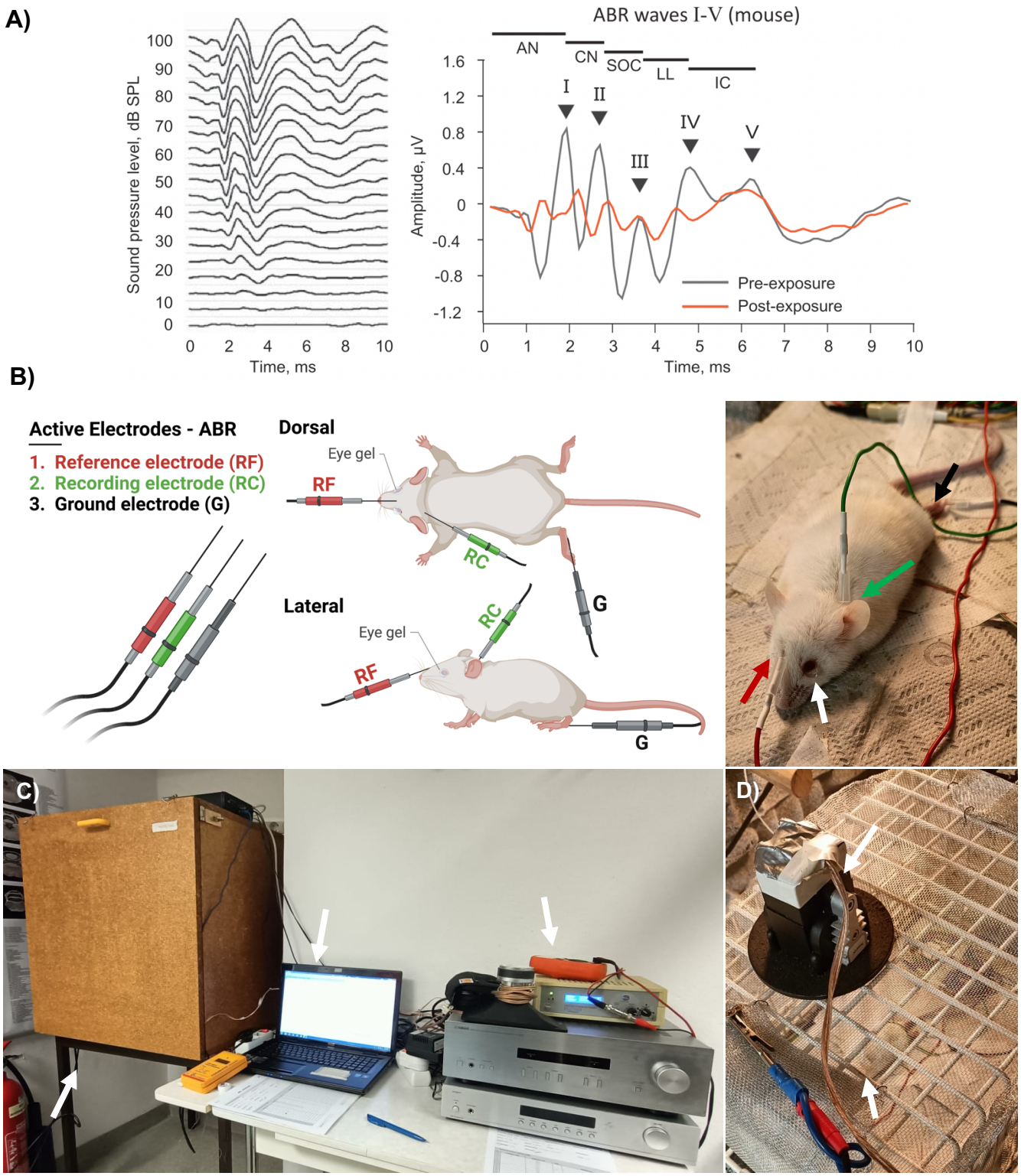

Figure 8. Auditory brainstem recordings (ABR): (A) A normal ABR recording in mice consists of 5 waves labeled from I-V. Wave I: Auditory nerve (AN); Wave II: Cochlear nucleus (CN); Wave III: Superior olivary complex (SOC); Wave IV: Lateral lemniscus (LL); Wave V: Inferior Colliculus (IC). (B-D) ABR recording procedure: (B) Active electrodes and schematic representation of their position during ABR recordings. Red: Reference electrode (RF); Green: Recording electrode, placed on the mastoid; Black: Ground electrode (G), placed on the left foot; placed subdermally on the forehead above the scalp. Eyes were protected with eye gel. (C) ABR recordings were made inside a soundproof chamber and identified by visual inspection. Evoked potentials were recorded using a high-frequency loudspeaker and a sine-wave generator that was adjusted with an audio amplifier. Respiration as well as animal activity were constantly monitored. (D) The loudspeaker was placed on the cage right above the animals in order to ensure equally binaural distribution of the sound waves and avoid external electrical contamination. *Source: (A) Rüttiger et al., 2017; Copyright (2017) Silverchair Publisher (B). Illustrated with Biorender.com.*

Were used per mouse, and during the whole perfusion step, the fixation status of the tissue was indicated by an onset of rigidity in the extremities. Finally, the perfused animal was then decapitated, and the skin removed from the head. Following perfusion, brains were carefully removed from the skull and stored in 0.1% PFA until the start of the posterior post-fixative processes. In cases where perfusion of the tissue was not completed successfully, brains were stored in 4% PFA O/N and then transferred to 0.1% PFA. This protocol was taken into account if tissue presented an inappropriate state of hardness in order to be posteriorly embedded into paraffin blocks.

Afterwards, neural tissue was embedded in Formalin O/W in order to post-fixate the neural tissue. Then, brain tissue was embedded in paraffin blocks using an embedding workstation (Epredia HistoStar Embedding Workstation, Thermo Fisher Scientific) and stored at room temperature until the following microtomy processes. All the post-fixative as well as blocking processes were performed in cooperation with the Unfallkrankenhaus Berlin Institut für Pathologie.

2.9. PREPARATION OF HISTOLOGICAL SLICES

After paraffin embedding, microscope slides (Microscope slides Corners cut, Carl Roth GmbH, Germany) were coated manually following an immersion protocol consisting of sequential baths of 99% Ethanol (1x, 20sec, RT), H_2O dest. (1x, 20sec, RT) and 1% Gelatin coating solution (1x, 20sec, RT) (Gelatine, extra pure, gold, 180 Bloom, Carl Roth GmbH, Germany) due to its adhesive properties for holding brain slices on the slide. Coated microscope slides were dried out at RT for at least two days before being used in following microtomy procedures.

Neural tissue was sectioned in 5-µm-thick slices in the frontal plane using a rotation microtome (Rotationsmikrotom Microm HM 325, Thermo Fisher Scientific). The sectioning of the brain tissue was performed from the beginning of the CN (Bregma, -6.48 mm; Interaural, -2.68 mm) until the end of the vMGB (Bregma, -2.80 mm; Interaural, 1.00 mm). This procedure was carried out following the histological mouse brain atlas by Paxinos and Franklin (Paxinos & Franklin, 2001). The collected slices were placed in cold water. Then, they were organized and mounted into microscope slides following a detailed procedure (see Figure 9). When properly mounted, microscope slides were carefully immersed into a hot water bath (Medax WB 24, Labexchange GmbH, Germany) kept at between 50-52 °C using a temperature probe (USPS-600, Voltcraft GmbH, Germany) in order to stretch the tissue. Finally, all mounted microscope slides

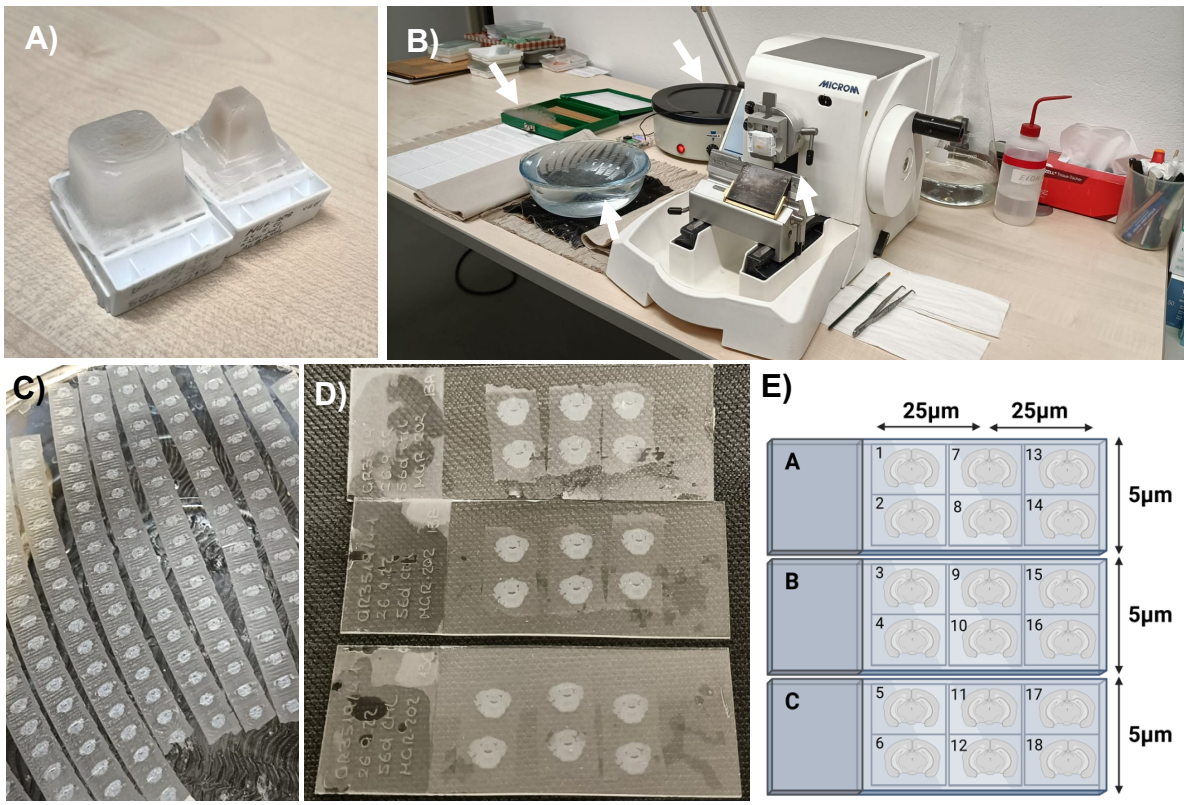

Figure 9. Histological preparation. A) Paraffin blocking: brains were embedded in paraffin after post-fixation in formalin. B)-E) Microtomy setup: brains embedded in paraffin blocks were sectioned in slices of 5 µm thickness using a rotation microtome. The obtained sections were mounted into microscope slides following sequential cold and hot baths, and were stored in microscope slide boxes at RT. *(E) Illustrated with Biorender.com*

were collected into microscope slide boxes (Microscope slide box ROTILABO, Carl Roth GmbH, Germany) and were kept at RT until the subsequent histological procedures. The cutting angle of the brain tissue was constantly checked during the whole duration of the microtomy procedure by visual inspection as well as under the microscope (Zeiss Axio Lab.A1, Carl Zeiss Microscopy GmbH, Germany).

2.10. FLUORESCENCE IMMUNOHISTOCHEMISTRY (FIHC)

After microtomy procedures were carried out, FIHC techniques were performed directly on top of each microscope slide containing paraffin-embedded mounted tissue sections. Therefore, two microscope slides were selected from each experimental subject: The first one contained regions of the CIC; the second one contained regions of the MGV. During each staining session, microscope slides belonging to 12 experimental subjects (115 dB: $n = 4$; 90 dB: $n = 4$; Ctrl: $n = 4$) included in only one experimental time point were stained at the same time. In other words, experimental subjects included in different experimental time points were stained on different sessions performed on different experimental days. Nevertheless, microscope slides belonging to

experimental subjects included in one experimental time point were not stained with more than two days of difference, and the usage of the same reagents was ensured as much as possible between staining experiments in order to avoid reagent quality interferences.

The selection of the region of interest (ROI) was performed taking into account the anatomical location of the CIC and MGV, and the objective of each experiment. Then, depending on the objective of the experiment being performed, slightly different neural regions were selected:

1. Experiment 1: Neurodegeneration analysis
    i. CIC: Bregma from -5.02 mm to -4.96 mm, Interaural from -1.22 mm to -1.16 mm
    ii. MGV: Bregma from -3.28 mm to -3.16 mm, Interaural from -0.52 mm to -0.16 mm
2. Experiment 2: Neuroconnectivity analysis
    i. CIC: Bregma from -5.20 mm to -5.02 mm, Interaural from -1.40 mm to -1.22 mm
    ii. MGV: Bregma from -3.40 mm to -3.28 mm, Interaural from -0.40 mm to -0.52 mm
3. Experiment 3: Neurotransmission analysis
    i. CIC: Bregma from -5.02 mm to -4.96 mm, Interaural from -1.22 mm to -1.16 mm
    ii. MGV: Bregma from -3.16 mm to -3.08 mm, Interaural from -0.64 mm to -0.72 mm

This protocol was applied because during the performance of the neuroconnectivity analysis (Experiment 2), more rigorous area selection criteria were needed in order to accurately target the projections of interest in the present study. Areas of interest were selected using image data from neurotracing experiments derived from the anatomical mouse brain connectivity atlas of the Allen Institute (Experiment 304857992 – IC) (Kuan et al., 2015) (see Figure 10). Combining the data derived from the Allen mouse brain connectivity atlas and the mouse brain atlas from Paxinos and Franklin (Kuan et al., 2015; Paxinos & Franklin, 2001), it was revealed that major neurofilament density from travelling fibers of the BIC could be found in the CIC between Bregma from -5.20 mm to -5.02 mm, and in the MGV between Bregma from -3.40 mm to -3.28 mm. This procedure was carried out in order to minimize the effect of heterogenic distribution of neurofilament density across the CIC and MGV. Then, microscope slides including sections from these areas were selected to undergo neuroconnectivity analysis. Subsequently, different microscope slides containing different CIC and MGV sections were included into the neurodegeneration and neurotransmission analysis. Finally, microscope slides containing a high degree of histological artifacts were not selected to undergo staining procedures.

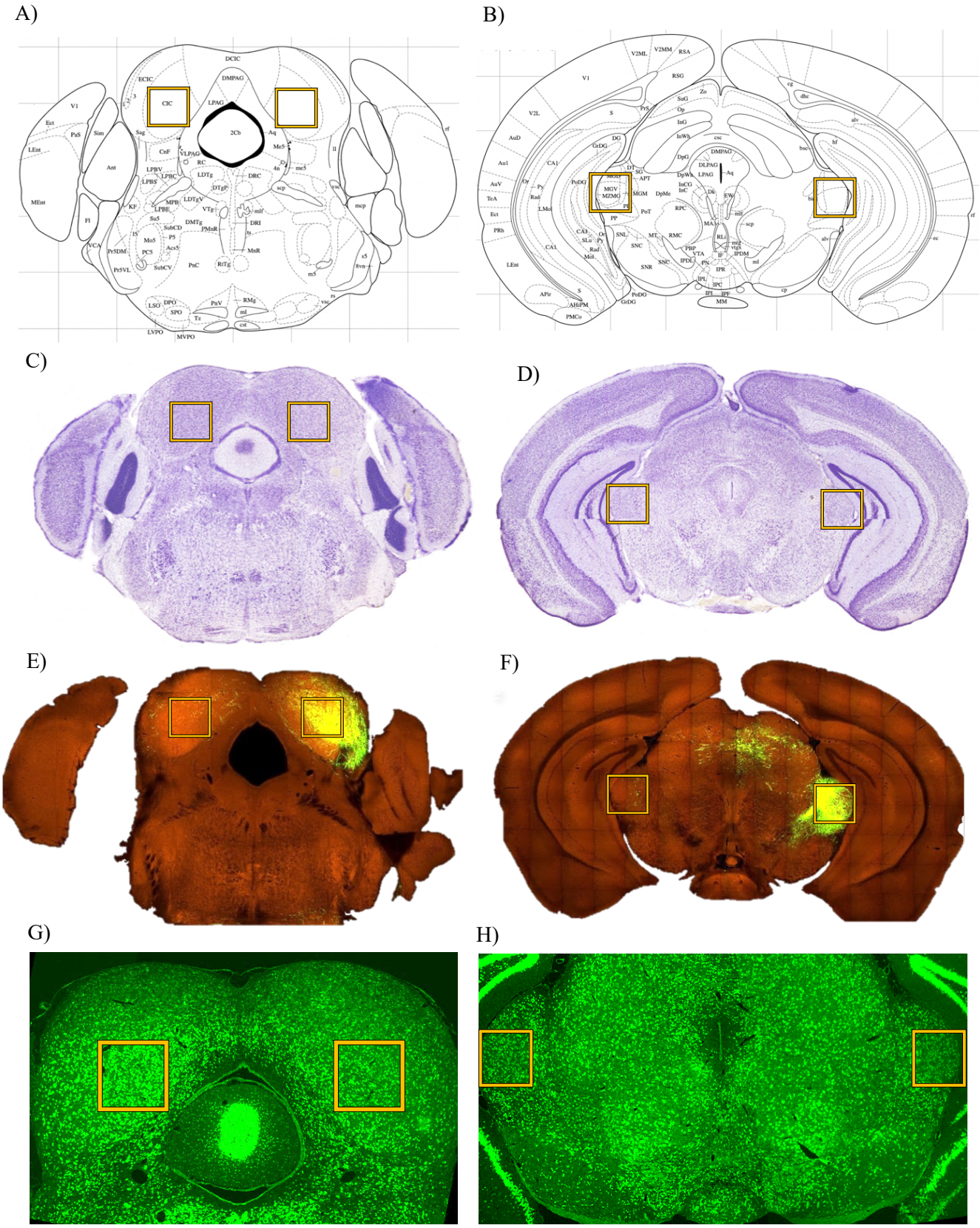

Figure 10. ROI selection. (A-D) Anatomical study of the CIC and MGV using Paxinos & Franklin mouse brain atlas. (E-F) Anatomical study of the brachium of the inferior colliculus was performed. Axonal bundles travelling from the CIC to the MGV were studied using image data derived from the anatomical Allen mouse brain connectivity atlas (Experiment 304857992 – IC). (G-H) Representative images from Neuronal Nuclei protein (NeuN) stainings in which CIC (G) and MGV (H) sections could be observed. Those areas were selected for posterior image analysis and data acquisition. *Source: Kuan et al., 2015 (E-F).*

2.10.1. Deparaffination and hydration

Deparaffinization and hydration steps were performed in order to remove the paraffin that had penetrated into tissue. First, mounted brain slices were embedded in Roti Histol organic solvent (Roti Histol, Roth, Germany) (1x, 10 min, RT). Subsequently, the Roti Histol was removed, and the brain slices were hydrated using sequential baths of descending alcohol concentrations of 90% (1x, 5 min, RT), 80% (1x, 5 min, RT) and 70% (1x, 5 min, RT) and a final wash with 1x PBS (1x, 5 min, RT) (PBS, Gibco, USA). The quality of the process was ensured by observing the whiten of the brain slices when they were transferred from xylene to ethanol (see Figure 11).

2.10.2. Heat-induced epitope retrieval for immunofluorescence (HIER-IFA) protocol

To prevent the loss of antigenicity that can occur with some epitopes in formalin-fixed and paraffin-embedded tissues, an epitope or antigen retrieval procedure was carried out. The Heat Induced Epitope Retrieval for immunofluorescence protocol (HIER-IFA) protocol was performed (see Figure 11). Microscope slides were incubated in 100ml of 10 mM Sodium HIER Citrate Buffer (10X, pH 6.0, Biozol, Germany) inside slide containers. Then, sections were carefully placed and heated inside a high-pressure cooker (Pressure Cooker, RC-HPC6L, Royal Catering Inc. Poland) filled with approximately 500 ml of dest. water. Subsequently, samples were cooked for 5 minutes, and hot water steam pressure was removed from the high-pressure cooker. Afterwards, containers with embedded microscope slides were partially immersed in a tray with cool running tap water for 25 minutes in order to cool down the microscope slides. Finally, samples were washed and incubated in 1x PBS prior to the blocking step.

2.10.3. Blocking

In order to avoid non-specific binding of the antibodies, a blocking step using Normal Goat Serum (NGS) was carried out (see Figure 11 and 12). To carry out this step, two mounted microscope slides were partially dried from PBS, and sections were delineated with hydrophobic red liquid barrier marker (RotiLiquid, Roth, Germany) using a painting brush. This procedure was done in order to contain the blocking and/or incubation solution within this region and ensure humidified conditions during subsequent blocking and antibody incubation steps. Afterwards, 300 µl of blocking solution (5% Normal Goat Serum (NGS) in 0.3% Tritonx100 in 1x PBS) were incubated in each slide for 30 minutes at RT inside humid chambers, ensuring all brain slices were

fully covered with blocking solution and properly humidified. In addition, individual sections were delineated with hydrophobic liquid marker for performing negative control staining on top. This was performed in order to ensure the specificity and accuracy of the staining procedure. In these sections, 50 µl of the same blocking solution was applied.

2.10.4. Primary Antibody Incubation

After blocking, primary antibody incubation was performed. Different primary antibody incubation solutions were prepared and are described as follows.

For experiment 1, primary antibody incubation solution was prepared using NeuN (D3S3I) Rabbit mAb primary anti-NeuN antibody (Cell Signaling Technology, Inc) diluted 1:100 in 1% NGS, 0.3% Tx100 and 1x PBS incubation solution. The Neuronal Nuclear protein or NeuN is localized specifically in the nuclei and perinuclear cytoplasm of postmitotic neurons, and it has been extensively used in order to study the neuronal differentiation and functional as well as pathological state of neurons for more than 20 years (Gusel'nikova & Korzhevskiy, 2015; Mullen et al., 1992). Labelling against NeuN was used in order to precisely assess neuronal cell density changes as a consequence of acute noise exposure, whereas DAPI labelling was used in order to study cell density changes without discriminating between cell types. Different cell types including neurons and glial cell types (such as astrocytes or microglial cells) are expected to be labelled by DAPI.

For experiment 2, primary antibody incubation solution was prepared using purified mouse SMI312 anti-neurofilament marker antibody (pan axonal, cocktail) (Biolegend, Inc.) diluted 1:1000 in 1% NGS, 0.3% Tx100 and 1x PBS incubation solution. SMI312 is a mixture of monoclonal antibodies directed against phosphorylated epitopes on neurofilaments medium (NF-M) and neurofilaments heavy (NF-H). During the present study, SMI312 neurofilament marker was used with the aim to assess neurofilament density changes as a consequence of acute noise exposure.

For experiment 3, a primary antibody solution combining three different primary antibodies diluted 1:500 in 1% NGS and 0.3% Tx100 and 1x PBS incubation solution was prepared: polyclonal chicken antibody SySy 135 316 against VGLUT1 (Synaptic Systems, Inc.); polyclonal guinea pig antibody SySy 135 404 against VGLUT2 (Synaptic Systems, Inc.), and polyclonal rabbit antibody SySy 131 002 against VGAT (Synaptic Systems, Inc.). Vesicular glutamate transporter 1 (VGLUT1) and Vesicular glutamate transporter 2 (VGLUT2). In the

current study, fluorescence immunohistochemistry against vesicular glutamate and GABA transporters was used in order to study glutamatergic and GABAergic neurotransmission imbalances in the CNS as a consequence of NIHL.

Therefore, blocking solution was carefully removed, and microscope slides were slightly dried out with filter paper. Afterwards, microscope slides were placed horizontally inside the humid chamber and 300 µl of primary antibody incubation solution were applied for each microscope slide, ensuring all sections were fully covered and humidified. Then, humid chambers were sealed with Parafilm (Parafilm M, Laborbedarf Inc.) in order to ensure long-term humidified conditions. Finally, humid chambers with incubated microscope slides were carefully transported from the bench to the fridge and samples were incubated for 24h O/N at 4°C. It is important to highlight that no primary antibody solution was added to those slices in which a negative control staining was performed. Those slices were incubated O/N in only 50 µl of 1% NGS, 0.3% Tritonx100 and 1x PBS in order to induce negative signaling. Primary antibody incubation procedures can be seen in Figures 11 and 12.

2.10.5. Secondary Antibody Incubation

On the second day, humid chambers were carefully transported from the fridge to the bench and parafilm sealing was removed. Primary antibody incubation solution was dried out from the microscope slides and three washing steps of 10 minutes in 1x PBS at RT were performed in agitation in order to remove unspecific primary antibody bindings. During these washing steps, secondary antibody solutions were prepared for the subsequent steps.

For experiment 1, secondary antibody incubation was prepared using Invitrogen Goat anti-Rabbit IgG (H+L) Cross-Adsorbed secondary antibody, Alexa Fluor 488 (Thermo Fisher Scientific, Inc., USA) diluted 1:250 in 1% NGS, 0.3% Tx100 and 1x PBS incubation solution. For experiment 2, secondary antibody incubation was prepared using Invitrogen Goat anti-mouse IgG (H+L) Cross-Adsorbed secondary antibody, Alexa Fluor 488 (Thermo Fisher Scientific, Inc., USA) diluted 1:250 in 1% NGS, 0.3% Tx100 and 1x PBS incubation solution. For experiment 3, a cocktail of three different secondary antibodies diluted 1:500 in 1% NGS and 0.3% Tx100 in 1x PBS incubation solution was prepared: Invitrogen Goat anti-chicken IgY (H+L) Secondary Antibody, Alexa Fluor 647 (Thermo Fisher Scientific, Inc., USA); Invitrogen Goat anti-Guinea Pig IgG (H+L) Secondary Antibody, Alexa Fluor 546 (Thermo Fisher Scientific, Inc., USA); Invitrogen Goat anti-Rabbit IgG (H+L) Cross-Adsorbed secondary antibody, Invitrogen Alexa Fluor 488 (Thermo Fisher Scientific, Inc., USA).

After the washing steps were finished, microscope slides were slightly dried out with the remaining PBS solution and carefully placed inside the humid chambers. Afterwards, 300 µl of secondary antibody incubation solution was applied on top of each microscope slide for 1h at RT in dark conditions. During the secondary antibody incubation, all slices in which a negative control was performed were equally incubated with the same secondary antibody solutions as the ones used for performing positive staining. Secondary antibody incubation procedures are described in Figures 11 and 12.

2.10.6. DAPI Incubation

In addition, 4′,6-diamidino-2-phenylindole (DAPI) labelling was performed. DAPI is a blue-fluorescent DNA stain commonly used as a nuclear stain in fluorescence microscopy due to its strong binding to adenine–thymine-rich regions of dsDNA. In the present study, DAPI staining procedures were carried out in order to analyze total cell density changes as a consequence of NIHL.

After the secondary antibody incubation was finished, the secondary antibody incubation solution was carefully dried out from the microscope slides and sections were rinsed three times in 1x PBS (10 min, RT, dark). Subsequently, each microscope slide was incubated with 300 µl of DAPI 300µM in 1x PBS solution during 5 min at RT in dark conditions (4',6-Diamidino-2-phenylindole, Dihydrochloride, D1306, Thermo Fisher Scientific, Inc., USA). At the end, the DAPI incubation solution was removed from the microscope slides and three 1x PBS washing steps of 10 minutes at RT were performed in order to remove remaining DAPI solution. Finally, microscope slides were immersed into slide containers filled with 1xPBS until coverslipping. Negative control slices were also incubated in DAPI incubation solution (see Figure 11).

2.10.7. Coverslipping and sealing

Next, sections were carefully dried out from 1xPBS using filter paper. Then, red liquid barrier marker was removed with a scalpel in order to ensure proper coverslipping procedures, and stained microscope slides were mounted in Roti Mount FluorCare mounting media (ROTI®Mount FluorCare, Carl Roth GmbH & Co.). Then, brain slices were covered with coverslips (Deckgläser 24x60, H878, Carl Roth GmbH & Co.) and placed horizontally O/N at 4 °C inside microscope slide boxes in order to ensure proper distribution of mounting media across the microscope slide. Finally, between 1 and 3 days after coverslipping procedures were performed, coverslips were sealed with nail polish (Nagellack Superstay Forever Strong 7 Days 25, Maybelline Inc., USA) in

order to avoid penetration of any solution and tissue drying inside the microscope slides. The sealed microscope slides remained at 4 °C in dark conditions until posterior image acquisition.

Figure 11. Fluorescence immunohistochemistry (FIHC) incubation: Blocking, primary, secondary and/or DAPI solutions were incubated on top of the mounted object slides (surrounded by hydrophobic barrier) inside microscope slide boxes. Boxes were filled with dest. H_2O and paper towels to produce humid chambers. This procedure was carried out in order to ensure continuous humidified conditions and avoid drying of the object slides. Blocking solution incubation was performed at RT for 30 minutes. Subsequently, primary antibody incubation was performed and humid chamber boxes were sealed with Parafilm and carefully moved to the fridge. Primary antibody incubation was carried out inside the fridge at 4 °C O/N. Secondary (2h) and DAPI (5 min) incubation were performed on the same humid chambers at RT under dark conditions. Washing steps were performed using microscope slide containers filled with 1x PBS.

2.11. IMAGE ACQUISITION

16-bit microphotographs of the CIC and MGV were acquired under an optic fluorescence microscope Nikon Widefield Ti2 system equipped with a digital camera (PCO.edge camera (>80% QE, 2048x2048 pixels, 6.5 µm pixel size, 53 fps full frame, up to 500 fps in small area)) using the Widefield EPI fluorescence imaging mode. The system was provided by the Advanced Biomedical Core Imaging Facility of the Charité Universitätsmedizin Berlin (Figure 12). Depending on the experiment, different settings were taken into account.

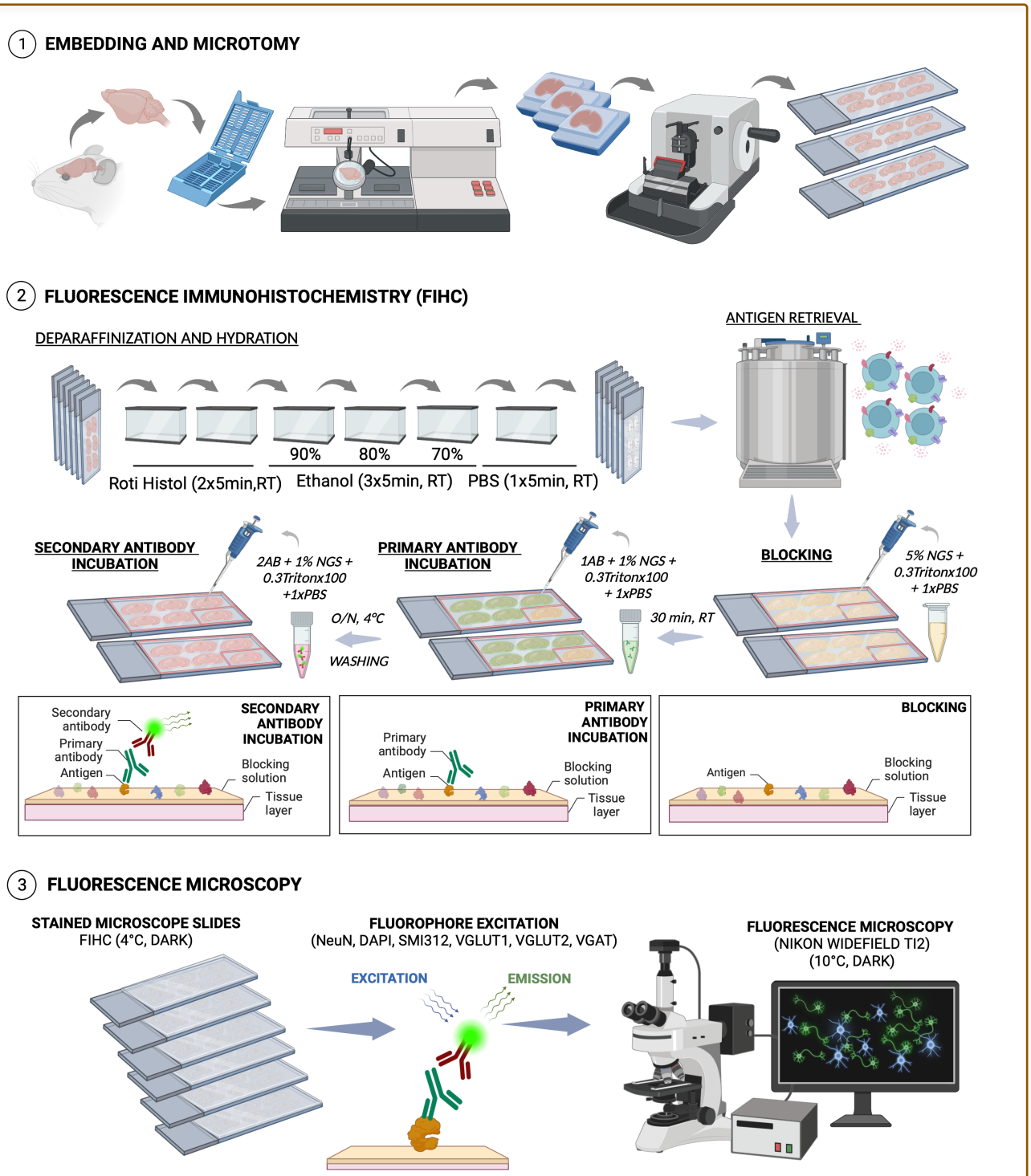

Figure 12. Histology overview**:** Brains were perfused with 4% PFA, dissected from the skull and embedded in paraffin. Then, brains were sectioned in 5 µm thickness using a rotation microtome, and slices were mounted into microscope slides. Fluorescence immunohistochemistry (FIHC) procedures were performed. First, object slides were deparaffinized and hydrated in order to remove paraffin embeddings using sequential baths of Roti Histol Xylene solution (2 x 5 min, RT), Ethanol (90%, 5 min, RT; 80%, 5 min, RT; and 70% 5 min, RT) and 1xPBS (1 x 5 min, RT). Then, heat-induced epitope retrieval for immunofluorescence (HIER-IFA) for unmasking antigens of interest was performed, and slices were incubated for 30 min at RT in blocking solution (5% NGS + 0.3% Tritonx100 + 1x PBS) in order to avoid unspecific antibody bindings. Brain slices were delineated with hydrophobic liquid barrier in order to contain the solutions and perform FIHC directly on top of the object slides. Subsequently, samples were incubated O/N (4 °C) in primary antibody solution (1AB + 1% NGS + 0.3% Tritonx100 + 1xPBS) in order to recognize the antigen of interest. On the second day, microscope slides were washed in 1xPBS and secondary antibody solution was applied for 1h at RT in dark conditions (2AB + 1%NGS + 0.3% Tritonx100 + 1xPBS). Slices were washed in 1x PBS and were incubated for 5 min in DAPI solution (300 µM, 1:1000). Finally, slices were coverslipped using RotiMount Fluorcare as the fluorescence preserving solution. Samples were stored in the dark at 4 °C until posterior fluorescence microscopy imaging techniques were performed under a Nikon Widefield Ti2 system. Illustrated with Biorender.com.

For experiment 1, a Plan Apo air objective with 20x magnification was used. The field of view (FOV) for this magnification was set at 664.54 µm x 663.30 µm. DAPI positive ($DAPI^+$) cells were detected in the first channel using an excitation/emission spectrum of 358/461 nm. NeuN positive ($NeuN^+$) cells were detected on the second channel using an excitation/emission spectrum of 499/520 nm. Images from negative control staining were also acquired in order to confirm positive staining presence.

For experiment 2, a Plan Apo air objective with 40x magnification was used. The FOV was set at 336.16 µm x 335.20 µm. DAPI positive ($DAPI^+$) cells were detected on the first channel, using an excitation/emission spectrum of 358/461 nm. SMI312 positive ($SMI312^+$) staining was detected on the second channel using an excitation/emission spectrum of 499/520 nm. Images from negative control staining were also acquired in order to perform background subtraction methods during fluorescence intensity quantification.

For experiment 3, a Plan Apo air objective with 40x magnification was used. The FOV was set at 336.16 µm x 335.20 µm. DAPI positive ($DAPI^+$) cells were detected on the first channel, using an excitation/emission spectrum of 358/461 nm. VGAT positive ($VGAT^+$) staining signal was acquired on the second channel using an excitation/emission spectrum of 499/520 nm. VGLUT2 positive ($VGLUT2^+$) staining signal was acquired on the third channel using an excitation/emission spectrum of 561/572 nm. VGAT positive ($VGLUT1^+$) staining signal was acquired on the fourth channel using an excitation/emission spectrum of 650/671 nm. Images from negative control staining from channel 2, channel 3 and channel 4 were also acquired in order to perform background subtraction methods during fluorescence intensity quantification for each of the vesicular neurotransmitter stainings performed.

During the acquisition, some considerations were taken into account to ensure the reliability and robustness of the method. First, microscope slides that were stained at the same time during one staining experiment were also imaged during one single imaging session in order to minimize fluorescence intensity differences between simultaneously stained samples due to the fading of fluorescent dyes. For that reason, simultaneously stained samples were kept in the dark at 4 °C from right after the sealing procedure until the subsequent day of imaging, which took place no longer than 1 week after fluorescence immunohistochemistry procedures were performed. Imaging sessions were always performed in dark conditions to avoid bleaching of the fluorescent dyes. Furthermore, images from representative experimental subjects from all conditions included in the study (115 dB, 90 dB and Ctrl) were acquired within each single imaging session in order

to minimize differences between our experimental treatments due to fluorescent fading. Moreover, all the images were acquired using the same settings and protocols for each experiment included into the study design as follows. Furthermore, in order to reduce bias in our data, all experimental subjects were treated equally during the image acquisition methodology. Finally, up to 12 images were acquired for each auditory brain region (CIC and vMGB) and for each experimental subject. Microphotographs from both hemispheres of each of the 6 slices mounted in each microscope slide were also acquired. Moreover, it is important to highlight that the number of images acquired depended on the presence of histological artifacts coming from previous histological procedures. Thus, all the sections and images that contained histological artifacts that potentially influenced data analysis were excluded from the study. Finally, images were taken under one single focal plane. Representative images from all histological procedures can be seen in Figure 13.

2.12. IMAGE ANALYSIS

Image analysis was performed using automated Image J macros developed in collaboration with the Advanced Biomedical Core Imaging facility of the Charité Universitätsmedizin Berlin. Hence, different image analysis approaches were taken into account.

2.12.1. Automated cell counting

During the neurodegeneration analysis, automated cell counting was performed in order to observe differences in cell ($DAPI^{+)}$ and neuronal ($NeuN^+/DAPI^+$) density. First, The $DAPI^+$ (Channel 1) and $NeuN^+$ (Channel 2) signal of fluorescently labelled neurons was segmented via machine learning by using cellpose. The image intensities were first normalized between the 1st and 99th intensity percentile, before using the ‘nuclei’ and ‘cyto’ model of cellpose for the segmentation of the $DAPI^+$ and $NeuN^+$ signal, respectively. Subsequently, the number of cells was counted for the first channel ($DAPI^+$ cells) and for the second channel ($NeuN^+$ cells), and cells expressing both NeuN and DAPI ($NeuN^+/DAPI^+$) were segmented by overlapping fluorescent intensities from both acquired channels. All processing steps were implemented into a custom python script for performing automated cell counting procedures.

Additionally, a quality assessment of the outcome of the raw data obtained from the automatic cell counting macro was performed. This procedure consisted of a comparison between the cell density values obtained through manual cell counting by visual inspection and those obtained by the automatic cell counting method. This procedure was performed for all images collected for the CIC region from 6 experimental subjects from the 115 dB group and from 6

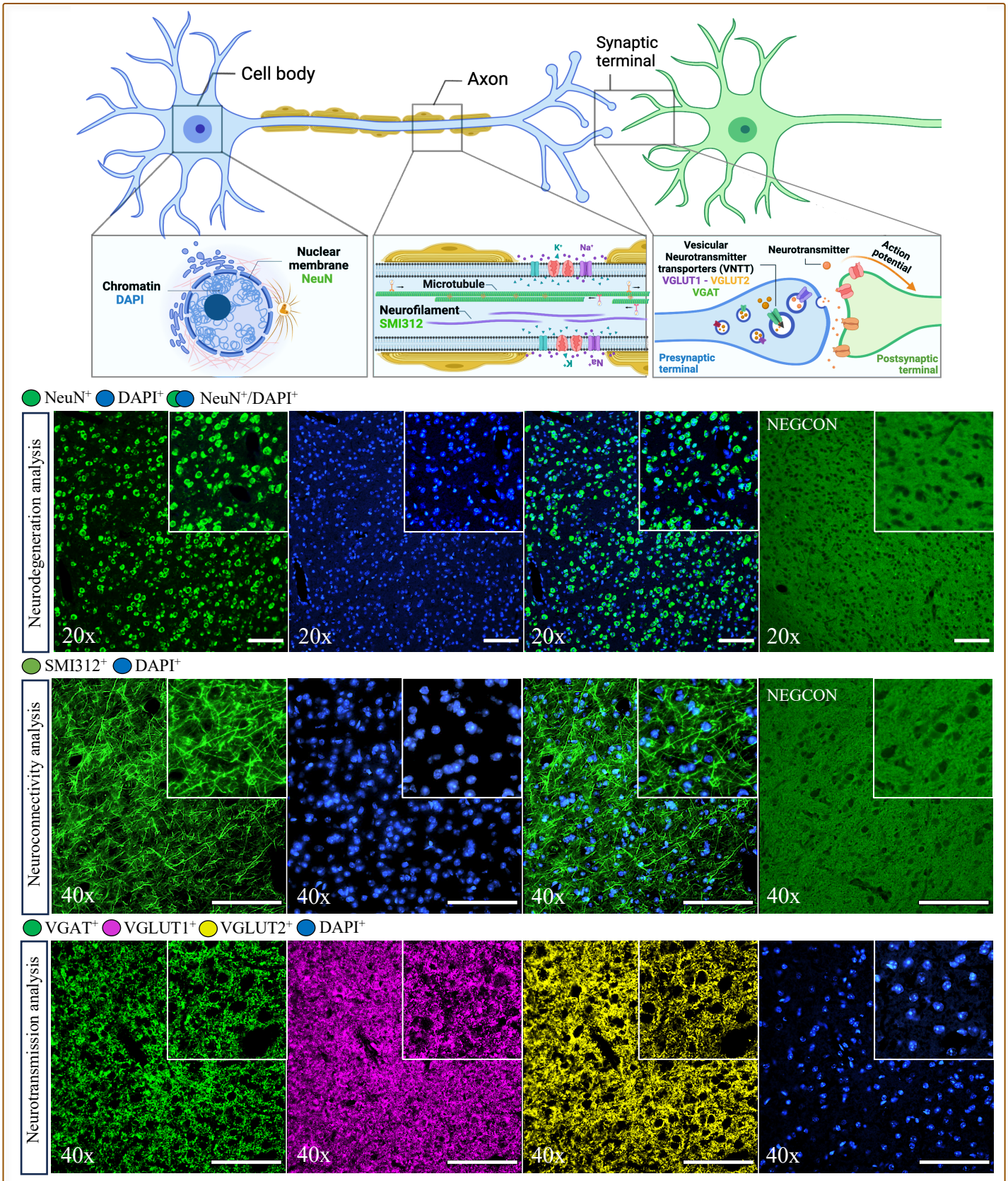

Figure 13. Fluorescence immunohistochemistry labeling: FIHC techniques were performed in order to label different structures within the neuronal cytoarchitecture (soma, axon and synaptic terminals). Fluorescence microphotographs were acquired under a Nikon Widefield Ti2 system. FIHC against NeuN (nuclei) & DAPI (Chromatin) was performed in order to study neurodegenerative changes, and two-channel images were acquired under a 20x magnification. FIHC against SMI312 (Neurofilament) and DAPI (Chromatin) was performed with the aim to assess changes in axonal density. Two-channel images were acquired under a 40x magnification. Finally, FIHC against VGAT, VGLUT1, VGLUT2 (VNTT) and DAPI was carried out in order to assess changes in vesicular GABA (VGAT) and glutamate (VGLUT1, VGLUT2) neurotransmitter transporters. Negative control (NEGCON) stainings were carried out as a quality control. No primary antibody solution was incubated when performing NEGCON stainings. *Scale bar: 100 µm. Illustrated with Biorender.com*

experimental subjects from the Ctrl groups. Next, manual cell counting was performed using the Image J Cell Counter plug-in, and the cell density for $DAPI^+$ cells (Channel 1) and cell density for $NeuN^+/DAPI^+$ (Channel 1 + 2) were counted separately. Finally, a correlation analysis between the automatic and manual cell counting methods was performed using Pearson correlation tests and Bland-Altman plots (Giavarina, 2014) (see Figure 16).

Additionally, $DAPI^+$ and $NeuN^+/DAPI^+$ density values were obtained for each image acquired from each of the experimental subjects included in the study, and an average of $DAPI^+$ and $NeuN^+/DAPI^+$ cell counting was calculated for each entire subject. Then, the total $DAPI^+$ and values previously calculated for each experimental subject were included into the respective experimental group. Finally, total average values were compared between noise exposure treatments included within one experimental time point (i.e., 1d: 115 dB vs. 90 dB vs. Ctrl). Results are given in cell counts/area (Mean ± Standard deviation).

2.12.2. Fluorescence Intensity Analysis: Corrected Total Cell Fluorescence (CTCF)

With the aim to assess the relative protein expression levels of SMI312, VGLUT1, VGLUT2 and VGAT, the Corrected Total Cell Fluorescence intensity (CTCF) in our samples was calculated using a custom Fiji macro following background subtraction calculations, which are described below. This procedure was performed in order to capture fluorescence intensity (FI) differences across our experimental groups coming from changes in protein expression.

Furthermore, this methodology was applied in order to obtain background-independent fluorescent readings, as differences in the background level can occur between different staining procedures and between investigated experimental conditions. Additionally, different auditory areas might also differ in background values due to differences in the autofluorescence baseline level. Hence, the average pixel intensity or "Mean" value was measured using a Fiji macro from loaded image sets containing both positively-stained and negatively-stained (negative control) samples. Taking into account that the FOV size (or area) was kept constant during acquisition, the following formula was applied in order to subtract the background from collected images:

$$Corrected\ Total\ Cell\ Fluorescence\ (CTCF) = Mean_{signal} - Mean_{background}$$

$Mean_{signal}$ refers to the "Mean" FI values measured from images obtained from positively-stained samples. $Mean_{background}$ refers to the average of all "Mean" values measured from all negatively-stained samples performed for each auditory area (IC and MGB) and for each staining

experiment. Thus, it is important to highlight that different $Mean_{background}$ values were calculated from negatively-stained slices for each staining session and for each auditory brain region (CIC and MGV) separately in order to reduce methodological and/or biological differences in FI due to the previously discussed reasons. Furthermore, "Mean" values coming from ImageJ were selected by "Integrated density" values in order to perform CTCF calculations. This decision was taken assuming that the FI intensity in our images had a homogeneous distribution. Finally, during the course of the experiments, it was observed that some overflow of primary and secondary antibody solution could happened in the negative control sections of the microscope slides, even if they were surrounded by hydrophobic liquid barrier. For these reasons, negative control stainings presenting any sign of positive signal were removed from the present study in order to avoid methodological artifacts during image analysis. Image analysis procedures described in the current sections are summarized in Figure 14.

Next, single $SMI312_{CTCF}$, VGLUT1 $_{CTCF}$, VGLUT2 $_{CTCF}$ and VGAT $_{CTCF}$ values were obtained for each image acquired. Then, all intensity values for each experimental subject were averaged in order to calculate an individual value for each respective experimental subject. Finally, a total intensity value was calculated for the entire experimental group, averaging individual intensity values obtained for each experimental subject included in the corresponding group. Those values were compared between experimental treatments within one experimental time point as previously described in the last sections. Results are given in Mean Fluorescence Intensity ($SMI312_{CTCF,}$ VGLUT1 $_{CTCF}$, VGLUT2 $_{CTCF}$ and VGAT $_{CTCF}$) levels (Mean ± Standard deviation).

2.12.3. Fluorescence Intensity Measurements: Quality Assessment

Additionally, it is well known that many variables can affect the performance of quantitative FI analysis (photobleaching, phototoxicity, temperature, differential fluorophore excitation, etc.) (Waters, 2009). These variables might vary differently between different staining sessions, leading to differences in the results observed. Therefore, a quality assessment was performed in order to assess the accuracy of the previously described FI analysis.

This quality assessment was carried out by staining different mounted microscope slides from the CIC and the MGV from the same experimental subject on different experimental days. Thus, two experimental subjects from each experimental treatment included into the 7d time point were investigated. In those subjects, an SMI312 staining was performed under similar conditions on two different staining sessions, which were performed on different days: Staining day 1 (D1) and Staining day 2 (D2). Then, FI (Mean $SMI312_{CTCF}$) and variability (Standard Deviation)

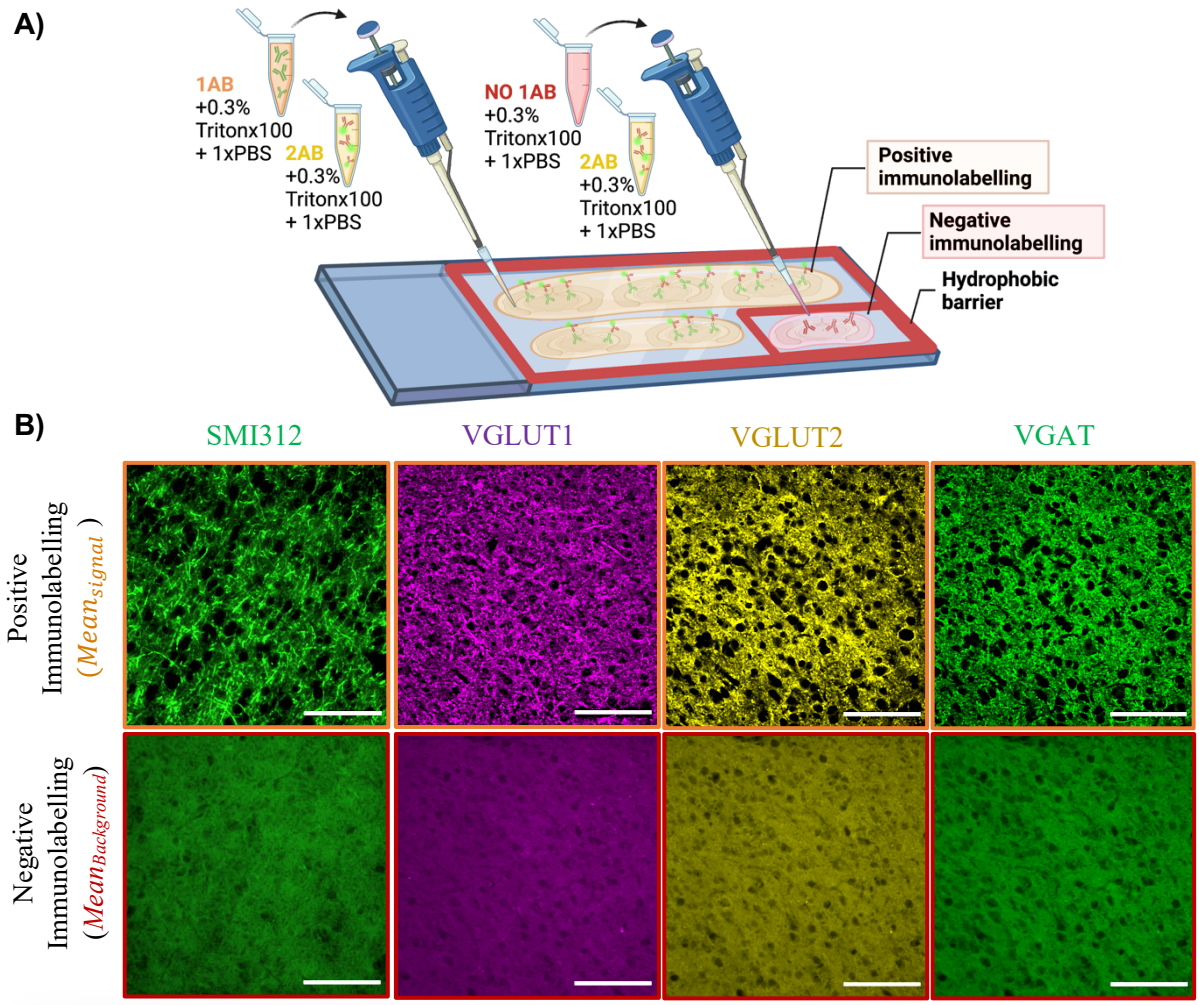

Figure 14: Image analysis workflow: (A) Performance of positive and negative immunolabelling (negative control). Negative control labelling was achieved by removing the primary antibody from the primary antibody incubation solution. Negative and Positive immunolabelling was performed on the same microscope slide. However, negative immunolabelling was separated from positive immunolabelling using a hydrophobic liquid barrier, and mixture of both solutions was avoided. (B) Relative protein quantification was performed using Fluorescence Intensity (FI) measurements of SMI312, VGLUT1, VGLUT2 and VGAT immunolabelling. The Mean FI intensity was calculated for each entire image acquired using a custom Fiji macro. Corrected Total Cell Fluorescence (CTCF) values were then assessed in order to perform background subtraction. CTCF values were calculated by subtracting the Mean FI values calculated from positively-stained ($Mean_{signal}$) (orange) slices from the Mean FI values calculated from negatively-stained ($Mean_{background}$) (red) slices. *Scale Bar: 100µM; (A) Illustrated with Biorender.com.*

measurements obtained for each experimental subject between each experimental day were qualitatively compared.

2.13. STATISTICS

This study has a mixed design. In the major part of the study, a between-subject design with 4 groups (experimental time point: 1d, 7d, 56d, 84d) for 3 treatments (115 dB, 90 dB, and

Ctrl), with 3 within-subject levels (Cell and neuronal density; axonal density; and glutamatergic and GABAergic vesicular neurotransmitter density) was established. Each of the hypotheses were tested separately for each auditory CNS area of interest (CIC and MGV). Since the primary objective of the current study was to track the pathological effects of various noise exposure conditions at 4 time points, the resulting data was compared between the experimental groups or treatments (115 dB, 90 dB and Ctrl) for each brain region within each experimental time point (1d, 7d, 56d and 84d). Moreover, statistical comparisons between experimental time points for each experimental treatment were not taken into account in the present study in order to avoid differences as a consequence of aging. The dependent variables were neuronal ($NeuN^+/DAPI^+$) and cell ($DAPI^+$) density in the CIC and MGV for experiment 1; axonal density (SMI312 fluorescence intensity ($SMI312_{CTCF}$)) in the CIC and MGV for experiment 2; and glutamatergic (VGLUT1 fluorescence intensity ($VGLUT1_{CTCF}$) and VGLUT2 fluorescence intensity ($VGLUT2_{CTCF}$)) and GABAergic vesicular neurotransmitter transporter density (VGAT fluorescence intensity ($VGAT_{CTCF}$)) in the CIC and MGV for experiment 3. The resulting means of the experimental groups were compared using one-way ANOVA and the Bonferroni post-hoc test was applied to account for multiple comparisons, as homogeneity of variances in the data was assumed. In cases where homogeneity of variances was not given, Welch's ANOVA followed by the Games-Howell post-hoc multiple comparisons test were performed. Taking into account the sample size collected and the robustness of the previously described statistical analysis against the normality assumption, violations of normality in data distribution were not taken into account in the present study. Additionally, t-tests for independent samples, Bland-Altman plots and linear regression analysis were performed in order to observe statistical correlation between automatic and manual cell counting. The software SPSS (version 29.0.0.0. (241); IBM SPSS Statistics) was used for all statistical analyses and the significance level for all statistical tests was set at $p \leq 0.05$.

03 RESULTS

3.1. AUDITORY BRAINSTEM RESPONSE (ABR)

Within each time point, auditory threshold shifts were significantly elevated after 7 days post-exposure in the 115 dB group (n = 8) when compared to both 90 dB ($p \leq 0.001$ for all tested frequencies (4, 8, 16, 32 kHz); n = 8) and Ctrl groups ($p \leq 0.001$ for all tested frequencies; n = 8). Furthermore, elevated threshold shifts in the 115 dB group ($p \leq 0.001$ for all tested frequencies; n = 8/time point) when compared to the 90 dB ($p \leq 0.001$ for all tested frequencies; n = 8/time point) and Ctrl groups ($p \leq 0.05$ for all tested frequencies; n = 8/time point) groups, were also observed 56 days and 84 days post-exposure. Threshold shift within the investigated frequencies ranged between 50- and 70-dB SPL in the 115 dB group, whereas a minimal threshold shift between 5- and 10-dB SPL could be observed in the 90 dB group for all investigated time points. Moreover, the 90 dB ($p \geq 0.05$ for all tested frequencies; n = 8/time point) and Ctrl ($p \geq 0.05$ for all tested frequencies; n = 8/time point) groups did not show significant differences for all tested time points (7d, 56d, 84d), whereas a slight increase in auditory threshold shift was observed for the 90 dB group 7 days post-exposure (see Figure 15, Table 1).

Table 1. ABR threshold shift after acute noise exposure. Significant differences in hearing thresholds (HT) (Mean ± SD) were observed between the 115 dB and the 90 dB and Ctrl groups at all investigated time points (7d, 56d, 84d) for all investigated frequencies (4, 8, 16, 32 kHz). No differences were obtained within and between the 90 dB and the Ctrl groups at 7d, 56d and 84d after noise exposure (p = 0.05) in any tested frequency.

ABR threshold Shift			
	4 kHz		
	115 dB	90 dB	Ctrl
7d	67.22 ± 20.3 ***	7.67 ± 9.36	1.50 ± 4.74
56d	56.00 ± 13.49 ***	14.50 ± 20.47	3.33 ± 4.33
84d	61.25 ± 16.20 ***	10.00 ± 20.950	6.50 ± 12.30
	8 kHz		
	115 dB	90 dB	Ctrl
7d	61.56 ± 19.08 ***	4.44 ± 6.34	4.50 ± 5.98
56d	57.50 ± 12.96 ***	12.50 ± 18.89	1.67 ± 5.00
84d	58.75 ± 16.42 ***	13.00 ± 17.02	3.00 ± 8.23
	16 kHz		
	115 dB	90 dB	Ctrl
7d	64.89 ± 12.70 ***	4.00 ± 7.55	1.50 ± 5.10
56d	55.50 ± 12.57 ***	10.50 ± 19.92	1.11 ± 4.16
84d	58.13 ± 11.93 ***	15.40 ± 22.39	5.50 ± 12.57
	32 kHz		
	115 dB	90 dB	Ctrl
7d	65.00 ± 19.36 ***	7.22 ± 10.34	4.40 ± 6.851
56d	57.00 ± 11.59 ***	14.00 ± 20.52	3.89 ± 6.009
84d	63.75 ± 14.82 ***	15.00 ± 20.950	8.40 ± 16.26

Significant differences are indicated by asterisks ($p \leq 0.001$:***).

In addition, between the investigated time points, all 115 dB groups included in all time points (7d 115 dB, 56d 115 dB and 84d 115 dB) showed significant differences with all of the Ctrl ($p \leq 0.001$ in all tested comparisons) and 90 dB ($p \leq 0.001$ in all tested comparisons) groups for all investigated frequencies. However, no significant differences were observed between any 115 dB groups across the time points ($p \geq 0.05$ in all tested comparisons). Furthermore, no Ctrl groups from any time point showed significant differences between each other ($p \geq 0.05$ in all tested comparisons), and when compared to any 90 dB group ($p \geq 0.05$ in all tested comparisons). Moreover, no significant differences between any 90 dB groups were observed between the time points ($p \geq 0.05$ in all tested comparisons) (see Table 1).

3.2. EXPERIMENT 1: NEURODEGENERATION ANALYSIS

3.2.1. Automated cell density analysis

First, in order to compare the effectiveness of automatic cell counting methods applied in the current work, a statistical analysis between the $NeuN^+/DAPI^+$ and $DAPI^+$ cell density values obtained both by automatic and manual counting was performed. This analysis revealed a significant difference in cell counts/area between the automatic and cell counting methods when estimating $NeuN^+/DAPI^+$ ($p = < 0.001$ by t-test; 115 dB: $n = 6$, Ctrl: $n = 5$) and the $DAPI^+$ ($p = < 0.001$ by t-test; 115 dB: $n = 6$, Ctrl: $n = 5$) cell density. Thus, a difference between the cell countings obtained by both methods was observed.

Furthermore, a significant correlation by Pearson r test was found between the automatic and manual counting cell densities calculated both for $NeuN^+/DAPI^+$ ($r = 0.818$; $p = 0.002$) and $DAPI^+$ ($r = 0.918$; $p = < 0.001$) cell counting. Similarly, after performing Bland-Altman plots, it was revealed that 95% of the data points lied within ± 1.96 SD of the mean difference and the limits of agreement for both $NeuN^+/DAPI^+$ (*Mean* = 202.3; SD = 84.35; *Upper Limit* =367.62; *Lower Limit* = 36.97) and $DAPI^+$ (*Mean* = 141.61; *SD* = 46.57; *Upper Limit* = 232.88; *Lower Limit* = 50.33) cell counting. Thus, a strong correlation between both methods was observed (see Figure 16).

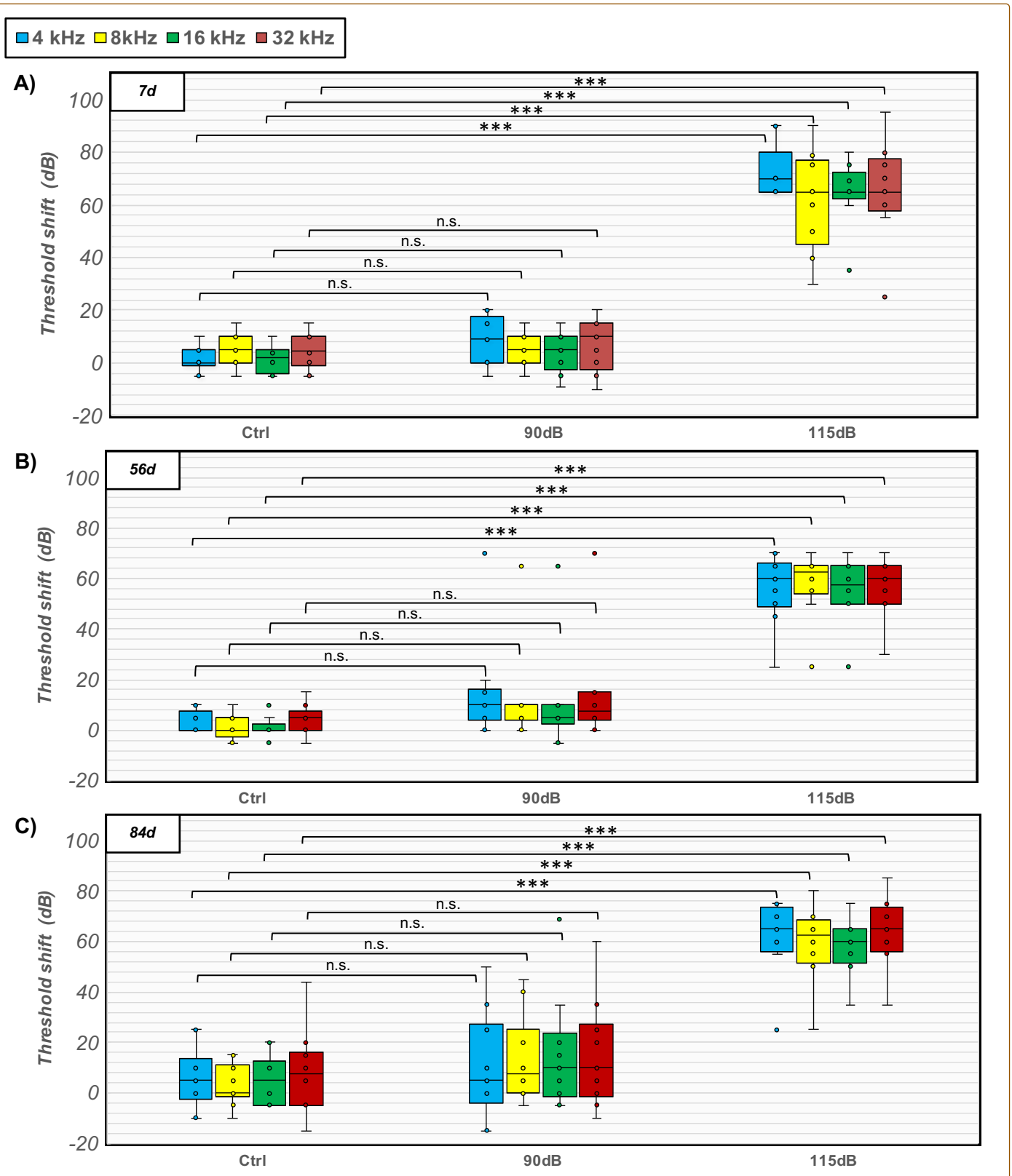

Figure 15. Auditory threshold shift after acute noise exposure: Threshold shift (Mean ± Standard Deviation) by means of ABR audiometry. Threshold shifts were calculated at 4 kHz (blue), 8 kHz (yellow), 16 kHz (green) and 32 kHz (red) within 7 days (A), 56 days (B) and 84 days (C) after acute noise exposure in noise-exposed (115 dB, n = 8/time point; 90 dB, n = 8/time point) and Control mice (Ctrl, n = 8/time point). A significant threshold shift was observed in the 115 dB group when compared to both 90 dB and Ctrl groups at all tested time points and for all investigated frequencies (7d (A): $p < 0.001$ (4 kHz, 8 kHz, 16 kHz, 32 kHz); 56d (B): $p < 0.001$ (4 kHz, 8 kHz, 16 kHz, 32 kHz); 84d (C): $p < 0.001$ (4 kHz, 8 kHz, 16 kHz, 32 kHz)). Additionally, no significant (n.s.) differences in hearing thresholds were observed between 90 dB and Ctrl mice within all investigated time points and all investigated frequencies after acute noise exposure (7d (A): $p \geq 0.05$ (4 kHz, 8 kHz, 16 kHz, 32 kHz); 56d (B): $p \geq 0.05$ (4 kHz, 8 kHz, 16 kHz, 32 kHz); 84d (C): $p \geq 0.05$ (4 kHz, 8 kHz, 16 kHz, 32 kHz). ($p \leq 0.001$: ***).

3.2.2. Neuronal density ($NeuN^+/DAPI^+$) differences in the CIC after acute noise exposure

After analyzing the effects of the different noise exposure treatments tested at earlier time points after noise exposure in the CIC, no significant differences in $NeuN^+/DAPI^+$ cell counts were detected between the 115 dB group when compared either to the 90 dB and Ctrl group 1d (p = 0.625 by one-way ANOVA; 115 dB: n = 8, 90 dB: n = 8, Ctrl: n = 7) and 7d (p = 0.140 by one-way ANOVA; 115 dB: n = 8, 90 dB: n = 8, Ctrl: n = 8) post-exposure (see Figure 17). Similarly, those differences were also not observed between noise-exposed and control animals 56d (p = 0.883 by one-way ANOVA; 115 dB: n = 8, 90 dB: n = 8, Ctrl: n = 7) and 84d (p = 0.658 by one-way ANOVA; 115 dB: n = 8, 90 dB: n = 8, Ctrl: n = 8) after noise exposure (see Figure 17). Thus, no significant differences in neuronal density in the CIC within earlier and later time points were found as a consequence of noise exposure (see Table 2). Thus, no evident signs of neuronal degeneration were observed in any of the studied time points after noise exposure (see Figure 18).

3.2.3. Cell density ($DAPI^+$) changes in the CIC after acute noise exposure

Equally, no significant differences in $DAPI^+$ cell counts were observed when comparing the 115 dB group both to the 90 dB and Ctrl groups 1d (p = 0.565 by one-way ANOVA; 115 dB: n = 8, 90 dB: n = 8, Ctrl: n = 7) and 7d (p = 0.085, by one-way ANOVA; 115 dB: n = 8, 90 dB: n = 8, Ctrl: n = 8) post-exposure. Additionally, no statistically significant differences were also found within 56d (p = 0.883 by one-way ANOVA; 115 dB: n = 8, 90 dB: n = 8, Ctrl: n = 7) and 84d (p = 0.815 by Welch's ANOVA; 115 dB: n = 8, 90 dB: n = 8, Ctrl: n = 8) post-exposure. Thus, no significant differences in total cell density were found as a consequence of noise exposure within any experimental time point in the CIC (see Figure 17, Table 2). Moreover, $DAPI^+$ cell morphology did not change in the CIC across the experimental time points included in the present study (see Figure 18).

Table 2. Numbers of neuronal ($NeuN^+/DAPI^+$) and cell ($DAPI^+$) cell counts in the CIC (Mean ± SD). No significant differences in neuronal and cell density were observed at either 1d, 7d, 56d or 84d after noise exposure in the 115 dB group when compared to the 90 dB and Ctrl groups. Furthermore, the 90 dB group did not show any significant difference in both neuronal and cell density when compared to the Ctrl group (p = 0.05).

CIC						
	$NeuN^+/DAPI^+$ *(Cell Counts/Area)*			***$DAPI^+$*** *(Cell Counts/Area)*		
	115 dB	90 dB	Ctrl	115 dB	90 dB	Ctrl
1d	903.12 ± 156.04	827.29 ± 159.00	821.87 ± 230.86	1088.40 ± 159.36	1097.17 ± 104.33	1089.63 ± 166.42
7d	1102.48 ± 100.98	1104.98 ± 130.56	965.94 ± 207.73	1361.49 ± 108.24	1346.60 ± 95.43	1238.19 ± 135.10
56d	974.58 ± 184.22	937.45 ± 207.79	924.23 ± 220.97	1230.89 ± 170.78	1208.67 ± 173.65	1135.37 ± 163.43
84d	837.12 ± 185.63	900.90 ± 180.38	914.47 ± 169.59	1255.15 ± 194.99	1197.12 ± 171.23	1212.14 ± 68.13

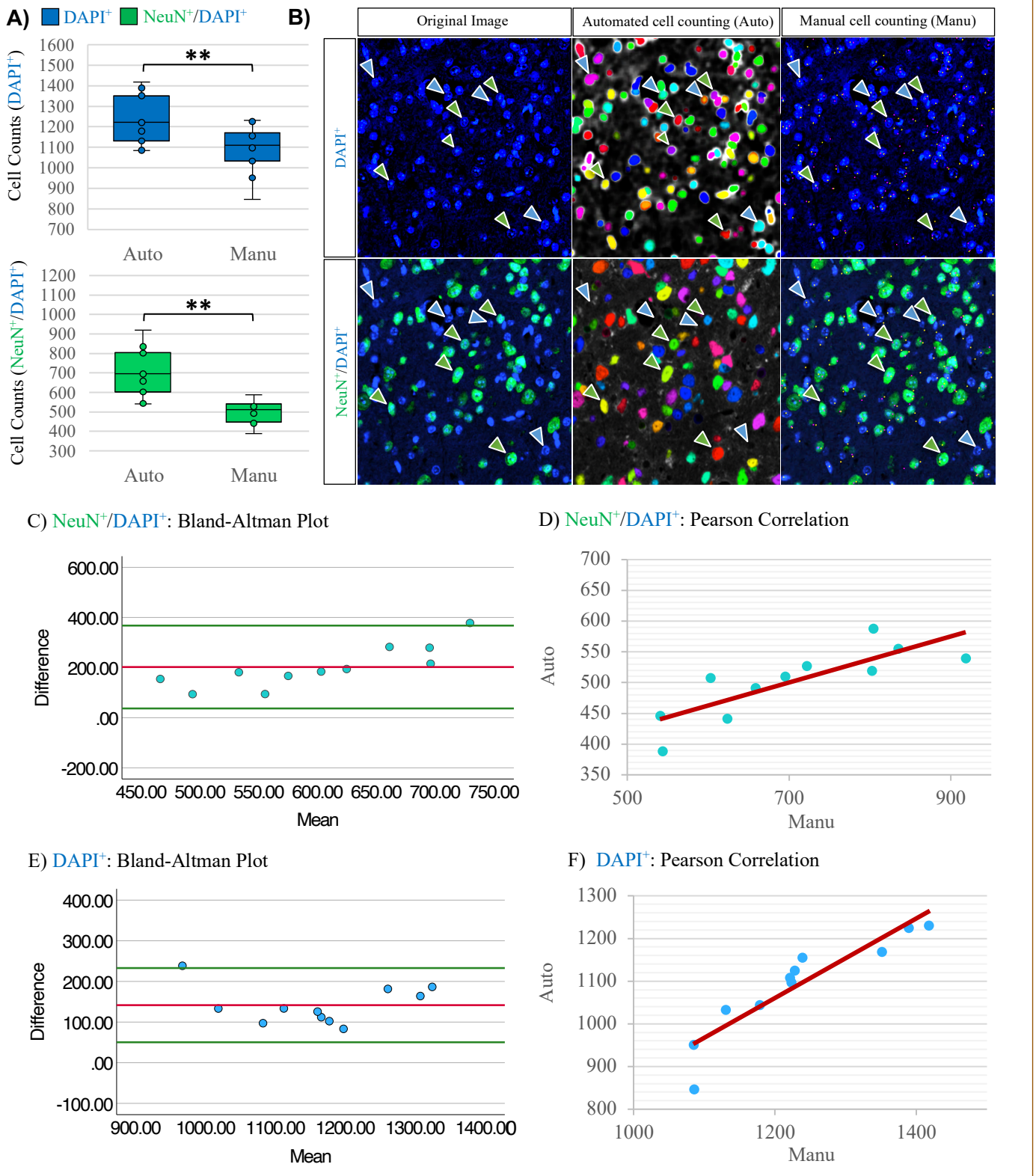

Figure 16: Automatic cell counting macro validation. (A) Neuronal (NeuN$^+$/DAPI$^+$) and Cell (DAPI$^+$) density measurements (Cell Counts/Area) in the CIC using manual (Manu) and automatic (Auto) cell counting methods (n = 12). Significant differences were found between Auto and Manu measurements of cell (DAPI$^+$) (p = 0.001) and neuronal (NeuN$^+$/DAPI$^+$) (p = 0.001 by t-test) density. (B) Examples of histological DAPI$^+$ (upper row) and NeuN$^+$/DAPI$^+$ (lower row) countings using the automatic and manual procedures. All DAPI$^+$ cells (blue arrows, yellow dots) were counted not taking into account co-localization in order to obtain the total number of cells. NeuN$^+$/DAPI$^+$ cells (green arrows, purple & yellow dots) were only counted when both markers (NeuN and DAPI) colocalized. Therefore, the DAPI$^+$ only cells (blue arrows) were not counted when obtaining the total number of neurons (see lower row). (C-F) Correlation analysis between Manu and Auto cell counting methods using Bland-Altman (BA) and Pearson correlation (PC). (C-D) BA & PC showed strong correlation in NeuN$^+$/DAPI$^+$ cell countings. (E-F) BA & PC showed strong correlation in DAPI$^+$ cell countings.

3.2.4. Changes in neuronal density ($NeuN^+/DAPI^+$) in the MGV after acute noise exposure

For the MGV, the effect of neuronal density was similar to that observed in the CIC. No statistically significant differences were detected either 1d ($p = 0.545$ by one-way ANOVA; 115 dB: $n = 8$, 90 dB: $n = 8$, Ctrl: $n = 7$) or 7d ($p = 0.672$ by one-way ANOVA; 115 dB: $n = 8$, 90 dB: $n = 8$, Ctrl: $n = 8$) post-exposure between any of the experimental groups. Equally, no significant differences in $NeuN^+/DAPI^+$ cell counts were observed as well 56d ($p = 0.197$ by one-way ANOVA; 115 dB: $n = 8$, 90 dB: $n = 8$, Ctrl: $n = 8$) and 84d ($p = 0.334$ by one-way ANOVA; 115 dB: $n = 8$, 90 dB: $n = 8$, Ctrl: $n = 8$) after noise exposure. For that reason, neuronal density differences were not detected within any experimental time point included in the study (see Figure 17, Table 3). Moreover, no qualitative morphological changes could be clearly observed in cells with a $NeuN^+/DAPI^+$ phenotype between all investigated time points and experimental treatments after noise exposure (see Figure 18).

3.2.5. Cell density ($DAPI^+$) differences in the MGV after acute noise exposure

According to the results obtained in the CIC, no statistically significant differences in $DAPI^+$ density were found within 1d ($p = 0.407$ by one-way ANOVA; 115 dB: $n = 8$, 90 dB: $n = 8$, Ctrl: $n = 7$) and 7d ($p = 0.590$, by one-way ANOVA; 115 dB: $n = 8$, 90 dB: $n = 8$, Ctrl, $n = 8$) after noise exposure. Equally, differences in $DAPI^+$ density were not detected 56d ($p = 0.666$ by one-way ANOVA; 115 dB: $n = 8$; 90 dB: $n = 8$, Ctrl: $n = 7$) or 86d ($p = 0.364$ by one-way ANOVA; 115 dB: $n = 8$; 90 dB: $n = 8$; Ctrl: $n = 8$) post-exposure. Thus, no statistically significant differences in cell density were found in the MGV at any of the experimental time points included in the study (see Table 3, Figure 17). In addition, no morphological differences in $DAPI^+$ cells were observed across the different experimental time points and treatments investigated (see Figure 18).

Table 3. Numbers of neuronal ($NeuN^+/DAPI^+$) and cell ($DAPI^+$) cell counts in the MGV (Mean ± SD). No significant differences in neuronal or cell density were observed in the MGV 1d, 7d, 56d or 84d after exposure ($p = 0.05$) in the 115 dB group when compared to both the 90 dB and Ctrl groups. Furthermore, no statistically significant differences were found between the 90 dB and Ctrl groups at any investigated time point ($p = 0.05$).

MGV						
	NeuN⁺/DAPI⁺ *(Cell Counts/Area)*			***DAPI⁺*** *(Cell Counts/Area)*		
	115 dB	90 dB	Ctrl	115 dB	90 dB	Ctrl
1d	493.01 ± 46.44	487.20 ± 70.08	458.46 ± 71.43	695.93 ± 56.80	714.61 ± 43.45	713.80 ± 66.85
7d	564.16 ± 86.20	580.54 ± 55.90	543.70 ± 98.25	863.74 ± 104.38	839.49 ± 57.20	821.23 ± 77.62
56d	538.64 ± 56.99	487.28 ± 70.51	536.04 ± 53.24	791.94 ± 56.27	766.27 ± 94.03	758.91 ± 67.65
84d	495.66 ± 136.97	510.72 ± 53.69	434.65 ± 109.87	774.13 ± 127.45	770.14 ± 50.04	712.95 ± 88.01

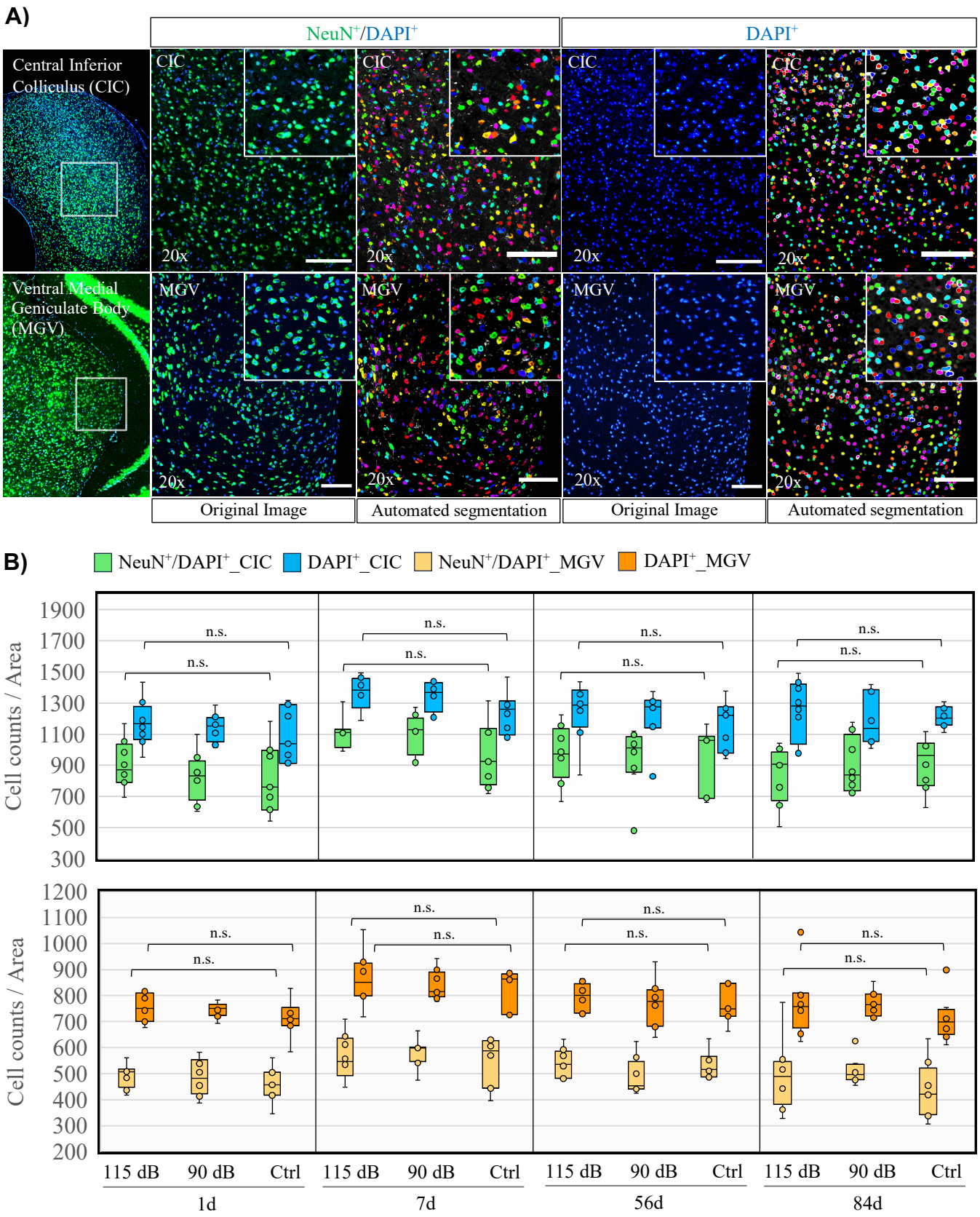

Figure 17. Effects of acute noise exposure on cell and neuronal density: (A) Histological examples of representative images from Neuronal (NeuN (NeuN$^+$/DAPI$^+$)) and Cell (DAPI (DAPI$^+$)) FIHC labelling after acute noise exposure in the Central Inferior Colliculus (CIC) and Ventral Medial Geniculate Body (MGV). Original images and their respective automatic segmentation are shown for both NeuN$^+$/DAPI$^+$ and DAPI$^+$. (B) Total cell counts/Area (Mean ± Standard Deviation) in the CIC and MGV for NeuN$^+$/DAPI$^+$ (CIC: green; MGV: yellow) and DAPI$^+$ (CIC: blue; MGV: orange) countings 1d, 7d, 56d and 84d after noise exposure. No significant (n.s) differences were observed between any experimental treatment either within 1d (115 dB: n =8; 90 dB: n = 8; n = 7), 7d (115 dB: n =8; 90 dB: n = 8; n = 8), 56d (115 dB: n =8; 90 dB: n = 8; n = 8) or 84d (115 dB: n =8; 90 dB: n = 8; n = 8) in both NeuN$^+$/DAPI$^+$ and DAPI$^+$ ($p \geq 0.05$ in all tested comparisons). *Scale bar*: 100 µM.

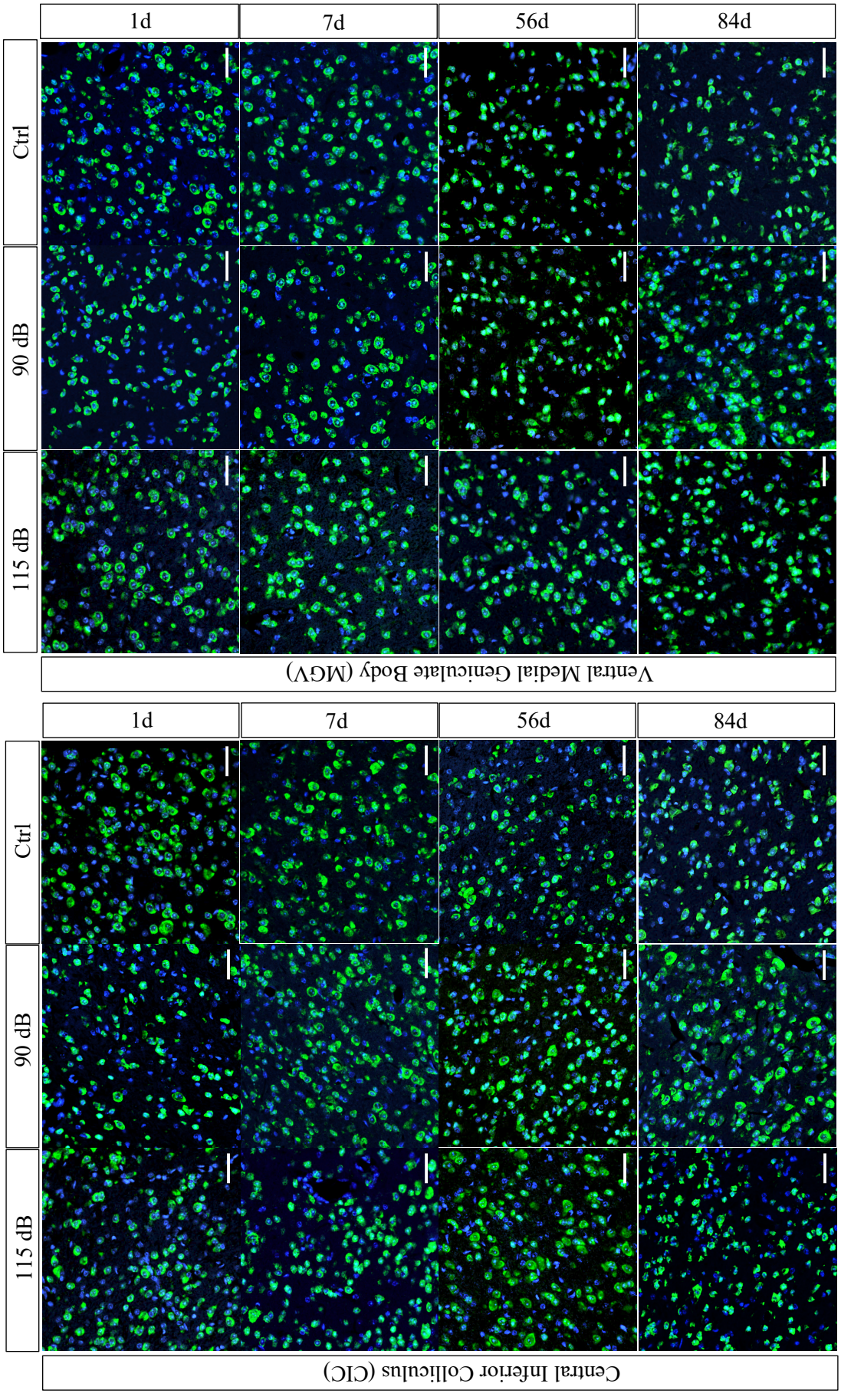

Figure 18. Cell morphology after noise exposure: NeuN$^+$/DAPI$^+$ (neurons, green & blue) and DAPI$^+$ (cell nuclei, blue) cells between each experimental time point (1d, 7d, 56d and 84d) and each experimental treatment (115 dB, 90 dB and Ctrl) in the CIC and MGV. In both neural structures, no evident morphological changes in cells with either NeuN$^+$/DAPI$^+$ or DAPI$^+$ phenotype were observed between all investigated time points and noise exposure treatments. Moreover, clear neurodegenerative evidences were also not observed from a qualitative perspective. The zoom was increased by 75% from the original images and the display settings were manually adjusted for proper visualization. *Scale Bar*: 100 µM.

3.3. EXPERIMENT 2: NEUROCONNECTIVITY ANALYSIS

3.3.1. Axonal density changes in the CIC upon noise exposure

In the CIC, a significant increase in $SMI312_{CTCF}$ values was detected 1d after noise exposure between the 115 dB and the 90dB ($p = 0.035$ by Bonferroni Post-hoc test; 115 dB: $n = 8$, 90dB: $n = 8$) groups, but no significant differences were found when comparing the 115 dB to the Ctrl group ($p = 0.141$ by Bonferroni Post-hoc test; 115 dB: $n = 8$, Ctrl: $n = 7$). Furthermore, no significant differences were also observed between the 90 dB and Ctrl group ($p = 1.000$ by Bonferroni Post-hoc test; 90 dB: $n = 8$, Ctrl: $n = 7$,). In addition, no statistically significant differences were found 7d ($p = 0.641$ by one-way ANOVA; 115 dB: $n = 8$, 90 dB: $n = 8$, Ctrl: $n = 8$), 56d ($p = 0.613$ by one-way ANOVA; 115 dB: $n = 8$, 90 dB: $n = 8$, Ctrl: $n = 7$) or 84d ($p = 0.691$ by one-way ANOVA; 115 dB: $n = 8$, 90 dB: $n = 8$, Ctrl: $n = 8$) post-exposure between any experimental time point included in the study. For these reasons, an increase in neurofilament density 1d after noise exposure in the 115 dB group when compared to the 90dB group could be observed, but not when compared to the Ctrl group. Those effects were not present 7d, 56d and 84d after noise exposure (see Figure 19, Table 4).

3.3.2. Neurofilament density changes in the MGV after acute noise exposure

Similar differences were found in the MGV 1d post-exposure to those detected in the CIC. Hence, a significant increase in $SMI312_{CTCF}$ values was observed in the 115 dB group when compared to both the 90 dB ($p = 0.012$ by Games-Howell post-hoc test; 115 dB: $n = 8$, 90 dB: $n = 8$) and Ctrl ($p = 0.017$ by Games-Howell post-hoc test; 115 dB: $n = 8$, Ctrl: $n = 7$,) groups in the MGV 1d post-exposure. However, no significant differences were observed between the 90 dB and Ctrl mice ($p = 0.530$ by Games-Howell post-hoc test; 90 dB: $n = 8$, Ctrl: $n = 7$). Additionally, no significant increases were observed 7d ($p = 0.486$ by Welch's ANOVA; 115 dB: $n = 8$, 90 dB: $n = 8$; Ctrl: $n = 8$), 56d ($p = 0.793$ by one-way ANOVA; 115 dB: $n = 8$, 90 dB: $n = 8$, Ctrl: $n = 7$) and 84d ($p = 0.274$ by one-way ANOVA; 115 dB: $n = 8$, 90 dB: $n = 8$, Ctrl: $n = 8$) after noise exposure. In this regard, a significant increase in neurofilament density was observed 1d after acute noise exposure in the MGV, but those effects were not present 7d, 56d or 84d post-exposure (see Figure 19, Table 4).

Table 4. Neurofilament density ($SMI312_{CTCF}$) in the CIC and MGV (Mean ± SD) after noise exposure. A significant increase in $SMI312_{CTCF}$ could be observed 1d post-exposure. In the CIC, $SMI312_{CTCF}$ was significantly elevated in the 115 dB group when compared to the Ctrl group, but not with the 90 dB group. In the MGV, the 115 dB showed higher $SMI312_{CTCF}$ when compared both to 90 dB and Ctrl group. No significant differences were observed between any experimental treatment within other time points after noise exposure (7d, 56d and 84d) ($p = 0.05$).

SMI312$_{CTCF}$						
	CIC			***MGV***		
	115 dB	90 dB	Ctrl	115 dB	90 dB	Ctrl
1d	2235.92 ± 1094.39*	1059.51 ± 594.18	1305.21 ± 769.94	1415.75 ± 805.48*	271.32 ± 176.21	354.56 ± 112.44
7d	1779.27 ± 773.44	1484.68 ± 435.87	1765.00 ± 817.69	580.98 ± 487.74	516.19 ± 312.16	906.64 ± 813.62
56d	1283.47 ± 818.36	1608.66 ± 910.14	1714.17 ± 907.63	262.72 ± 202.64	367.10 ± 405.31	331.00 ± 281.33
84d	1733.42 ± 937.04	1852.25 ± 683.15	2058.46 ± 616.37	293.78 ± 357.09	546.46 ± 527.21	697.34 ± 564.48

Significant differences are indicated by asterisks ($p \leq 0.05$: *).

3.4. EXPERIMENT 3: NEUROTRANSMISSION ANALYSIS

3.4.1. Glutamatergic neurotransmission after acute noise exposure in the CIC

In the CIC, no significant differences in $VGLUT1_{CTCF}$ and $VGLUT2_{CTCF}$ were observed between the investigated experimental treatments within any experimental time point studied. Thus, no significant changes in glutamatergic neurotransmission could be detected either 1d (VGLUT1: $p = 0.206$ by one-way ANOVA; 115 dB: $n = 8$, 90 dB: $n = 8$, Ctrl: $n = 7$; VGLUT2: $p = 0.501$ by one-way ANOVA; 115 dB: $n = 8$, 90 dB: $n = 8$, Ctrl: $n = 7$), 7d (VGLUT1: $p = 0.699$ by one-way ANOVA; 115 dB: $n = 8$, 90 dB: $n = 8$, Ctrl: $n = 8$; VGLUT2: $p = 0.666$ by one-way ANOVA; 115 dB: $n = 8$, 90 dB: $n = 8$, Ctrl: $n = 8$), 56d (VGLUT1: $p = 0.823$ by one-way ANOVA; 115 dB: $n = 8$, 90 dB: $n = 8$, Ctrl: $n = 8$; VGLUT2: $p = 0.852$ by one-way ANOVA; 115 dB: $n = 8$, 90 dB: $n = 8$, Ctrl: $n = 8$) or 84d (VGLUT1: $p = 0.789$ by one-way ANOVA; 115 dB: $n = 8$, 90 dB: $n = 8$, Ctrl: $n = 8$; VGLUT2: $p = 0.089$ by one-way ANOVA; 115 dB: $n = 8$, 90 dB: $n = 8$, Ctrl: $n = 8$) after noise exposure in the CIC (see Figure 20, Table 5).

3.4.2. Glutamatergic influences after acoustic overstimulation in the MGV

No statistically significant changes in glutamatergic neurotransmission could be found in the MGV at 1d (VGLUT1: $p = 0.495$ by one-way ANOVA; 115 dB, $n = 8$, 90 dB, $n = 8$, Ctrl, $n = 7$; VGLUT2: $p = 0.690$ by one-way ANOVA; 115 dB, $n = 8$, 90 dB, $n = 8$, Ctrl, $n = 7$), 7d (VGLUT1: $p = 0.752$ by one-way ANOVA; 115 dB, $n = 8$, 90 dB, $n = 8$, Ctrl, $n = 8$; VGLUT2: $p = 0.714$ by one-way ANOVA; 115 dB, $n = 8$, 90 dB, $n = 8$, Ctrl, $n = 8$), 56d (VGLUT1: $p = 0.815$ by one-way ANOVA; 115 dB, $n = 8$, 90 dB, $n = 8$, Ctrl, $n = 8$; VGLUT2: $p = 0.618$ by one-way

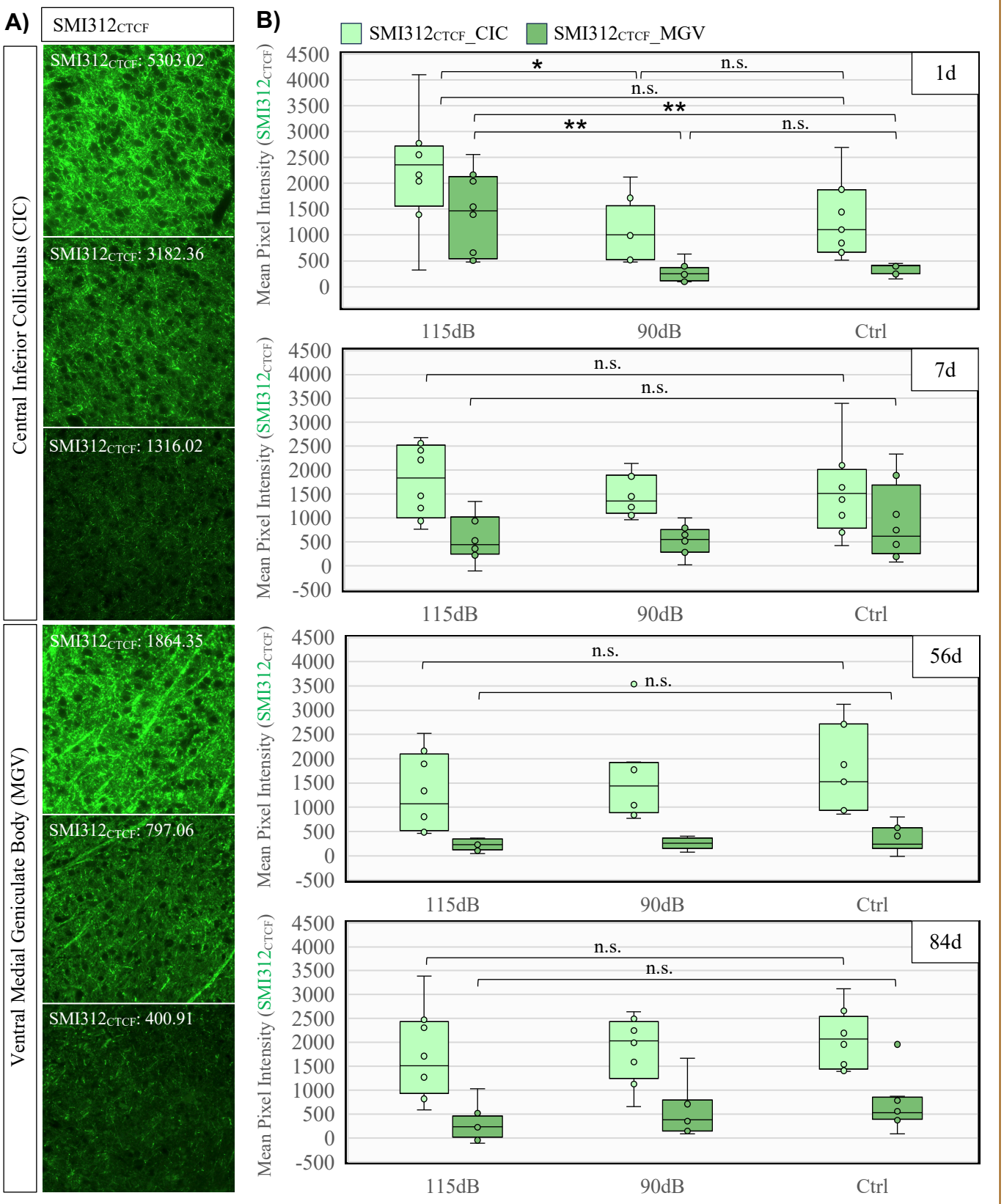

Figure 19. Neurofilament density after acute noise exposure: (A) Comparison of different Corrected Total Cell Fluorescence (CTCF) levels from SMI312 FIHC immunolabelling in the CIC and the MGV. Brightness and contrast settings were manually adjusted differently in the CIC and MGV for proper display. Differences between acquired CTCF levels could be observed. (B) Mean Pixel Intensity ($SMI312_{CTCF}$ ± SD) between all investigated treatments (115 dB, 90 dB and Ctrl) within each experimental time point (1d, 7d, 56d, 84d). Significant increases in $SMI312_{CTCF}$ were observed in the CIC 1d post-exposure between the 115 dB ($n = 8$) and the 90dB ($n = 8$) groups ($p = 0.035$), whereas no significant (n.s.) differences were detected between the 115 dB ($n = 8$) and the Ctrl ($n = 7$) groups ($p = 0.141$). No additional differences were found between the 90 dB and the and Ctrl ($p = 1.000$) groups. In the MGV, the 115 dB ($n = 8$) group had significantly increased $SMI312_{CTCF}$ levels when compared to both the 90 dB ($n = 8$, $p = 0.012$) and Ctrl ($n = 8$, $p = 0.017$) groups. 7d (115 dB, $n = 8$; 90 dB, $n = 8$; Ctrl, $n = 8$), 56d (115 dB, $n = 8$; 90 dB, $n = 8$; Ctrl, $n = 8$) and 84d (115 dB, $n = 8$; 90 dB, $n = 8$; Ctrl, $n = 8$) after acute noise exposure, no significant (n.s.) differences were found between any experimental treatment in either in the MGV or CIC ($p \geq 0.05$ in all investigated time points).

ANOVA; 115 dB: n = 8, 90 dB: n = 8, Ctrl: n = 8) or 84d (VGLUT1: p = 0.307 by one-way ANOVA; 115 dB: n = 8, 90 dB: n = 8, Ctrl: n = 8; VGLUT2: p = 0.178 by one-way ANOVA, 115 dB: n = 8, 90 dB: n = 8, Ctrl: n = 8) after acute noise exposure (see Figure 20, Table 5).

3.4.3. GABAergic neurotransmission after acute noise exposure in the CIC

No significant changes in GABAergic neurotransmission were found at 1d (VGAT: p = 0.474 by one-way ANOVA; 115 dB: n = 8, 90 dB: n = 8, Ctrl: n = 7), 7d (VGAT: p = 0.309 by one-way ANOVA; 115 dB: n = 8, 90 dB: n = 8, Ctrl: n = 8), 56d (VGAT: p = 0.355 by Welch's ANOVA; 115 dB: n = 8, 90 dB: n = 8, Ctrl: n = 8), or 84d (VGAT: p = 0.764 by Welch's ANOVA; 115 dB: n = 8, 90 dB: n = 8, Ctrl: n = 8) post-exposure (see Figure 20, Table 5).

Table 5. Vesicular glutamate transporter density ($VGLUT1_{CTCF}$, $VGLUT2_{CTCF}$) in the CIC and MGV (Mean ± SD). No significant differences were observed for both $VGLUT1_{CTCF}$ and $VGLUT2_{CTCF}$ at any time point after noise exposure between the 115 dB and both the 90 dB and Ctrl groups in the CIC and MGV. Equally, no significant differences were found between the 90 dB and the Ctrl group for $VGLUT1_{CTCF}$ and $VGLUT2_{CTCF}$ at 7d, 56d or 84d after noise exposure (p = 0.05).

CIC						
	$VGLUT1_{CTCF}$			**$VGLUT2_{CTCF}$**		
	115 dB	90 dB	Ctrl	115 dB	90 dB	Ctrl
1d	192.23 ± 59.21	144.57 ± 39.03	161.64 ± 56.58	2676.37 ± 1058.0	2183.01 ± 716.06	2601.97 ± 838.67
7d	115.26 ± 55.64	122.81 ± 39.73	99.62 ± 67.43	3963.76 ± 631.89	4124.93 ± 631.89	3702.95 ± 1030.15
56d	181.74 ± 65.87	202.23 ± 88.70	185.99 ± 45.43	2236.79 ± 1458.4	2652.88 ± 1718.1	2366.04 ± 1295.5
84d	206.15 ± 61.23	197.45 ± 41.13	217.56 ± 68.84	2800.68 ± 963.65	3251.02 ± 627.22	3859.25 ± 1082.10
MGV						
	$VGLUT1_{CTCF}$			**$VGLUT2_{CTCF}$**		
	115 dB	90 dB	Ctrl	115 dB	90 dB	Ctrl
1d	274.57 ± 171.63	338.84 ± 87.66	260.69 ± 134.34	1396.61 ± 657.09	1124.65 ± 475.57	1285.89 ± 742.00
7d	136.29 ± 59.80	133.49 ± 71.25	161.65 ± 106.34	2549.15 ± 776.05	2241.55 ± 637.18	2438.69 ± 832.34
56d	301.55 ± 71.22	314.35 ± 77.42	335.47 ± 152.06	1063.24 ± 664.16	1369.34 ± 719.52	1084.11 ± 682.62
84d	200.07 ± 123.26	275.76 ± 77.72	228.88 ± 82.26	960.54 ± 449.49	1447.02 ± 460.40	1322.96 ± 635.13

3.4.4. GABAergic neurotransmission imbalances in the MGV after noise exposure

No significant differences in $VGAT_{CTCF}$ were detected in the MGV 1d (VGAT: p = 0.348 by one-way ANOVA; 115 dB: n = 8, 90 dB: n = 8, Ctrl: n = 7), 7d (VGAT: p =0.717 by one-way ANOVA; 115 dB: n = 8, 90 dB: n = 8, Ctrl: n = 8), 56d (VGAT: p = 0.806 by one-way ANOVA; 115 dB: n = 8, 90 dB: n = 8, Ctrl: n = 8) or 84d (VGAT: p = 0.789 by one-way ANOVA; 115 dB: n = 8, 90 dB: n = 8, Ctrl: n = 8) after acute noise exposure. For that reason, in the present study, no significant changes in GABAergic neurotransmission could also be observed in the MGV after

acute noise exposure within any experimental time point due to the expression of VGAT (see Figure 20, Table 6).

Table 6. Vesicular GABA transporter density ($VGAT_{CTCF}$) in the CIC and MGV (Mean ± SD). No significant changes in $VGAT_{CTCF}$ were detected in the CIC or the MGV at 1d, 7d, 56d and 84d after noise exposure. No statistically significant differences in $VGAT_{CTCF}$ were observed between the 115 dB and the 90 dB or Ctrl groups at any time point. Similarly, no differences were found between the 90 dB and the Ctrl groups ($p = 0.05$).

VGAT$_{CTCF}$						
	CIC			***MGV***		
	115 dB	90 dB	Ctrl	115 dB	90 dB	Ctrl
1d	1560.93 ± 427.55	1300.61 ± 366.49	1463.88 ± 472.71	928.65 ± 384.07	826.45 ± 308.34	686.64 ± 211.79
7d	1568.73 ± 282.62	1545.64 ± 228.37	1342.34 ± 409.92	897.37 ± 334.02	775.49 ± 187.04	967.70 ± 388.19
56d	1463.19 ± 396.82	1838.06 ± 567.50	1606.75 ± 258.50	875.78 ± 1094.04	1094.04 ± 449.24	853.95 ± 406.81
84d	1307.98 ± 361.40	1449.54 ± 372.05	1476.27 ± 671.62	557.13 ± 427.66	998.66 ± 451.44	550.40 ± 345.72

3.4.5. Qualitative assessment of FI measurements

Finally, results from quantitative $SMI312_{CTCF}$ measurements (Mean ± SD) performed on different days (Day 1: D1, Day 2: D2) on stained samples from the same experimental subjects can be observed in Table 7. Overall, no significant qualitative differences either in CTCF or SD values from staining performed on different animals could be observed. Therefore, external influences have played a minor role in the accuracy of FI measurements.

Table 7. Analysis of Fluorescence Intensity (FI) measurement accuracy. No major qualitative differences in neurofilament density ($SMI312_{CTCF}$) (Mean ± SD) were observed either in the CIC or the MGV for any mice investigated between different staining days (D1: Day 1; D2: Day 2).

SMI312$_{CTCF}$				
	CIC		***MGV***	
Animal Number	D1	D2	D1	D2
MGR-30	2373.48 ± 546.93	2250.05 ± 727.74	1408.38 ± 401.00	1032.69 ± 483.77
MGR-31	2513.88 ± 599.30	2074.61 ± 674.99	939.41 ± 294.64	736.32 ± 293.26
MGR-33	2202.63 ± 662.71	2560.56 ± 898.58	1037.79 ± 356.99	941.84 ± 537.85
MGR-34	1569.37 ± 380.97	1349.54 ± 494.14	659.01 ± 294.34	420.61 ± 248.67
MGR-37	1274.29 ± 522.89	1216.70 ± 561.77	210.40 ± 160.54	524.38 ± 358.36
MGR-39	2042.65 ± 441.75	2076.07 ± 695.72	619.84 ± 320.20	750.72 ± 293.99

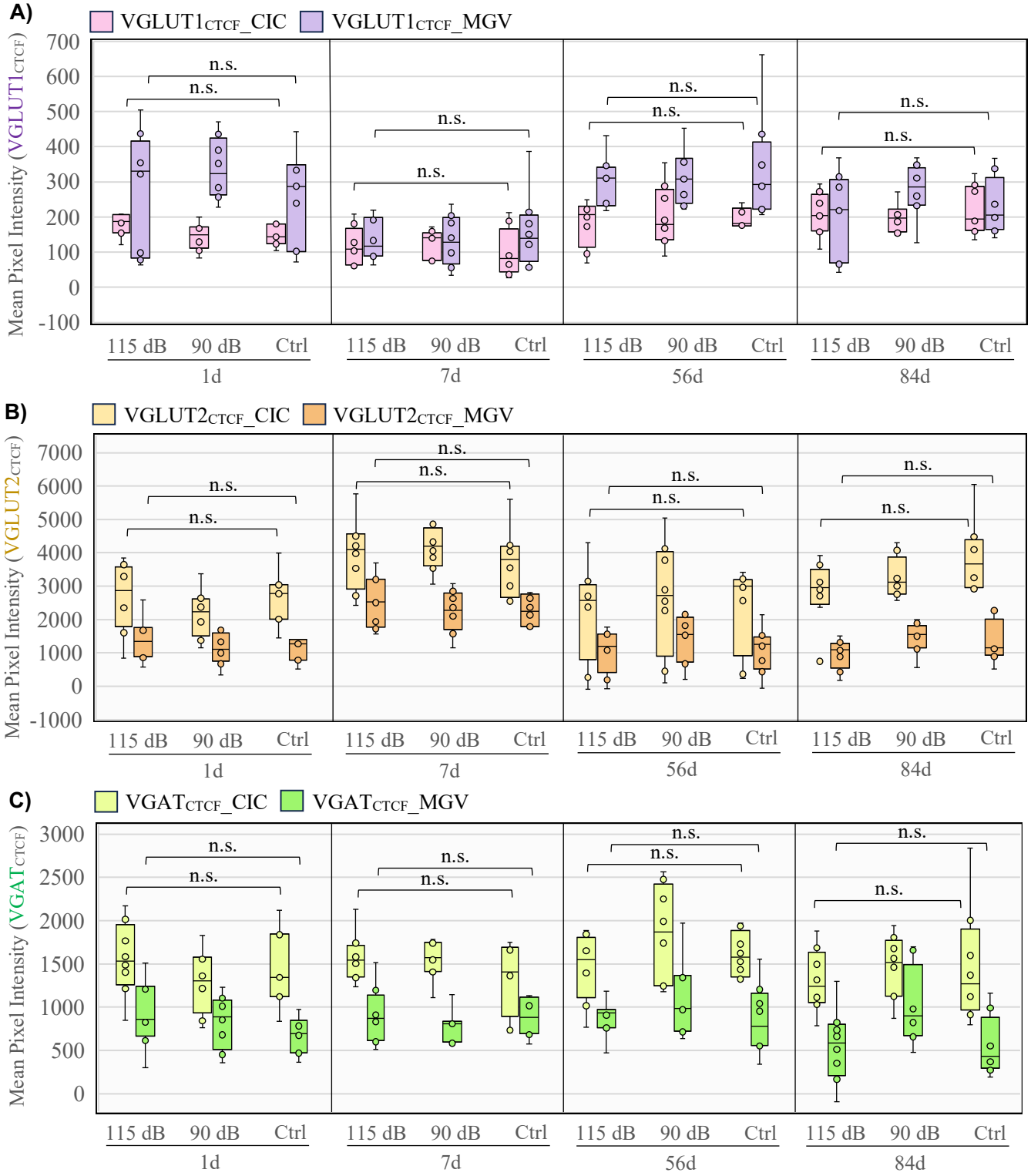

Figure 20. Glutamate (VGLUT1, VGLUT2) and GABA (VGAT) vesicular neurotransmitter transporter expression after acute noise exposure: Mean Pixel Intensity (Mean ± SD) of VGLUT1 ($VGLUT1_{CTCF}$) (A), VGLUT2 ($VGLUT1_{CTCF}$) (B) and VGAT ($VGLUT1_{CTCF}$) (C) immunolabelling after 1d (115 dB: $n = 8$; 90 dB $n = 8$; Ctrl $n = 7$), 7d (115 dB: $n = 8$; 90 dB $n = 8$; Ctrl $n = 8$), 56d (115 dB: $n = 8$; 90 dB $n = 8$; Ctrl $n = 8$) and 84d (115 dB: $n = 8$; 90 dB $n = 8$; Ctrl $n = 8$) post-exposure. (A) No significant (n.s.) differences in $VGLUT1_{CTCF}$ were observed between 115 dB and 90 dB and Ctrl-exposed mice ($p \geq 0.05$ in all tested comparisons) at all investigated time points after noise exposure. Moreover, no significant differences between the 90 dB and both 115 dB and Ctrl groups ($p \geq 0.05$ in all tested comparisons) were observed. (B) No statistically significant changes in $VGLUT2_{CTCF}$ could be found either between the 115 dB group and the 90 dB and Ctrl groups ($p \geq 0.05$ in all tested comparisons), or between the 90 dB and the 115 dB and Ctrl groups ($p \geq 0.05$ in all tested comparisons). No significant changes were observed at any time point investigated. (C) No significant differences were detected $VGAT_{CTCF}$ at any time point studied after noise exposure. Significant differences were not detected between the 115 dB group and both the 90 dB and Ctrl groups ($p \geq 0.05$ in all tested comparisons). No significant changes were also observed between the 90 dB and the 115 dB and Ctrl groups ($p \geq 0.05$ in all tested comparisons).

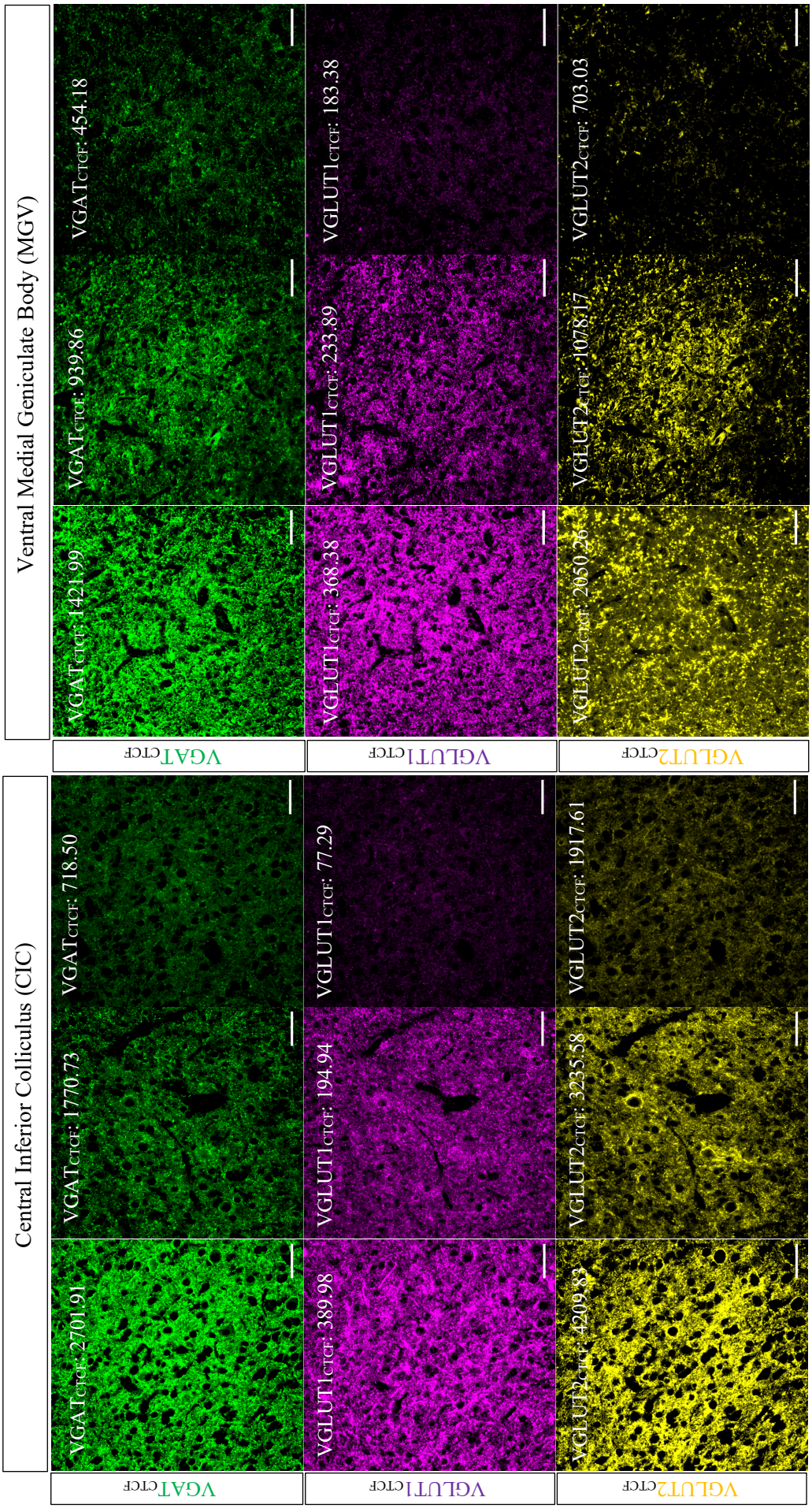

Figure 21. Corrected Total Cell Fluorescence (CTCF) measurements from VGAT, VGLUT1 and VGLUT2 immunolabelling: Representative example images with different CTCF values calculated from VGAT ($VGAT_{CTCF}$), VGLUT1 ($VGLUT1_{CTCF}$) and VGLUT2 ($VGLUT2_{CTCF}$) labelling in the CIC and MGV. Different CTCF levels observed corresponded with differences in VGAT, VGLUT1 and VGLUT2 relative expression. Brightness and contrast were manually adjusted in order to properly display fluorescence intensity differences. *Scale Bar:* 100 µm

04 DISCUSSION

4.1. HEARING LOSS UPON NOISE EXPOSURE

The experimental animals from the 115dB group showed a significant threshold shift when compared with the 90 dB group and the Ctrl group at all investigated time points (7d, 56d, 84d after noise exposure) and tested frequencies (4 kHz, 8kHz, 16kHz, 32 kHz). Thus, a significant difference in HT was found between the high (115 dB), moderate (90 dB) and control (Ctrl) noise exposure treatments by means of the experimental design. These results indicated that a profound acoustic injury followed by a non-recoverable threshold shift after acute noise exposure was induced in high-noise exposed mice, whereas no evident signs of noise trauma were observed in the moderate and sham exposed subjects. Thus, a NIHL phenotype derived from our experimental design was confirmed.

On the one hand, the present work showed that a significant PTS in the 115 dB group could be clearly observed 7d, 56d and 84d after trauma. Those effects are in line with the previously listed literature in which similar experimental designs in terms of noise-induced trauma were carried out (Basta et al., 2005; Gröschel et al., 2010, 2011). Thus, comparable inner ear injury might have been present in the 115 dB group, but should have been absent in the 90 dB and Ctrl groups. Nonetheless, the threshold shifts observed in the present work were much higher when compared to previous studies, even when using the same mouse strain (NMRI). Gröschel et al. (2010) and Gröschel et al. (2011) observed a threshold shift between 33- and 42-dB SPL 7d after a similar noise exposure paradigm was applied (115 dB SPL, 5-20 kHz, 3h). In the current study, the detected threshold shifts ranged from 70- to 90 dB SPL 7d post-exposure, from 45- to 70 d B SPL 56d post-exposure, and from 60- to 75 dB SPL 84d post-exposure. It is challenging to explain the reason behind these differences. Nevertheless, it is well known that different factors such as sex (Lauer & Schrode, 2017; Milon et al., 2018; Wang et al., 2021), hormonal concentration (Delhez et al., 2020; Shuster et al., 2021), estrous cycle stage (Krizman et al., 2021) and/or circadian rhythms (Meltser et al., 2013) might differentially affect noise susceptibility between individuals. As will be discussed further, the present study included more females than males when compared to the cited studies. In addition, ABR measurements were preferentially performed during early mornings, an issue that might produce differences in noise susceptibility. Moreover, slight changes in the positioning of the experimental subjects inside the soundproof chamber might produce differences in hearing thresholds, as noise intensity was observed to be not equally distributed through the whole soundproof chamber.

On the other hand, the absence of acute hearing loss in the 90 dB group is in accordance with the effects described by Kujawa & Liberman (2009), in which moderate noise exposure did not result in PTS during the first weeks of noise exposure. In addition, no significant threshold shifts 7d after noise exposure to 90 dB SPL were also reported by Gröschel et al. (2011). Similarly, as was reported by the present study, threshold shifts after 90 dB exposure observed by Gröschel et al. (2011) were also within the range of 10dB, and were not significantly different from non-exposed control animals. Subsequently, Singer et al. (2020) also did not detect elevated threshold shifts after 80 dB SPL (10 kHz, 2h) noise exposure when compared to controls. Therefore, although some detrimental effects might happen after moderate noise exposure which might be undetected by conventional audiometry (Kujawa & Liberman, 2015), permanent damage might be absent.

Certainly, this increase in HT occurring only in high-noise exposed mice could be explained by deeply investigated pathological mechanisms occurring in inner ear structures after profound acoustic overstimulation, such as structural damage (Ding et al., 2019), irreversible loss of sensory HC (Kurabi et al., 2017), loss of synaptic connectivity between the HC and the ANF and/or the subsequent degeneration of the SGN and the auditory nerve (Cranial Nerve VIII) (Kujawa & Liberman, 2015), which are responsible for carrying neural auditory information to central higher auditory pathways. In this context, this acute inner ear injury could arise under different noise-induced pathological circumstances such as profound mechanical damage (Kurabi et al., 2017), increased oxidative stress (Henderson et al., 2006), pronounced immune and inflammatory responses (Frye et al., 2019), and altered spontaneous release of glutamate from damaged HC (Muly et al., 2004), leading to hyperexcitability and excitotoxic mechanisms (Knipper et al., 2013; Salvi et al., 2000). Therefore, all these pathological processes can severely disrupt the transduction of neural auditory information to higher auditory structures and affect neural activity in those brain auditory areas (Singer et al., 2020). Therefore, though the use of ABR as a diagnostic tool can be controversial because subjects with moderate hearing dysfunctions can present a normal audiogram, it is widely accepted that severe damage in the inner ear can have an impact on the amplitude of recorded ABR waveform peaks, which can be associated with several physiological alterations in both the peripheral and central auditory system (Eggermont, 2019; Habib & Habib, 2021; Heeringa & van Dijk, 2014; Hickox & Liberman, 2014; Liberman, 2016; Milloy et al., 2017; Singer et al., 2020). Up to the current knowledge, these central noise-induced mechanisms are mainly related to the activation of apoptotic cell death pathways (Aarnisalo et al., 2000; Coordes et al., 2012; Gröschel et al., 2018), cell loss (Basta et al., 2005; Gröschel et al.,

2010), changes in synaptic connectivity and neural activity (Muly et al., 2002; Salvi et al., 2000; Zeng et al., 2009), and changes in the inhibitory and excitatory balance in the CNS (Heeringa et al., 2016; Browne et al., 2012; Park et al., 2020). So far, the previous literature has reported well-documented ABR-related changes in the HT of similarly noise-exposed experimental subjects followed by the aforementioned pathological mechanisms in the CNS (Basta et al., 2005; Basta & Ernst, 2004; Gröschel et al., 2010, 2011; Park et al., 2020; Schrode et al., 2018; Singer et al., 2020). Nevertheless, as will be explained, this study successfully detected an early elevation in central connectivity after noise in association with a clear elevation of HT, whereas no cell loss or glutamatergic and GABAergic imbalances were able to be described. For that reason, an extensive discussion about the implications, considerations and limitations of the current findings will be performed.

Additionally, up to the present knowledge, the present study provides the first insights into the consequences of acute noise trauma in HT at later time points after noise exposure, suggesting that similar pathological mechanisms observed 7 days post-exposure could also be observed 56 days and 84 days after intense acoustic overstimulation. This contributes to the evidence that loud noise exposure for prolonged periods of time produces a permanent and non-recoverable hearing impairment. In this regard, the HT was observed to be stable during the entire investigated time (12 weeks after noise exposure). However, the variance observed in the 90 dB and Ctrl groups was slightly higher when compared to the 115 dB group. In order to explain this phenomenon, it is possible to think that early signs of ARHL and/or physiological differences in noise susceptibility might be present in experimental subjects from the 90 dB and Ctrl groups to a more major extent than in the 115 dB group. These differences might produce slight changes in auditory function, which might be shown by the increased variability. Moreover, those differences might be partially masked in the 115 dB group, probably due to noise-induced damage. Nevertheless, it is also important to mention the reduced sample size used in each experimental group.

In addition, some limitations must be taken into account. First, ABR data from the 1d group was not collected and analyzed due to the reasons described in previous sections (see Section 2.7). For that reason, conclusions about the exact time-frame in which the first evident signs of acoustic noise trauma started to appear in the current study cannot be directly extracted from the collected data. Hence, determining the HT of the experimental subjects at early time points after noise exposure would help to assess if detrimental effects on hearing capacity are either produced immediately or generated during the first week after noise exposure. Nevertheless, previous publications described changes in higher auditory regions both immediately and during the first

hours after acute noise trauma (Coordes et al., 2012; Gröschel et al., 2014; Noreña & Eggermont, 2003). Moreover, in previous studies, it was difficult to observe any ABR response 1 day after loud noise exposure. Thus, similar ABR audiometry results as well as pathological mechanisms might be present 1d after noise exposure.

Equally, there is a lack of ABR data in order to study the noise-induced effects happening between 7d and 56d post-exposure. Furthermore, collecting ABR data from 14 days and 28 days post-exposure might also add follow-up information to the time-course of NIHL related changes between earlier and later time points after noise exposure. However, no significant differences in ABR thresholds would be expected during the testing of those intermediate time points, as similar elevations of HT have been described 14 and 28 days after noise exposure (Fröhlich et al., 2017, 2018; Gröschel et al., 2014). Furthermore, it is also important to take into account that ABR audiometry was performed in different experimental mice for each investigated time point, and no longitudinal studies were performed on the same individuals due to the experimental design applied in the present study. Thus, studying how HT changes in the same experimental subjects by means of ABR audiometry would help analysis of the time-frame of physiological response in individual animals in order to add consistent value for future studies.

Finally, performing a classic structural metric of inner ear damage by counting the number of HC along the cochlear duct (a method known as a cytocochleogram) between the high, moderate, and sham-exposed mice, would help to finally assess if the observed increase in HT by means of ABR audiometric data could be related to the previously listed HC death mechanisms after inner ear damage.

4.2. CELL DENSITY IN THE CIC AND MGV

After analysing the effects of noise exposure on cell ($DAPI^+$) and neuronal ($NeuN^+/DAPI^+$) density in the CIC and MGV, the presented results indicated that no evident changes either on $DAPI^+$ or $NeuN^+/DAPI^+$ cell densities could be observed in the present study between the 115 dB, the 90 dB and the Ctrl groups 1d, 7d, 56d or 84d after noise exposure. Thus, the observed noise-induced trauma present in the 115 dB group could not be explained either by cell or neuronal loss in the CNS after noise exposure in the present study. In line with the current results, some studies did not observe cell or neuronal density changes after noise exposure (Heeringa et al., 2016; Aarnisalo et al., 2000; Kurioka et al., 2016; Reuss et al., 2016). Nevertheless, these results do not support previous findings published by our research group, which suggested that extensive cell

death is produced after acute noise trauma through the ascending auditory pathway (Basta et al., 2005; Gröschel et al., 2010).

In this regard, Basta et al. (2005) and Gröschel et al. (2010) detected an increase in HT by means of ABR audiometry together with a significant reduction in cell density in the CN, IC and MGB 7 days after acute noise exposure. In these studies, the animal mouse model (*Mus Musculus*, NMRI strain), the experimental group sizes, the noise exposure paradigm and the ABR recording setup were comparable to those performed in the present study. During both experiments, NMRI strain mice were noise exposed for 3h inside a soundproof chamber to broadband white noise (5-20 kHz and 9.5-10.5 kHz) under anesthetic conditions to 115 dB SPL, and frequency-specific ABR responses (from 4 to 32 kHz) were measured following similar procedures. Furthermore, a clear evidence of acute threshold shift by means of ABR audiometry was also observed by Basta et al. (2005) and Gröschel et al. (2010), with similar characteristics to those described in this study. Bearing this in mind, subtle differences between diverse experimental designs that were carried out might potentially lead to controversial results. These are described in the following paragraphs.

4.2.1. Moderate noise exposure under MRI acquisition: Its impact on neuronal and cell density

First, in previous publications, animals were sacrificed immediately following the performance of ABR recordings, and no additional techniques were applied before starting the histological procedures. In the present study, MR techniques were performed directly prior to the perfusion and sacrifice of the animals. Although functional MR techniques are considered a valuable diagnostic tool used in auditory research, they can present some limitations, as acoustic noise associated with image acquisition represents a challenge in the application of those techniques to auditory neuroscience (Beam et al., 2021; Boyen et al., 2013; Koops et al., 2020; Landgrebe et al., 2009; Lauer et al., 2012; McJury & Shellock, 2000; Talavage et al., 2014). Noise levels inside MRI scan rooms are frequently below the maximum limit permissible, but they can vary depending on the type of scanner and image sequence being performed. In addition, stress derived from noise exposure inside some MRI scans can elevate the heart rate, increase blood pressure and alter metabolic states, issues that could affect animals' well-being and research outcomes (Lauer et al., 2012). As explained previously, it is not recommended to exceed a noise exposure of 85dB over a prolonged period of time in order to avoid hearing damage, and noise levels produced by MRI scans can range from 80 to 130 dB over time (Coskun, 2011; Counter et al., 1997; Nakai et al., 2012). For that reason, an assessment of the noise levels produced during the MR acquisition was performed in order to observe its influence on the current data. MR noise

levels were measured inside the MRI scan room at a distance of 2 meters during all VBM, DTI and 1H MRS sequences, and the results are shown in Table 8. The measurements revealed that an additional moderate noise exposure that ranged from 80 to 100dB during approximately 30 minutes was applied to all experimental subjects during MR image acquisition. Thus, the introduction of an additional moderate noise exposure by means of MR techniques must be discussed, as one could think that the cell numbers observed in the Ctrl or the 90dB groups could be affected due to the additional MRI noise. If these differences were large enough to fall under the limit of our cell density counting method, this issue could lead to undetected cell density differences. However, even if it is likely that an additional noise exposure could possibly influence hearing thresholds, it is unlikely that it could induce cell loss within the limited time between MRI measurement and tissue fixation (10-15 minutes). A fast cell loss upon noise exposure was described only for the VCN as the terminal structure of the auditory nerve. Higher centers of the auditory pathway have never been shown to be affected in such a time frame (Coordes et al., 2012; Gröschel et al., 2010). Furthermore, previous studies from our group described that an elevation in the number of apoptotic cell bodies ($TUNEL^+$ cells) in the MGV could be observed in mice exposed two times to 115 dB SPL (5-20kHz) when compared to one-time exposed mice 14 days after noise exposure, but not 7 days post-exposure (Fröhlich et al., 2017). However, these elevations were not detected in the CN and IC at either 14 or 7 days after exposure (Fröhlich et al., 2018). Therefore, it seems possible that repeated noise exposure could activate additional apoptotic pathways, which might later be later translated into cell death and the reduction of cell density. Moreover, the noise exposure performed during repeated noise exposure experiments was significantly higher than the one observed during MRI sequences.

Table 8. MRI noise exposure levels across different sequential MR image acquisition sequences performed on a Bruker BioSpec 70/20 USR system (Mean ± SD). Noise levels indicated that an additional moderate noise exposure that ranged from 80 dB to 100 dB was applied during MRI acquisition for approximately 30 minutes.

MR acquisition sequence	Sound pressure level (dB SPL)	Exposure Time
Localizer_multi_slice	85dB ± 5dB	00:00:40
TurboRARE (VBM)	85dB ± 5dB	00:08:30
DTI_b100_6dir (DTI_1)	95dB ± 5dB	00:01:30
DTI_b900_13dir (DTI_2)	95dB ± 5dB	00:03:05
DTI_b1600_25dir (DTI_3)	95dB ± 5dB	00:05:40
DTI_2500_18dir (DTI_4)	93dB ± 5dB	00:04:24
DTI_b2500_18dir (DTI_5)	94dB ± 5dB	00:04:10
2_STEAM_1H (MRS)	40dB ± 5dB	00:50:00

Unfortunately, ABR recordings after noise exposure in the MRI in order to test hearing deficits after MRI were not performed due to the design of the present work. Therefore, it was not possible to observe if MRI noise could affect hearing function. For these reasons, the current study might suggest that the possible influence of MRI in the central auditory system should be deeply investigated by further studies.

4.2.2. Different histological methods

Additionally, Basta et al. (2005) and Gröschel et al. (2010) detected cell density differences between exposed and non-exposed mice using Hematoxylin-Eosin (H&E) (Gröschel et al., 2010) or modified Kluever-Barrera (KB) (Basta et al., 2005) staining techniques. In the present study, such differences were studied by the expression of NeuN and DAPI using FIHC techniques. H&E and KB stainings allow for visualizing the architecture as well as the cellular components of tissue using different types of dyes, providing valuable information about structure and composition. In contrast, FIHC are a range of histological techniques used for detecting and visualizing specific proteins or antigens of interest by the usage of antibody-based stains that specifically bind to target structures and molecules, and not dyes that react to structural and molecular elements within tissues. This property allows immunohistochemistry techniques to detect even small amounts of target molecules of interest with a high degree of specificity (Webster et al., 2021). For that reason, despite all histological techniques giving valuable insights into the structural and functional status of biological tissues, different immunohistochemistry techniques might provide different information. Thus, they cannot always be directly compared to each other, mainly due to their underlying specificity in recognizing molecular components of interest. One example supporting this statement can be seen when comparing studies Aarnisalo et al. (2000) and Gröschel et al. (2010). Using cresyl violet or Nissl staining techniques (which selectively labels DNA and RNA from neuronal and glial cells in the CNS), no differences in neuronal density in the VCN were found by Aarnisalo et al. (2000), whereas a decrease was found by Gröschel et al. (2010) in the same structure applying H&E staining techniques. Although these two studies were performed in different animal models (mouse and guinea pig) and under different noise exposure conditions, controversial results produced by different staining techniques are shown. Furthermore, H&E and KB staining by themselves are not always informative about the morphological difference between different types of cell death (Janke et al., 2019). Therefore, one feasible explanation of the undetected cell density differences in the present study might be the differences in specificity and sensitivity between H&E, KB, Nissl and FIHC staining. In other words, detected biological

processes of interest might differ when compared to the previously listed literature due to the application of different histological techniques. In addition, it was also assumed that the activation of cell death pathways leads to the clearance of dying cells from the damaged tissue over time. This is because cellular components are degraded gradually, and target antigens of interest can undergo different molecular and structural changes that make them unrecognizable by tagged antibodies during FIHC (Elmore, 2007). These processes might lead to the non-detection of these apoptotic cell bodies, and thus, to a decreased cell density. However, contrary to the hypotheses, the expression of NeuN and DAPI in the CIC and MGV did not decrease in all investigated time points after acute noise exposure in the 115 dB group when compared to the 90 dB or Ctrl groups. One potential explanation might be that NeuN and DAPI immunoreactivity persists 1d and 7d post-exposure even after the initiation of noise-induced apoptotic cell death pathways. This might happen because the initiation of apoptotic mechanisms may not lead immediately to the clearance of dying cells, and therefore, immunoreactivity may not be lost during the whole apoptotic process. Supporting this statement, some studies show that it is possible to observe co-expression of TUNEL, NeuN and DAPI (Hong et al., 2014; Jiang et al., 2017; Newcomb et al., 1999). This co-expression phenomenon was observed by Jiang et al. (2017), in which different neurons co-expressing NeuN and TUNEL together with Hoechst 33342 were found 7 days after an ischemic stroke was induced in adult mice. Similarly, Newcomb et al. (1999) detected double NeuN and TUNEL immunoreactivity in neurons of adult mice 6h, 1 day, 3 days and 14 days after traumatic brain injury (TBI) was induced (Figure 22). Per contra, some

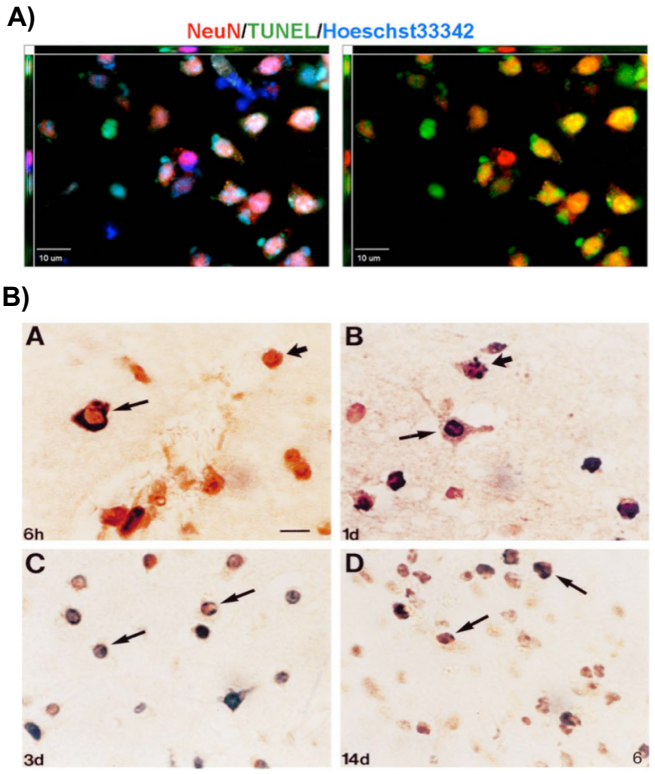

Figure 22: NeuN, DAPI and TUNEL co-expression: A) Representative images showing neuronal populations co-expressing NeuN, TUNEL and Hoeschst33342 observed in adult mice 7 days after a severe ischemic stroke was induced. This provides evidence about the possibility of detecting apoptotic cells labelled with NeuN and DAPI several days in the CNS several days after inducing acute injury. B) Neuronal populations showing NeuN and TUNEL immunoreactivity 6 hours, 1 day, 3 days and 14 days after traumatic brain injury. *Source: Jiang et al., 2017, Copyright (2016) International Society of Neuropathology Newcomb et al., 1999*

studies go against this assumption and report a decrease in NeuN immunoreactivity after various pathological mechanisms, a phenomenon mainly explained by neuronal cell death (Gusel'nikova & Korzhevskiy, 2015; Karuppagounder et al., 2007; Yousef et al., 2017). Additionally, this decrease in NeuN and DAPI immunoreactivity was also not observed at 56d and 84d after acute noise trauma, time points in which decreased immunoreactivity and clearance of dying cells should have already happened. However, up to the current knowledge, this is the first study in which neuronal degeneration 56d and 84d after noise exposure has been investigated, and there is no previous evidence against the current observations. These results might be explained by different mechanisms happening in the CNS due to aging, such as changes in brain size and tissue shrinkage, mechanisms that may hinder the observation of changes in cell density over such a long period of time (Peters, 2006).

4.2.3. Different cell counting methods

Additionally, there are substantial differences between the cell counting methods used by previous works. Basta et al. (2005) and Gröschel et al. (2010) performed manual cell counting methods, counting the number of visible nuclei on printed photographs by hand. In this work, an automated cell counting method was carried out to automatically assess $DAPI^+$ and $NeuN^+/DAPI^+$ density differences. As described before, both methods showed a difference in terms of the number of cell countings performed in each of them. Nevertheless, a clear correlation was observed between them, and therefore, it was concluded that both methods could be equally informative. Then, a deeper analysis was performed in order to understand the nature of the detected differences. These analyses revealed that manual cell counting led to a slight underestimation of the cell numbers. This occurred mainly because differences in FI between different images could lead to the non-observation of some cells and the misinterpretation of the $NeuN^+/DAPI^+$ phenotype, even if the same image settings were propagated between images. Then, human error was shown to be higher than the automatic error observed when counting all cells observed in each image. These issues were avoided during the automatic counting procedure, as image intensities were normalized in the first steps of the process. Moreover, automatic cell counting using the software Cellpose was blinded to the treatment performed in each experimental subject. Nevertheless, despite the reasons listed above, the application of an automated method during image analysis must be accounted for during a proper interpretation of the current data, as it may lead to substantial differences when compared to previous studies.

4.2.4. Cell density changes after diverse experimental designs: The need for standardization

Having described all the discrepancies between the present work and previous research, it is important to discuss why some studies were also not successful in reporting cell density changes. Interestingly, Reuss et al. (2016) were not able to quantify neuronal degeneration within the first two weeks after noise exposure in the olivocochlear complex (OC) of the SOC. First, though the SOC is known to play an important role in modulating the neural activity (Buras et al., 2006; Mulders et al., 2010; Reuss 2000), no study has investigated cell density changes after noise exposure in this region. Therefore, cell death might not be equally represented in the SOC when compared to other auditory CNS structures. Additionally, it is worth noting that OC neurons do not constitute the entire neuronal population in the SOC. Furthermore, Reuss et al. (2016) applied a narrower-band noise exposure treatment (120 dB SPL, 10kHz, 2h) when compared to Basta et al. (2005) and Gröschel et al. (2010) (115 dB SPL, 5-20 kHz, 3h). Therefore, the noise trauma induced by Reuss et al. (2016) was more restricted. Additionally, Reuss et al. (2016) applied retrograde neural tracing by injections of Fluorogold (FG) in order to observe olivocochlear neurons. As seen before, differences in histological procedures might explain these controversial results. Finally, the manual cell counting protocols described by Reuss et al. (2016) were slightly different from previous studies. Furthermore, no information about the sexes included was given by Reuss et al. (2016).

Additionally, Kurioka et al. (2016) also did not detect cell density differences in the VCN after similar loud noise exposure treatments (120 dB SPL, 2-20 kHz, 3h) to those used by Gröschel et al. (2010), even observing clear evidences of HC death. These results contradict the decreased neuronal density observed in the VCN by Gröschel et al. (2010). In this regard, the noise exposure paradigm performed by Kurioka et al. (2016) was similar to that performed by Gröschel et al. (2010). However, Nissl stainings were performed by Kurioka et al. (2016), as compared to the H&E staining used by Gröschel et al. (2010). In both studies, manual countings were also performed, auditory thresholds shifts and group sizes were comparable and mice of both sexes were included, although the mouse strains used was different (The NMRI strain was used by Gröschel et al. (2010) whereas Kurioka et al. (2016) used the C57/BL6 strain). According to Kurioka et al. (2016), Aarnisalo et al. (2000) did not observe neuronal degeneration between noise-exposed and control animals in the anteroventral cochlear nucleus (AVCN) even 25 days after excessive noise exposure was delivered (130dB SPL, 4kHz, 5 hours). Surprisingly, an increase in apoptotic cell nuclei was clearly observed in both the AVCN and SOC, which suggested that an early increase in $TUNEL^{+}$ cells might not always lead to decreased cell density in later time points

after noise exposure. However, Aarnisalo et al. (2000) observed these effects in guinea pigs, an issue that could potentially influence the results due to interspecies differences (Kiefer et al., 2022). Moreover, the AVCN does not constitute the entire CN, and differences in auditory responsiveness within the different subnuclei of the CN might happen. Furthermore, as performed by Kurioka et al. (2016), Aarnisalo et al. (2000) used Nissl stainings to identify neuronal cell loss. Finally, Aarnisalo et al. (2000) also did not indicate the ratio between males and females included.

All the presented results demonstrate that under slightly different experimental designs in terms of the noise exposure paradigm applied or histological technique performed, diverse results can be observed. For this reason, developing new standard techniques for studying noise trauma in the CNS could help to establish a final consensus about how noise exposure can produce cell death. Finally, the static limitations of histology were evidenced in terms of studying cell loss in the CNS. These techniques only allow for the studying of noise-induced consequences in a specific time-frame, which creates a loss of information about the dynamic properties that characterize *in vivo* conditions. So, the implementation of techniques that allow the study of neuronal cell loss *in vivo* during the whole time-course of NIHL would finally help the assessment of how these neurodegenerative processes happen in real time under physiological situations.

4.3. EARLY NOISE-INDUCED CONNECTIVITY CHANGES IN THE CIC AND MGV

Although cell density changes were not observed, an evident increase in neurofilament density was present in the MGV 1d after acute noise exposure in the 115 dB group when compared to the 90 dB and the Ctrl mice. In the CIC, a significant increase was also detected between the 115 dB- and the 90dB-exposed mice, but this increase was not observed between 115 dB and Ctrl groups, as well as between the 90 dB and Ctrl groups. Furthermore, no significant neurofilament density changes were detected within 7d, 56d and 84d in the CIC and in the MGV. These changes were observed together with an elevation of HT in the 115 dB group for all investigated frequencies in all investigated time points after noise exposure, which suggested that dramatic and non-recoverable inner ear damage was present. Therefore, in line with the hypothesis, these results indicate that loud noise exposure can induce changes in synaptic connectivity in higher auditory structures of the CNS. However, in the present study, this could not be related to cell loss or changes in VNTT expression in those auditory brain areas. Therefore, a proper interpretation of the presented data must be precisely performed.

4.3.1. Axonal density changes and their relationship with central hyperactivity

It was demonstrated that axonal growth events can happen in the CIC and the MGV during the first day after noise exposure, experiencing a transient decline at later time points. Due to this observation, it is reasonable to speculate that a possible relationship between increases in synaptic connectivity and hyperactivity events through the auditory CNS may exist. This is because intense and prolonged acoustic overstimulation and cochlear damage produce a decreased signal transmission to the central auditory pathway, mainly due to HC, ribbon synapse and ANF loss. In order to mitigate and restore this deprived peripheral auditory output, the central auditory system can enhance its intrinsic neural activity and spread those patterns through all the auditory pathway. These effects can be accompanied by different synaptic remodeling events, probably with the aim to reinnervate lower auditory areas after auditory damage (Benson et al., 1997; Bilak et al., 1997; Dehmel et al., 2012; Knipper et al., 2013; Lin et al., 2011; Mao & Chen, 2021; Muly et al., 2002; Salvi et al., 2000; Singer et al., 2020; Zhao et al., 2016). However, one might ask why and how are these hyperactivity and connectivity events exactly related with each other? How could these mechanisms turn into pathological consequences?

In this context, it is possible to think that early axonal sprouting events may precede and even evoke late hyperactivity in CNS areas like the IC or the MGB. In other words, early synapse formation in the CNS could gradually lead to increased neural activity during later time points after noise exposure. This probably happens with the aim of compensating the loss of auditory function in lower and peripheral auditory areas. In support of this hypothesis, some studies report that hyperactivity mechanisms might be a transiently developing phenomenon rather than an immediate consequence, happening within the first two weeks after noise exposure (Gröschel et al., 2014; Manzoor et al., 2012). Gröschel et al. (2014) found enhanced central hyperactivity in the CN and IC 14 days post-exposure, but not 7 days after noise exposure. This was consistent with the hyperactivity found in those regions by Manzoor et al. (2012) and Ma et al. (2006) within 2-3 weeks after noise exposure. Similarly, Dong et al. (2010) found hyperactivity in the IC within 2-4 weeks after noise trauma, but not immediately. Equivalently, increases in neural activity in the MGB were demonstrated *in vivo* long after tinnitus was induced in rats by Kalappa et al. (2014). This hyperactivity might be produced by an elevated Ca^{+2} intracytoplasmatic influx produced by excessive overstimulation, which in turn could lead to an excessive release of glutamate into the synaptic cleft. Equally, this calcium influx is crucial for the induction of long-term potentiation (LTP), which is critical for the formation and strengthening of new synapses and for the maintenance of neural activity (Eccles, 1983). Supporting this statement, an increase in the Ca^{+2}

dependent activity was observed in the CN 1d after acute noise exposure by Gröschel et al. (2011). Then, 7 days after, the elevation was also detected in the SOC and in the MGB, and 14 days after, the signal was again only observed in the CN. Futhermore, Çakır et al. (2015) demonstrated an enhancement of LTP mechanisms in the CN of mice suffering from tinnitus 1d after noise exposure. This may be produced in part by alterations in the function of AMPA and NMDA glutamatergic receptors, as different studies report enhanced protection against NIHL using AMPA and NMDA antagonists (Chen et al., 2004; Duan et al., 2006; Hu et al., 2020). As an example, Tagoe et al. (2017) showed how NMDA receptor antagonists could decrease extracellular calcium concentration, restoring normal LTP function in the CN following loud noise exposure. In addition, this may also have a possible link with the observed changes in VGLUT1 and VGLUT2 in the CN (Heeringa et al., 2016; Barker et al., 2012; Kurioka et al., 2016). Therefore, an enhancement of LTP due to a massive Ca^{+2} influx might lead to a gradual formation and strengthening of new and maybe pre-existing glutamatergic synapses, causing an excessive excitation in several areas of the auditory pathway. If these connections are maintained due to prolonged and repetitive noise exposure, this may produce a permanent elevation of central activity with profound physiological alterations like tinnitus or hyperacusis.

These hypotheses are also supported by different studies. Benson et al. (1997), Bilak et al. (1997) and Muly et al. (2002) observed that after destruction of HC and ANF after noise exposure or after cochlear removal, a decrease in synaptophysin and evidences of axonal degeneration were observed in the CN during the first 7 days. However, both synaptophysin and axonal density were recovered transiently from 7d to 150 days post-exposure, which was explained by a slow formation of new synaptic contacts in this region. In this regard, a gradual increase in GAP-43, which was associated to axonal growth, was observed in the SOC, CN and IC by extensive studies performed by Kari Suzanne Kraus and Robert-Benjamin Illing. This increase was detected from the 7th day after noise exposure until several weeks or months after noise exposure. Moreover, it may probably rise as an attempt of the CNS to reinnervate deprived peripheral auditory input in lower auditory brainstem areas like the CN (Illing et al., 1997; Kraus et al., 2011; Kraus et al., 2009). Nevertheless, it is not clear when this expression in GAP-43 exactly starts, until when it can be conserved, and what its defined implications are for the time-course of NIHL. Moreover, some studies were not successful in even finding altered protein expression of GAP-43 in the CN, IC and AC, either after some days or months after noise-induced trauma (Browne et al., 2012).

Nevertheless, it is still challenging to assess if hyperactivity is a cause or a consequence of an increased axonal growth. In this regard, different studies show how this increase in neural

activity can be also recorded in the first minutes after auditory damage (Mossop et al., 2000; Noreña & Eggermont, 2003; Salvi et al., 2000). Mossop et al. (2000) detected that a significant increase in excitatory responses could be recorded in gerbils in the first minutes after cochlear ablation. Similarly, Noreña & Eggermont (2003) and Salvi et al. (2000) recorded such hyperactivity during the first few hours after noise exposure and/or cochlear ablation. In this regard, Salvi et al. (2000) explained that if hyperactivity is produced right after noise trauma, it is reasonable to think that hyperactivity could be related to changes in pre-existing neural circuits rather than being due to immediate and fast synapse formation. In this context, a loss of pre-established synaptic inhibitory inputs would be enough for observing changes in excitatory neural activity. However, the current observations may add valuable information to this hypothesis, suggesting that together with connectivity rearrangements in pre-existing synapses, synaptic growth could start even earlier than was thought. Consequently, both pre-existing connectivity changes and *de novo* synaptic formation might contribute to the generation of hyperactivity in the CNS. Nonetheless, this hypothesis cannot be concluded from the current data, and must be extensively confirmed in further studies.

Furthermore, adding further complexity, some studies were not successful in reporting changes in central activity after noise exposure or even detected a decrease in neural activity in the IC (Basta & Ernst, 2004; Qiu et al., 2000; Sun et al., 2012; Wang et al., 1996). As explained before, these diverse observed results in the literature might be produced due to fact that different performed noise exposure treatments can produce differences in auditory damage, auditory responsiveness and/or auditory susceptibility. Furthermore, differences between *in vivo* and *in vitro* recording methods can also lead to uneven results. However, when compared, studies using *in vivo* methods also show different results (Basta & Ernst, 2004; Gröschel et al., 2014; Mossop et al., 2000; Salvi et al., 2000). Moreover, the impact of acoustic trauma can be largely variable, as it can differ between animal models, between different groups of central auditory neurons or brain nuclei, and also depending on the area of the receptive field in which damage is produced (Kiefer et al., 2022; Niu et al., 2013; Scholl & Wehr, 2008). Once again, controversies may arise because there is a lack of available techniques to study the dynamics of noise-induced neuroplasticity *in vivo*. Therefore, noise-induced neuroplasticity can be extremely dependent on several environmental factors, which could be misinterpreted or underestimated during *in vitro* experiments. These ambiguities make it challenging to establish a clear relation between central increases in neural connectivity and hyperactivity imbalances found in the central auditory system.

Therefore, despite their intrinsic nature being still under debate, the evidences given suggest the existence of both short-term and long-term hyperactivity mechanisms in the central auditory system as a consequence of peripheral damage, and therefore, related physiological processes like connectivity reorganizations may occur within both time-frames in order to produce such alterations (Gröschel et al., 2014; A. N. Heeringa & van Dijk, 2014; Henry, 2013; Kaltenbach et al., 1998; Knipper et al., 2013; Mossop et al., 2000). Moreover, it has been observed that central hyperactivity in the IC and the CN might be dependent on pathological changes in the peripheral auditory system (Mulders & Robertson, 2009). Accordingly, elevations of HT observed by ABR audiometry might suggest that increases in axonal density in the CIC and MGV could be related to traumatic injury in the inner ear. Within this context, the reported synaptic connectivity increases 1d post-exposure might suggest that formation of new synapses might happen in the CIC and MGV in the first moments of noise exposure. Although it is difficult to know if this axonal growth is a cause or a consequence of central hyperactivity, both mechanisms may be intrinsically related due to the reasons described above. However, it is worth mentioning the speculative characteristics of the present arguments. Having only integrated the current data with published literature, it is difficult to extract reliable conclusions about how concretely this biological relation between connectivity and hyperactivity could happen. Therefore, these observations must be extensively studied in future studies.

Moreover, although an increase in axonal connectivity could happen in the CIC and MGV 1d post-exposure, it is not clear which could be the main source of those rising connections. Furthermore, our results suggest that early axonal growth could be expressed differently between the CIC and MGV. It is reasonable to think that these issues may reflect biological differences in neuroplastic events happening in these regions after loud noise exposure

4.3.2. Axonal innervation in the CIC and MGV after noise exposure: An intrinsic or an extrinsic phenomenon?

Additionally, the current study could not provide a precise indication about where the observed axonal tracts detected 1d after noise exposure in the CIC and the MGV might originate from. This is because no neurotracing experiments were performed, and both the IC and MGB present a complex network of ascending and descending inputs from different classical and non-classical auditory areas (Cai et al., 2014; Ito & Oliver, 2010, 2012a; Ito, 2016). Hence, it is challenging to evaluate the contributions of each central auditory nuclei to this phenomenon. However, finding the origin of these increasing axon projections could reveal many functional

properties of different areas of the auditory system. In addition, it may help to assess how noise exposure shapes the neural response in the CNS right after noise exposure.

On the one hand, it is possible to hypothesize that axonal projections are originated extrinsically from the IC or MGB. Thus, the pronounced increase in HT observed by means of ABR audiometry in the 115 dB group suggests that severe pathological mechanisms occurred in the inner ear structures that could potentially produce such changes in the central auditory system, and therefore, central axonal growth might be primarily evoked as a consequence of peripheral auditory damage. Accordingly to Manzoor et al. (2012), ablation of the DCN was shown to produce a significant reduction in the central hyperactivity in the IC 2 and 3 weeks after noise exposure (10 kHz, 115dB, 4h). This might have been caused by a decrease in projecting axons from the DCN to the IC and/or MGB due to noise exposure. Therefore, central hyperactivity in the IC seemed to be dependent on some lower auditory areas that include at least, the CN. Thus, it may be possible that axonal tracts implicated in IC hyperactivity might originate from extrinsic sources such as the CN. Equally, Kraus & Illing (2004) showed that increases in GAP-43 expression observed in the CN 7 days after severe inner ear damage could originate in lower brainstem nuclei such as the SOC. Moreover, different studies show how glutamatergic connections probably linked with neuronal hyperactivity in the CN might arise from alternative somatosensory areas like the spinal trigeminal nucleus (Sp5), the cuneate nucleus (Cu) or the lateral vestibular nucleus (LVN) (Barker et al., 2012; Dehmel et al., 2012; Shore et al., 2008; Zeng et al., 2011, 2012). Thus, there is robust evidence to demonstrate that at least some the connections observed in the CIC and MGV might originate outside these areas.

On the other hand, connectivity increases could also be produced and/or maintained as a consequence of intrinsic neural activity of the IC and/or the MGB without peripheral influences. Relevant literature suggests that the persistence of hyperactivity over time could be associated to biological mechanisms happening within the auditory CNS, particularly in the IC (Hickox & Liberman, 2014; Kaltenbach et al., 1996). Moreover, due to the inner complexity of the auditory neural pathways, there is a possibility that a combination of extrinsic and intrinsic sources might play a role in the observed elevations of neurofilament density in the CIC and MGV.

Thus, it is challenging to determine where these axonal tracts detected within the CIC and MGV originate from. Therefore, care must be taken when rejecting any hypothesis, as additional robust studies must be done in order to extract reliable conclusions about this issue. Nevertheless, it seems clear that both areas present different connectivity mechanisms that could be translated

into functional differences. For that reason, differences in axonal density expression found between the IC and MGB may have a possible biological explanation. These issues will constitute the following point of discussion.

4.3.3. Functional differences and early axonal density changes between the CIC and MGV: its relationship with NIHL

It is worth noting that a clear early central axonal growth in the MGV was observed in the 115 dB group when compared to both the 90dB and Ctrl groups, together with an elevation of HT by means of ABR audiometry. For that reason, the observed connectivity increase might be probably related to pathological mechanisms elicited by loud noise exposure. Alternatively, in the CIC, despite an elevation of HT being also detected in 115 dB-exposed mice at all tested frequencies, a significant increase in neurofilament density was observed in the 115 dB group only when compared to the 90 dB group. Interestingly, no statistically significant differences were observed between the 115dB and the Ctrl groups. Therefore, an evident difference in noise-induced connectivity events was observed between the CIC and the MGV.

On the one hand, the different results found in the CIC and the MGV might reflect differences in auditory function and/or noise susceptibility between those auditory areas after peripheral auditory damage. This is shown by the fact that neuroconnectivity increases were more dramatic in the MGV when compared to the CIC. It is possible to speculate that the biological mechanisms behind these observations may be partially related to a pronounced loss of inhibitory neurotransmission in the MGB after noise exposure when compared to the IC. Equally, anatomical, physiological or functional differences could also explain why prolonged noise exposure can produce diverse effects in neural connectivity between those auditory neural areas.

Due to its position within the ascending auditory neural pathway, the IC could be more directly exposed to the effects of noise exposure than the MGB. Principally, due to the crucial connectivity between the IC and the CN, it is one of the first neural regions affected after noise exposure. In addition, it is known that from 20 to 40% of IC neurons projecting to the MGB are GABAergic (Mellott et al., 2014). Previous studies found out that these neurons are mainly large GABAergic cells that send their inhibitory projections to both the auditory thalamus and the contralateral IC, thus being one of the main sources of inhibition of the MGB (Chen et al., 2018; Ito et al., 2009; Ito & Oliver, 2010, 2012; Winer et al., 1996). Thus, synaptic activity of the MGB could be potentially influenced by the function of the large GABAergic cells found in the IC.

Therefore, a downregulation of this GABAergic-mediated inhibition due to noise-induced damage to large GABAergic neurons present in the IC may lead to increases in the MGB excitability. This issue could lie behind the differential increase in neural connectivity between the CIC and the MGV, as excitatory influences might be upregulated in the MGB due to the loss of suppression previously exerted by those large GABAergic projections. Hence, it is possible that those alterations can be translated into more prominent increases in neurofilament density in the MGV. Unfortunately, it is difficult to conclude from the present data which specific mechanisms in the IC and/or the MGB could produce damage to large GABAergic neurons that could lead to differences in neural connectivity after noise exposure, and in particular, because no changes in VGAT expression were observed across any noise exposure treatments and/or time points investigated. Nevertheless, some processes may explain how these alterations can be produced. Some studies highlight the importance of fast and slow changes in the GABAergic activity of GABA Receptors such as GABA Receptor A ($GABA_AR$) (Sametsky et al., 2015; Caspary & Llano, 2017). Furthermore, additional studies described how inhibitory neurons could be more susceptible to peripheral deafferentation due to their high metabolic vulnerability (Ibrahim & Llano, 2019). Thus, it might be possible that GABAergic neurons in the CIC could be potentially more vulnerable to noise exposure than other cell types like glutamatergic neurons. Despite those effects having been mainly associated to ARHL, there is a possibility that the mechanisms may also play a role in NIHL. Hence, this aspect could constitute an alternative explanation for the observed downregulation of synaptic inhibition after auditory damage. Nevertheless, robust evidence would need to be observed about this hypothetical increased susceptibility of large GABAergic neurons in the IC in such a narrow time-frame after noise exposure, an issue that cannot be concluded from the presented results. For these reasons, further research is needed in order to confirm the presence of clear connectivity increases in the CIC during the first moments after noise exposure.

On the other hand, as will be extensively discussed in further sections, it could be possible that the high variability observed between CTCF measurements and/or reduced sample sizes might influence the observable differences between experimental groups. In this case, it might be possible that connectivity increases in the CIC between the 115dB and the Ctrl groups could also be present in similar ways as those observed for the MGV. Nevertheless, due to the limit of detection of the present techniques, these effects could be masked, leading to unobservable differences between those groups. In this scenario, similar noise-induced mechanisms could occur in the IC and the MGB, leading to analogous changes in neural connectivity between both areas.

For this reason, new methodologies must be applied by future studies in order to confirm the existence of different connectivity mechanisms between the IC and the MGB after loud noise exposure.

To sum up, due to the described evidences, the present study has shown how different noise exposure conditions might lead to significantly different effects in neural connectivity through the whole auditory system. This might be produced by the extensive detrimental effects of noise exposure in higher auditory brain areas. Nonetheless, it is challenging to assess the detailed implications of the early connectivity events in the NIHL pathophysiology. This makes it difficult to fully assess which specific pathological mechanisms might lie behind these increases in neural connectivity in the CNS. In addition, no significant cell loss or changes in VNTT expression were observed. For these reasons, those findings must be extensively discussed.

4.4. VNTT EXPRESSION AFTER NOISE TRAUMA IN THE CIC AND MGV

4.4.1. Increases in HT were not associated to VGLUT1, VGLUT2 or VGAT imbalances

In this context, no significant changes in vesicular glutamate (VGLUT1 and VGLUT2) and GABA (VGAT) transporters were detected in the present study within any experimental time point after noise exposure between all experimental conditions investigated. Although a significant threshold shift was observed in 115 dB-exposed mice, no changes in glutamatergic and GABAergic imbalances could be found as a consequence of loud noise exposure by studying the expression of these markers. Thus, the detected elevations in axonal growth and possible related hyperactivity phenomena may not have been produced by changes in VNTT. Nevertheless, the current results show some differences with previous studies that observed neurotransmission-related changes as a consequence of NIHL (Heeringa et al., 2016; Hakuba et al., 2000; Lee & Godfrey, 2014; Ma et al., 2021; Muly et al., 2004; Park et al., 2020; Zhang et al., 2021). Therefore, these results must be closely explored.

4.4.2. VGLUT1, VGLUT2 or VGAT expression in the IC

Within this context, only studies made by Park et al. (2020a) investigated changes in the expression of VNTTs in the IC after noise exposure. Interestingly, this study was not successful in finding VGLUT1 changes in the IC after either mRNA or protein quantification. However, significant increases in VGLUT2 were detected under both these two methods 30 days after exposing Sprague-Dawley rats. Together with these findings, elevations of HT were also found.

Finally, levels of VGAT and GAD also did not differ between noise-exposed and control groups, even after such a pronounced loud noise exposure. Thus, although the current results agree with VGLUT1 and VGAT changes found by Park et al. (2020a), an increase in VGLUT2 contradicts the current observations derived from the present work. Nonetheless, it must be noted that Park et al. (2020a) used a noise exposure paradigm which differed significantly from the one performed in the present work, as 115 dB SPL (2-20kHz) for 4h were administrated for 10 days, and real-time reverse transcription polymerase chain reaction (RT-PCR) or western blot (WB) techniques were used in order to study mRNA and protein expression. Therefore, the uneven results might have been produced due to the different analytical techniques used, as well as the profoundly different noise exposure that was induced. Finally, rats and mice might present different susceptibilities to noise exposure (Kiefer et al., 2022). Therefore, more research needs to be done in this direction in order to understand how these markers change in the IC. Moreover, no additional study investigated these changes in the MGB.

4.4.3. Changes in VNTT expression after cochlear lesion in the CN

Different evidences seem to agree that after cochlear lesion, VGLUT1 expression is decreased, and VGLUT2 expression is increased in the CN. Probably, this is due to differential distribution of these VNTTs on auditory, and non-auditory synaptic terminals, respectively (Heeringa et al., 2016; Barker et al., 2012; Kurioka et al., 2016; Zeng et al., 2009; Zhou, 2007). Some of the studies reported similar elevations of HT together with extensive damage in the inner ear. Furthermore, some of them also used FIHC to study VNTT expression in the CN. First, Zeng et al. (2009), Heeringa et al. (2016) and Kurioka et al. (2016) used similar FIHC immunolabelling as performed in this work, successfully finding a decrease in VGLUT1 and an increase in VGLUT2 in the CN. Conversely, Zeng et al. (2009) and Heeringa et al. (2016) both performed kanamycin injections as a method of noise trauma, contrary to noise exposure used here. However, Kurioka et al. (2016) found HT elevations under similar noise exposure conditions. Furthermore, contrary to common belief, Fyk-Kolodziej et al. (2011) showed increased gene expression of VGLUT1 in the VCN and DCN, and a significant decrease in VGLUT2 only in the VCN after cochlear ablation. In addition, in studies made by Schrode et al. (2018), despite a slight decrease being shown, the study did not detect a significant decrease in VGLUT1 in the CN of mice exhibiting threshold shifts after exposing them to broadband noise (100dB, 2-50kHz, 2h). Interestingly, immunohistochemistry techniques were also performed in the present study. However, FIHC detection was used. This, primarily constitutes an additional piece of evidence

about how controversial results may arise during the implementation of different experimental designs. Moreover, none of them studied VNTT expression in the IC or the MGB, and therefore, different mechanisms may occur in this last auditory region.

Furthermore, despite it having been demonstrated that changes in glutamatergic and GABAergic expression can occur after noise exposure, the information on this topic is still scarce. Most of the current bibliography is mainly focused on the VNTT alterations happening in the CN. Consequently, this study provides one of the few pieces of evidence of unchanged expression of VNTTs after noise exposure in the IC. Additionally, up to the present knowledge, no studies have investigated the expression of VGLUT1, VGLUT2 and/or VGAT in the MGB. Thus, it must be also considered that some kind of alternative synaptic process must happen in these areas in order to explain the presence of neuroplastic changes, such as increases in axonal density.

4.4.4. Alternative presynaptic and postsynaptic alterations: Synaptic transmission after NIHL

At this stage, the relevance of additional pathways in the NIHL pathophysiology must be extensively evaluated. First, it is worth noting that the role of vesicular glutamate transporter 3 (VGLUT3) was not investigated in the present study. Moreover, little is known regarding VGLUT3 expression in the auditory CNS (Kurioka et al., 2016; Zeng et al., 2009; Zhang et al., 2020; Zhou, 2007). In the peripheral auditory system, VGLUT3 knock-out ($VGLUT^{KO}$) mice can develop profound hearing impairment and deficits in synaptic connectivity between IHCs and auditory nerve fibers (Kim et al., 2019). Furthermore, mice lacking the expression of VGLUT3 suffer from dramatic deafness due to the inability of HC to load glutamate into synaptic vesicles. Additionally, different increases in VGLUT3 after noise exposure in the inner ear and auditory CNS have been reported during the first week after noise exposure (Boero et al., 2021; Kim et al., 2019; Ma et al., 2021). In the CNS, only Zhang et al. (2020), after sodium salicylate application, showed no significant differences in VGLUT3 expression in either the CN or the IC. However, no significant differences in the HT of rats treated with salicylate compared to untreated controls were observed, which differed significantly from the pronounced HT shift reported by the present study. Additionally, studies made by Ito et al. (2009) were not even successful in finding VGLUT3 immunoreactivity in the IC, and Fyk-Kolodziej et al. (2011) detected decreased VGLUT3 gene expression three weeks after induced deafness. Therefore, it should be extensively investigated if the role of VGLUT3 in the CIC and MGV could be more relevant than was thought.

Additionally, alterations in neurotransmitter re-uptake metabolism and/or changes in post-synaptic elements like glutamate and GABA receptors could also be potentially affected after noise exposure (Caspary & Llano, 2017; Dong et al., 2010; Hakuba et al., 2000; Ma et al., 2021; Muly et al., 2004; Sametsky et al., 2015). In line with this hypothesis, some studies successfully reported changes in different isoforms of the enzyme Glutamate Decarboxylase (GAD), which is responsible for the synthesis of GABA through glutamate decarboxylation. Mossop et al. (2000) and Milbrandt et al. (2000) correlated a decrease in GAD67 and/or GAD65 with elevated excitatory responses in the IC both 24h and 7 days after cochlear ablation or high noise exposure, which recovered by 30 days. However, Abbott et al. (1999) reported an increase in GAD67 expression immediately after moderate noise exposure which decreased by 30 days post-exposure, also in the IC. Furthermore, Kou et al. (2013) observed that two weeks after noise exposure, the expression of GABA receptor B ($GABA_BR$) was decreased, whereas the expression of the enzyme glutamate decarboxylase 67 (GAD67) (responsible for metabolizing glutamate into GABA) was unchanged. As described before, alterations in NMDA and AMPA receptors might be related to noise-induced neuroplastic mechanisms like LTP (Chen et al., 2004; Duan et al., 2006; Hu et al., 2020; Tagoe et al., 2017). Accordingly, Ma et al. (2021) detected an increase in VGLUT3 together with a reduction in the expression of GLAST in the cochlea during the first 30 days after noise exposure. Furthermore, some studies have suggested that both the release and uptake mechanisms can be impaired after noise exposure, leading to glutamate excitotoxicity (Lee & Godfrey, 2014). Therefore, these evidences showed how alterations in alternative synaptic pathways to VNTT can also produce the central neuroplastic mechanisms found in the CNS. For this reason, further studies must observe if these alternative pathways might be compromised in the IC and MGB after acoustic overstimulation in order to obtain a much broader view.

Once again, reported statements provide clear evidences contributing to the ongoing debate with regard to trying to understand the role of VNTTs in different noise-induced excitatory and inhibitory imbalances in the CNS. Unchanged levels of VGLUT1, VGLUT2 or VGAT reported by the present study add valuable further information about the role of these VNTTs in the time course of NIHL pathophysiology. First, they raise the question of the significant role of additional synaptic alterations, such as changes in VGLUT3 or alterations in glutamate and GABA receptor and reuptake metabolism in the CNS following inner ear damage. Second, they also support the crucial need for experimental design standardization between future studies in terms of the induced auditory trauma or methodological approach carried out. Additionally, there is a crucial need to develop new methodological techniques in order to study the inner mechanisms of NIHL.

Currently, despite several methods have been proposed for this, there is no powerful technique which allows for studying how neuroplasticity changes in real time *in vivo* in a living human brain. This step would promote the translation from basic experimental science into clinical applications in human patients, opening a new era in the field which could be extended to several related scientific disciplines.

4.4.5. Metabolic imbalances and noise-induced inhibitory influences

Additionally, besides the mainly discussed hypotheses of a downregulation of inhibitory influences as a consequence of compensatory mechanisms in the CNS, it has been proposed that metabolic imbalances happening in inhibitory GABAergic neurons might also lie behind the observed decrease in inhibitory influences. Studies made by Ibrahim & Llano (2019) suggest that GABAergic neurons are more vulnerable to hearing impairment due to their high metabolic demands when compared to glutamatergic neurons. This high energy demand might lead to the production and accumulation of a large amount of ROS as a consequence of excessive ATP production in the electron transport chain of their mitochondria. Consequently, the ability to remove the intracellular excess of ROS might be impaired, an issue that could lead to extensive damage in GABAergic neurons. Therefore, though this effect might happen mainly as a consequence of aging, similar mechanisms could play a role in noise-induced overexcitation.

This may be an additional explanation of why an increase in axonal density 1d after noise exposure can be produced without a decrease of VGAT. Additional metabolic imbalances happening in GABAergic neurons together with a peripheral deafferentation might also explain this phenomenon. Nevertheless, these considerations must be extensively investigated in future studies in order to extract reliable conclusions.

4.5. CURRENT LIMITATIONS IN THE STUDY OF NOISE-INDUCED VNTT AND AXONAL DENSITY CHANGES

As described in the last few sections, an increase in axonal connectivity 1d after noise exposure could not be associated to changes in VNTT expression, even if a clear elevation of HT was detected. In this regard, some limitations must be taken into account in order to understand the data derived from these experiments.

4.5.1. Moderate noise exposure under MR acquisition: Possible effects on neurotransmission and synaptic activity

DTI and 1H MRS are both useful tools for analyzing connectivity and metabolic changes in the CNS. Some studies successfully reported changes in connectivity as well as in glutamate and GABA in higher auditory and non-auditory structures of the CNS after hearing loss or tinnitus. However, they were performed using either human models or *in vitro* animal models, as animals were sacrificed before the acquisition in the MRI scan (Aldhafeeri et al., 2012; Brozoski et al., 2012; Cacace & Silver, 2007; Gao et al., 2015; Husain et al., 2011; Isler et al., 2022; Kilicarslan et al., 2014; Leaver et al., 2016; Profant et al., 2013; Sedley et al., 2015). Up to the current knowledge, this is the first study in which neural tracts and/or glutamate and GABA concentration at different time points after noise exposure were measured *in vivo* using DTI and 1H MRS in mice inside a 7T MRI scanner. As discussed before, MRI-derived noise could be a potential influencing factor, leading to uneven results when compared to previous literature. Furthermore, results obtained from measuring MRI noise levels, summarized in Table 8, indicate that, in addition to the fact that mice were noise-exposed from 85 to 100 dB during approximately 30 minutes, the loudest sequences recorded were those related to DTI measurements. Therefore, though 1H MRS sequences are thought to emit silent MRI-derived noise, it is especially important to take into account that the 1H MRS techniques were carried out right after the DTI sequences were finished, and therefore, the loudness measured during the DTI sequences may have potentially influenced neurotransmitter levels in the auditory CNS, especially in the 90 dB and Ctrl groups. Supporting this hypothesis, the various cited literature which reported having detected changes using 1H MRS did not apply loud MRI acquisition sequences. Furthermore, Niu et al. (2013) detected an increase in the firing rates of neurons in the IC after exposing mice to 105 dB SPL (20kHz) for only 30 minutes, and Salvi et al. (1990) detected an increase in the amplitudes of auditory evoked potentials after similar noise exposure treatments. Therefore, these results indicate that similar noise exposure treatments may lead to a transient change in the excitatory/inhibitory balance of the IC. Therefore, similar excitatory and inhibitory imbalances could transiently happen in the Ctrl groups when compared to the 115 dB and 90 dB-exposed mice due to a sudden response of the CNS in order to adapt to loud DTI sequences. This might lead to unobservable VNTT changes between those groups. Additionally, perfusion and sacrifice of the animals was performed immediately after the end of the MRI image acquisition in order to maintain the physiological state of the animals and achieve a representative histological picture of the functional changes investigated during the MRI acquisition. For this reason, the histological data must reflect the physiological status of the animals during MRI image acquisition.

Furthermore, as discussed before, a third ABR audiometry measurement was not performed directly after the MRI measurements due to the intrinsic objectives of the present study, as this would have affected the physiological status of the animals, and no correlation would have been possible to be established between the MRI and histological measures. Thus, it was not possible to assess the impact of MRI-derived noise on changes in HT and auditory function. Therefore, the present results might suggest that adaptative neurotransmission changes as a consequence of moderate-to-loud noise overstimulation could happen in the central auditory pathway during noisy MRI scans. However, this hypothesis could not be concluded from the current data, as no testing of the hearing function was performed after MRI scans. This possibility remains open for deep evaluation in future studies.

Nevertheless, this hypothesis does not necessarily contradict the observation of an elevated neurofilament density 1d after noise exposure. Though axonal growth can be observed 1d post-exposure, it is difficult to think that a moderate exposure in the MRI could elicit those changes either during the measurement or during the first moments after the MRI acquisition finished. In addition, the mice were immediately sacrificed after MRI acquisition, and therefore, one would think it not likely that momentary changes in glutamatergic and GABAergic imbalances as a consequence of MRI noise could produce extensive changes in axonal density in such a narrow time-frame. Excitatory and inhibitory imbalances derived from MRI may only reflect a transient adaptative response of the central auditory system to induced noise, without probably leading to acute hearing impairment in the 90 dB and Ctrl groups or to axonal sprouting events. On the other hand, though MRI-derived noise could have an influence on neuronal cell density, it is also hard to extract reliable conclusions from the present study about its potential influence on it. Equally, it seems difficult to expect that a potential immediate neuronal cell loss could occur after the discussed exposures, but this hypothesis cannot be rejected from the current observations. For this reason, MRI noise limitations might be extensively considered when understanding the results reported by the present study, and this raises many important questions about MRI applicability in the study of NIHL.

4.5.2. Fluorescence intensity quantification: high variability in data distribution

First, a high degree of variability and a widespread data distribution was observed during the analysis of the performed FI measurements. This effect could be, in the first place, related to differences in noise susceptibility between different experimental mice. Important differences in auditory responsiveness have been reported as a consequence of different factors such as age, sex,

stress, differential gene expression, hormonal imbalances or even due to different circadian rhythms in both animal and human models (Caras, 2013; Henderson et al., 1993; Kiefer et al., 2022; Meltser et al., 2013; Nolan, 2020; Yang et al., 2015). Thus, differences in FI measurements may arise as a consequence of differences in responsiveness to auditory stimuli, which might be translated into structural and functional interindividual differences within the central auditory system. Nevertheless, although it is well known that fluorescence microscopy is a critical tool in biological research, it should be acknowledged that many biological and/or methodological factors could influence FI measurements. Therefore, the observed data distribution might be partially related to methodological aspects intrinsically associated to the current techniques performed. Implementing quantitative fluorescence microscopy imaging protocols could be a laborious process in order to accurately monitor the biological mechanism desired to be investigated. Extensive factors such as photobleaching, phototoxicity, differences in fluorophore excitation, background noise, differences in antibody binding and incubation solution properties, histological artifacts and image acquisition differences can influence FI measurements greatly (Im et al., 2019; Verdaasdonk et al., 2014; Waters & Wittmann, 2014).

In the current study, all efforts were taken in order to minimize differences in FI due to methodological artifacts through the standardizing of sample preparation, image acquisition and image analysis setup, applied with the aim to maximize signal-to-noise ratio (SNR) and avoid photobleaching during the entire process. Widefield microscopy was then selected due to its large advantages in optimizing imaging workflow during imaging sessions. Nevertheless, it is important to notice that significant out-of-focus fluorescence was measured using this technique when compared to Confocal microscopy, which could compromise the SNR obtained. Moreover, using confocal microscopy, images in more than one focal plane can be acquired. This technique can acquire more data from a large tissue area, an issue that may avoid differences in FI if proteins are non-homogeneously distributed in biological tissues (Waters, 2009; Waters & Wittmann, 2014). The application of those techniques may lead to differing results, an issue evidenced by the controversial previously discussed results from Heeringa et al. (2016), Kurioka et al. (2016) and Zeng et al. (2009). Therefore, it is possible to consider that neurofilament density changes happening at later time points after noise exposure (7d, 56d or 84d) could not be detected due to the sensitivity of the techniques performed in the present study. Equally, a reduced sensitivity due to high variability may also hinder the observation of neurofilament density differences, especially in the CIC between the 115dB and Ctrl groups 1d after noise exposure. In this regard, the

implementation of additional imaging techniques and/or new methodologies in further experiments might help to expand the knowledge presented by the current work.

Finally, as shown in previous sections (see Table 7), though a low sample size was collected in order to extract statistical inferences, variability might have probably originated from methodological and/or physiological differences intrinsically detected by the method itself. From our observations, external influences such as the performance of staining on different days would not have a profound effect on the variability observed. Nevertheless, these observations could not allow us to conclude if this variability is produced by methodological or physiological influences, or both. Due to the observed data distribution, it is reasonable to think that a combination of both kinds of influences could affect the present results. For that reason, further research must be made to clarify the main origin of this pronounced variability.

4.5.3. Sex influences in the study of noise-induced neuroplasticity

Additionally, in contrast to previous studies in which both sexes were equally represented (Basta et al., 2005; Gröschel et al., 2010), more females than males were included into the experimental design. This effect must be particularly taken into account, as different studies report sex-dependent differences in auditory physiology and the susceptibility to noise between males and females. These effects are mainly explained by the effects of estrogen signaling in the mammalian auditory system (Caras, 2013; Villavisanis et al., 2020; Lauer & Schrode, 2017; Milon et al., 2018). Shuster et al. (2021) described a protective effect from acute noise exposure in the peripheral auditory system exerted by estradiol in female mice. Findings made by Meltser et al. (2008) and Simonoska et al. (2009) suggested that this protective effect might be mediated at least by the expression of estrogen receptor-β (ERβ). Interestingly, although the exact mechanism is not clear, it has been shown that ERβ signaling can regulate the activation of apoptotic pathways through its action on apoptosis-related molecules like caspase-3 (Yang et al., 2019). In this regard, there are evidences for both the apoptotic-suppressing or -inducing effects of estrogen receptors found in many cancer types (Chimento et al., 2022). As observed by Duong et al. (2020), these diverse roles of estrogenic effects on cell viability might depend fundamentally on the cellular environment. Moreover, Lewis-Wambi & Jordan (2009) described how the activation of different molecular pathways could explain these diverse estrogen functions in apoptotic regulation. Therefore, it must be taken into account that the biological processes described in the present study might be affected in a different manner between males and females, influencing neurodegeneration, neuroplasticity and neurotransmission in the auditory pathway.

4.6. FUTURE PERSPECTIVES IN THE STUDY OF NOISE-INDUCED NEURODEGENERATION AND NEUROPLASTICITY

First, the present work evidences the crucial role of the CNS in the NIHL pathophysiology. Nevertheless, there is an extremely important need to develop more specific and standardized methods for studying NIHL consequences in the central auditory pathway. Right now, different kinds of experimental approaches are being performed due to the lack of potential available tools that could predict, assess and quantify the damage produced in the CNS after prolonged loud noise exposure, and especially, during *in vivo* conditions. This represents an important threat against translating basic science into robust clinical practices (Wang et al., 2020). Some techniques such as optogenetics, deep brain stimulation or MRI are being investigated due to their potential for modulating and observing central changes in real time after noise exposure (Boyen et al., 2013; Janssen & Jahanshahi, 2022; Landgrebe et al., 2009; Sato et al., 2017). However, there is an important limiting frontier in trying to assess NIHL consequences on the cellular level. In addition, it was reviewed that there is no consensus when understanding which are the detailed molecular pathways implicated in NIHL related symptoms such as poor speech perception in noise, which are proposed to be mainly related to central nervous processing disorders. However, currently no treatment can completely reverse NIHL derived consequences, and prevention and awareness are the most effective strategies to date. For these reasons, future studies must move towards a better understanding of the biological mechanisms of NIHL in the CNS in order to develop preventive, diagnostic and treatment strategies.

05 CONCLUSION

During the present study, it was demonstrated that excessive loud noise exposure could induce a significant auditory threshold shift, which might be associated with changes within the central auditory pathway. Increases in axonal connectivity in the CIC and MGV were observed 1d post-exposure in high-noise exposed mice when compared to moderate and/or sham-exposed mice. These effects are related to noise-induced neuroplastic changes such as changes in neural activity, which possibly act as compensatory mechanisms in order to counteract traumatic events occurring in the inner ear. Interestingly, the existence of early CNS noise-induced neuroplastic changes directly after noise exposure has been demonstrated. Understanding how early axonal growth can occur might contribute to the understanding of noise-induced pathologies in the CNS. Furthermore, it could represent a potential target for developing novel diagnostic and therapeutic strategies. Nevertheless, profound cell loss and excitatory as well as inhibitory changes by means of VNTT expression were not observed. Those effects might be related to several intrinsic properties of newly implemented methodologies in order to observe changes in cell density or glutamatergic and GABAergic influences. Unfortunately, remarkably variable experimental approaches have been used in the field, which limits clear comparisons between different studies. Therefore, the current work highlights the important need for methodological standardization in the field in order to extract reliable conclusions about neurodegenerative and neuroplastic changes after noise exposure.

To conclude, the present work reported neuroplastic changes in the CNS after high-intensity noise exposure. This could help in the understanding of the underlying mechanisms of clinical sequelae induced by acoustic overstimulation such as tinnitus and poor speech understanding in noisy conditions.

06 BIBLIOGRAPHY

Aarnisalo, A. A., Pirvola, U., Liang, X. Q., Miller, J., & Ylikoski, J. (2000). Apoptosis in auditory brainstem neurons after a severe noise trauma of the organ of corti: Intracochlear GDNF treatment reduces the number of apoptotic cells. *Orl*, *62*(6), 330–334. doi: 10.1159/000027764

Abbott, S. D., Hughes, L. F., Bauer, C. A., Salvi, R., & Caspary, D. M. (1999). Detection of glutamate decarboxylase isoforms in rat inferior colliculus following acoustic exposure. *Neuroscience*, *93*(4), 1375–1381. doi: 10.1016/S0306-4522(99)00300-0

Akil, O., Oursler, A., Fan, K., & Lustig, L. (2016). Mouse Auditory Brainstem Response Testing. *Bio-Protocol*, *6*(6), 1–11. doi: 10.21769/bioprotoc.1768

Alberti, P. W. (1992). Noise induced hearing loss. *British Medical Journal*, *304*(6826), 522. doi: 10.1136/bmj.304.6826.522

Aldhafeeri, F. M., MacKenzie, I., Kay, T., Alghamdi, J., & Sluming, V. (2012). Neuroanatomical correlates of tinnitus revealed by cortical thickness analysis and diffusion tensor imaging. *Neuroradiology*, *54*(8), 883–892. doi: 10.1007/s00234-012-1044-6

Almasabi, F., Janssen, M. L. F., Devos, J., Moerel, M., Schwartze, M., Kotz, S. A., Jahanshahi, A., Temel, Y., & Smit, J. V. (2022). The role of the medial geniculate body of the thalamus in the pathophysiology of tinnitus and implications for treatment. *Brain Research*, *1779*, 147797. doi: 10.1016/J.BRAINRES.2022.147797

American Speech Language-Hearing Association. (2022). Effects of Hearing Loss on Development. accessed 11 July 2022, <https://www.asha.org/public/hearing/effects-of-hearing-loss-on-development>

Anderson, L. A., & Linden, J. F. (2011). Physiological differences between histologically defined subdivisions in the mouse auditory thalamus. *Hearing Research*, *274*(1–2), 48–60. doi: 10.1016/j.heares.2010.12.016

Barker, M., Solinski, H. J., Hashimoto, H., Tagoe, T., Pilati, N., & Hamann, M. (2012). Acoustic overexposure increases the expression of VGLUT-2 mediated projections from the lateral vestibular nucleus to the dorsal cochlear nucleus. *PLoS ONE*, *7*(5). doi: 10.1371/journal.pone.0035955

Bartolomé, M.V., Ibáñez, M.A,, López-Sánchez, J.G., Merchán-Pérez, A., Gil-Loyzaga, P. Synaptophysin immunoreactivity in the cochlear nuclei of mammals: a comparative study. *J Otorhinolaryngol Relat Spec*, *55*(6), 317-21. doi: 10.1159/000276447

Basner, M., Babisch, W., Davis, A., Brink, M., Clark, C., Janssen S, Stansfeld S. (2014). Auditory and non-auditory effects of noise on health. *Lancet*, *383*(9925), 1325-1332. doi: 10.1016/S0140-6736(13)61613-X.

Basta, D., & Ernest, A. (2004). Noise-induced changes of neuronal spontaneous activity in mice inferior colliculus brain slices. *Neuroscience Letters*, *368*(3), 297–302. doi: 10.1016/j.neulet.2004.07.030

Basta, D., Tzschentke, B., & Ernst, A. (2005). Noise-induced cell death in the mouse medial geniculate body and primary auditory cortex. *Neuroscience Letters*, *381*(1–2), 199–204. doi: 10.1016/j.neulet.2005.02.034

Beam, A. S., Moore, K., Berry, S. D., Brown, L., Smith S., Wilcher A., Bibbs A., Beemon I. (2021) An Investigation of MR Imaging Scanner Noise and its Effect on Technologists. *Radiol Technol*, *92*(6), 568-576

Benson, C. G., Gross, J. S., Suneja, S. K., & Potashner, S. J. (1997). Synaptophysin immunoreactivity in the cochlear nucleus after unilateral cochlear or ossicular removal. *Synapse*, *25*(3), 243–257. doi: 10.1002/(SICI)1098-2396(199703)25:3<243::AID-SYN3>3.0.CO;2-B

Berger, J. I., & Coomber, B. (2015). Tinnitus-related changes in the inferior colliculus. *Frontiers in Neurology*, *6*(3), 1–12. doi: 10.3389/fneur.2015.00061

Bilak, M., Kim, J., Potashner, S. J., Bohne, B. A., & Morest, D. K. (1997). New growth of axons in the cochlear nucleus of adult chinchillas after acoustic trauma. *Experimental Neurology*, *147*(2), 256–268. doi: 10.1006/exnr.1997.6636

Boero, L. E., Payne, S., Gómez-Casati, M. E., Rutherford, M. A., & Goutman, J. D. (2021). Noise Exposure Potentiates Exocytosis From Cochlear Inner Hair Cells. *Frontiers in Synaptic Neuroscience*, *13*(9). doi: 10.3389/fnsyn.2021.740368

Boyen, K., Langers, D. R. M., de Kleine, E., & van Dijk, P. (2013). Gray matter in the brain: Differences associated with tinnitus and hearing loss. *Hearing Research*, *295*, 67–78. doi: 10.1016/j.heares.2012.02.010

Fyk-Kolodziej, B., Shimano, T., Gong, T.W., Holt, A.G. (2011). Vesicular Glutamate Transporters: Spatio-Temporal Plasticity following Hearing Loss. *Neuroscience*, *178*(5), 218–239. doi: 10.1016/j.neuroscience.2010.12.059

Brinkmann, P., Kotz, S. A., Smit, J. V., Janssen, M. L. F., & Schwartze, M. (2021). Auditory thalamus dysfunction and pathophysiology in tinnitus: a predictive network hypothesis. *Brain Structure and Function*, *226*(6), 1659–1676. doi: 10.1007/s00429-021-02284-x

Brookhouser, P. E., Gorga, M. P., & Kelly, W. J. (1990). Auditory brainstem response results as predictors of behavioral auditory thresholds in severe and profound hearing impairment. *Laryngoscope*, *100*(8), 8803–810. doi: 10.1288/00005537-199008000-00002

Browne, C. J., Morley, J. W., & Parsons, C. H. (2012). Tracking the expression of excitatory and inhibitory neurotransmission-related proteins and neuroplasticity markers after noise induced hearing loss. *PLoS ONE*, *7*(3). doi: 10.1371/journal.pone.0033272

Brozoski, T. J., Bauer, C. A., & Caspary, D. M. (2002). Elevated fusiform cell activity in the dorsal cochlear nucleus of chinchillas with psychophysical evidence of tinnitus. *Journal of Neuroscience*, *22*(6), 2383–2390. doi: 10.1523/jneurosci.22-06-02383.2002

Brozoski, T. J., Odintsov, B., & Bauer, C. (2012). Gamma-aminobutyric acid and glutamic acid levels in the auditory pathway of rats with chronic tinnitus: A direct determination using high resolution point-resolved proton magnetic resonance spectroscopy (1H-MRS). *Frontiers in Systems Neuroscience*, *6*(2), 1–12. doi: 10.3389/fnsys.2012.00009

Buras, E. D., Holt, A. G., Griffith, R. D., Asako, M., & Altschuler, R. A. (2006). Changes in Glycine Immunoreactivity in the Rat Superior Olivary Complex Following Deafness. *J Comp Neurol.*, *494*(1), 179–189. doi: 10.1002/cne.20795

Cacace, A. T., & Silver, S. M. (2007). Applications of magnetic resonance spectroscopy to tinnitus research: initial data, current issues, and future perspectives. *Progress in Brain Research*, *166*, 71–81. doi: 10.1016/S0079-6123(07)66007-5

Cai, R., Kalappa, B. I., Brozoski, T. J., Ling, L. L., & Caspary, D. M. (2014). Is GABA neurotransmission enhanced in auditory thalamus relative to inferior colliculus? *Journal of Neurophysiology*, *111*(2), 229–238. doi: 10.1152/jn.00556.2013

Çakır, A., Ecevit, M. C., Bal, R., Gürkan, S., Alpay, H. C., & Şerbetçioğlu, M. B. (2015). Assessment of synaptic plasticity via long-term potentiation in young mice on the day after acoustic trauma: Implications for tinnitus. *Journal of International Advanced Otology*, *11*(3), 196–201. doi: 10.5152/iao.2015.1047

Caras, M. L. (2013). Estrogenic modulation of auditory processing: A vertebrate comparison. *Frontiers in Neuroendocrinology*, *34*(4), 285–299. doi: 10.1016/j.yfrne.2013.07.006

Caspary, D. M., Ling, L., Turner, J. G., Hughes, L. F. (2008). Inhibitory neurotransmission, plasticity and aging in the mammalian central auditory system. *J Exp Biol*, *211*(11), 1781-91. doi: 10.1242/jeb.013581.

Caspary, D. M., Llano, D. A. (2017) Auditory thalamic circuits and $GABA_A$ receptor function: Putative mechanisms in tinnitus pathology. *Hear Res*, *349*,197-207. doi: 10.1016/j.heares.2016.08.009.

Centers for Disease Control and Prevention. (2021). Preventing Noise-Induced Hearing Loss, accessed 11 July 2022, <https://www.cdc.gov/ncbddd/hearingloss/noise.html>

Chang, H., Chen, K., Kaltenbach, J. A., Zhang, J., & Godfrey, D. A. (2002). Effects of acoustic trauma on dorsal cochlear nucleus neuron activity in slices. *Hearing Research*, *164*(1–2), 59–68. doi: 10.1016/S0378-5955(01)00410-5

Chen, C., Cheng, M., Ito, T., & Song, S. (2018). Neuronal organization in the inferior colliculus revisited with cell-type-dependent monosynaptic tracing. *Journal of Neuroscience*, *38*(13), 3318–3332. doi: 10.1523/JNEUROSCI.2173-17.2018

Chen, G. D., Sheppard, A., & Salvi, R. (2016). Noise trauma induced plastic changes in brain regions outside the classical auditory pathway. *Neuroscience*, *315*(12), 228–245. doi: 10.1016/j.neuroscience.2015.12.005

Chen, Z., Ulfendahl, M., Ruan, R., Tan, L., & Duan, M. (2004). Protection of auditory function against noise trauma with local caroverine administration in guinea pigs. *Hearing Research*, *197*(1–2), 131–136. doi: 10.1016/j.heares.2004.03.021

Chimento, A., De Luca, A., Avena, P., De Amicis F., Casaburi I., Sirianni R., Pezzi V. Estrogen Receptors-Mediated Apoptosis in Hormone-Dependent Cancers. *Int J Mol Sci*, 23(3), 1242. doi: 10.3390/ijms23031242

Clopton, B. M., & Spelman, F. A. (2003). Auditory system. *Biomedical Imaging*, 5-1-5–13. doi: 10.1201/b17094-23

Cook, J. A., Barry, K. M., Zimdahl, J. W., Leggett, K., & Mulders, W. H. A. M. (2021). Spontaneous firing patterns in the medial geniculate nucleus in a guinea pig model of tinnitus. *Hearing Research*, *403*, 108190. doi:10.1016/j.heares.2021.108190

Coordes, A., Gröschel, M., Ernst, A., & Basta, D. (2012). Apoptotic cascades in the central auditory pathway after noise exposure. *Journal of Neurotrauma*, *29*(6), 1249–1254. doi: 10.1089/neu.2011.1769

Coskun, O. (2011). Magnetic resonance imaging and safety aspects. *Toxicology and Industrial Health*, *27*(4), 307–313. doi: 10.1177/0748233710386413

Counter, S. A., Olofsson, A., Grahn, H. F., & Borg, E. (1997). MRI acoustic noise: Sound pressure and frequency analysis. *Journal of Magnetic Resonance Imaging*, *7*(3), 606–611. doi: 10.1002/jmri.1880070327

Dallos, P., & Harris, D. (1978). Properties of auditory nerve responses in absence of outer hair cells. *Journal of Neurophysiology*, *41*(2), 365–383. doi: 10.1152/jn.1978.41.2.365

Daniel, E. (2007). Noise and hearing loss: A review. *Journal of School Health*, *77*(5), 225–231. doi: 10.1111/j.1746-1561.2007.00197

Dawes, P., Cruickshanks, K.J., Fischer, M.E., Klein, B.E., Klein, R., Nondahl, D.M. (2015). Hearing aid use and long-term health outcomes: hearing handicap, mental health, social engagement, cognitive function, physical health and mortality. *Int J Audiol.*, *54*(1), 838–844. doi: 10.3109/14992027.2015.1059503.

Dehmel, S., Pradhan, S., Koehler, S., Bledsoe, S., & Shore, S. (2012). Noise overexposure alters long-term somatosensory-auditory processing in the dorsal cochlear nucleus-possible basis for tinnitus-related

hyperactivity? *Journal of Neuroscience*, *32*(5), 1660–1671. doi: 10.1523/JNEUROSCI.4608-11.2012

Delhez, A., Lefebvre, P., Péqueux, C., Malgrange, B., & Delacroix, L. (2020). Auditory function and dysfunction: estrogen makes a difference. *Cellular and Molecular Life Sciences*, *77*(4), 619–635. doi: 10.1007/s00018-019-03295-y

Dewey, R. S., Hall, D. A., Guest, H., Prendergast, G., Plack, C. J., & Francis, S. T. (2018). The physiological bases of hidden noise-induced hearing loss: Protocol for a functional neuroimaging study. *JMIR Research Protocols*, *7*(3). doi: 10.2196/resprot.9095

Ding-Pfennigdorff, D., Smolders, J. W. T., Müller, M., & Klinke, R. (1998). Hair cell loss and regeneration after severe acoustic overstimulation in the adult pigeon. *Hearing Research*, *120*(1–2), 109–120. doi: 10.1016/S0378-5955(98)00055-0

Ding, T., Yan, A., & Liu, K. (2019). What is noise-induced hearing loss? *British Journal of Hospital Medicine*, *80*(9), 525–529. doi: 10.12968/hmed.2019.80.9.525

Dobie, R. A. (2003). Depression and tinnitus. *Otolaryngologic Clinics of North America*, *36*(2), 383–388. doi: 10.1016/S0030-6665(02)00168-8

Dong, S., Rodger, J., Mulders, W. H. A. M., & Robertson, D. (2010). Tonotopic changes in GABA receptor expression in guinea pig inferior colliculus after partial unilateral hearing loss. *Brain Research*, *1342*, 24–32. doi: 10.1016/j.brainres.2010.04.067

Dong, Songyu, Mulders, W. H. A. M., Rodger, J., Woo, S., & Robertson, D. (2010). Acoustic trauma evokes hyperactivity and changes in gene expression in guinea-pig auditory brainstem. *European Journal of Neuroscience*, *31*(9), 1616–1628. doi: 10.1111/j.1460-9568.2010.07183

Duan, M., Chen, Z., Qiu, J., Ulfendahl, M., Laurell, G., Borg, E., & Ruan, R. (2006). Low-dose, long-term caroverine administration attenuates impulse noise-induced hearing loss in the rat. *Acta Oto-Laryngologica*, *126*(11), 1140–1147. doi: 10.1080/00016480500540519

Duong, P., Tenkorang, M. A. A., Trieu, J., McCuiston, C., Rybalchenko, N., & Cunningham, R. L. (2020). Neuroprotective and neurotoxic outcomes of androgens and estrogens in an oxidative stress environment. *Biology of Sex Differences*, *11*(1), 1–18. doi: 10.1186/s13293-020-0283-1

Durham, D., Park, D. L., & Girod, D. A. (2000). Central nervous system plasticity during hair cell loss and regeneration. *Hearing Research*, *147*(1–2), 145–159. doi: 10.1016/S0378-5955(00)00128-3

Eccles, J. C. (1983). Calcium in long-term potentiation as a model for memory. *Neuroscience*, *10*(4), 1071–1081. doi: 10.1016/0306-4522(83)90100-8

Eggermont J. J. (2019). Auditory brainstem response. *Handb Clin Neurol*, 160, 451-464. doi: 10.1016/B978-0-444-64032-1.00030-88

Eggermont, J. J. (2006). Cortical tonotopic map reorganization and its implications for treatment of tinnitus. *Acta Oto-Laryngologica*, *126*, 9–12. doi: 10.1080/03655230600895259

Eggermont, J. J., & Roberts, L. E. (2004). The neuroscience of tinnitus. *Trends in Neurosciences*, *27*(11), 676–682. doi: 10.1016/j.tins.2004.08.010

Elmore S. (2007). Apoptosis: A Review of Programmed Cell Death. *Toxicol Pathol*, *35*(4), 495–516.

Eriksen, J., Li, F., & Edwards, R. H. (2021). *The Mechanism and Regulation of Vesicular Glutamate Transport: Coordination with the Synaptic Vesicle Cycle*. 1–21. doi: 10.1016/j.bbamem.2020.183259.

Fetoni, A. R., Paciello, F., Rolesi, R., Eramo, S. L. M., Mancuso, C., Troiani, D., & Paludetti, G. (2015). Rosmarinic acid up-regulates the noise-activated Nrf2/HO-1 pathway and protects against noise-induced injury in rat cochlea. *Free Radical Biology and Medicine*, *85*, 269–281. doi: 10.1016/j.freeradbiomed.2015.04.021

Fligor, B.J., Levey, S., Levey, T. (2014). Cultural and Demographic Factors Influencing Noise Exposure Estimates From Use of Portable Listening Devices in an Urban Environment. *Journal of Speech, Language, and Hearing Research*, *1*(4), 164–173. doi: 10.1044/2014

Franklin, S. R., Brunso-Bechtold, & Henkel, C. K. (2006). Unilateral Cochlear Ablation Before Hearing Onset Lateral Lemniscus Projection Patterns in the Rat. *Neuroscience*, *143*(1), 105–115. doi: 10.1016/j.neuroscience.2006.07.039

Fröhlich, F., Basta, D., Strübing, I., Ernst, A., & Gröschel, M. (2017). Time course of cell death due to acoustic overstimulation in the mouse medial geniculate body and primary auditory cortex. *Noise & Health*, *19*(88), 133. doi: 10.4103/NAH.NAH_10_17

Fröhlich, F., Ernst, A., Strübing, I., Basta, D., & Gröschel, M. (2017). Apoptotic mechanisms after repeated noise trauma in the mouse medial geniculate body and primary auditory cortex. *Experimental Brain Research*, *235*(12), 3673–3682. doi: 10.1007/s00221-017-5091-4

Fröhlich, F., Gröschel, M., Strübing, I., Ernst, A., & Basta, D. (2018). Apoptosis in the Cochlear Nucleus and Inferior Colliculus Upon Repeated Noise Exposure. *Noise & Health*, *20*(97), 223. doi: 10.4103/NAH.NAH_30_18

Frye, M. D., Ryan, A. F., & Kurabi, A. (2019). Inflammation associated with noise-induced hearing loss. *The Journal of the Acoustical Society of America*, *146*(5), 4020–4032. doi: 10.1121/1.5132545

Fujimoto, H., Notsu, E., Yamamoto, R., Ono, M., Hioki, H., & Delano, P. H. (2021). *Positive Domains on Dendrites in the Mouse Medial Geniculate Body Receive Ascending Excitatory and Inhibitory Inputs Preferentially From the Inferior Colliculus*. *15*(September), 1–15. doi: 10.3389/fnins.2021.740378

Gao, F., Wang, G., Ma, W., Ren, F., Li, M., Dong, Y., Liu, C., Liu, B., Bai, X., Zhao, B., & Edden, R. A. E. (2015). Decreased auditory GABA+ concentrations in presbycusis demonstrated by edited magnetic resonance spectroscopy. *NeuroImage*, *106*, 311–316. doi: 10.1016/j.neuroimage.2014.11.023

Giavarina, D. (2014). Understanding Bland Altman Analysis. *Past, Present, and Future of Statistical Science*, *25*(2), 335–347. doi: 10.1201/b16720-37

Gil-Loyzaga, P. (1998). Synaptophysin immunoreactivity in the cat cochlear nuclei. *Histology and Histopathology*, *13*(2), 415–424. doi: 10.1159/000276447

Godfrey, D. A., Kaltenbach, J. A., Chen, K., Ilyas, O., Liu, X., Licari, F., Sacks, J., & Mcknight, D. (2012). Amino acid concentrations in the hamster central auditory system and long-term effects of intense tone exposure. *Journal of Neuroscience Research*, *90*(11), 2214–2224. doi: 10.1002/jnr.23095

Gopinath, B., McMahon, C., Tang, D., Burlutsky, G., & Mitchell, P. (2021). Workplace noise exposure and the prevalence and 10-year incidence of age-related hearing loss. *PLoS ONE*, *16*(7), 1–10. doi: 10.1371/journal.pone.0255356

Greenwood, S. M., Connolly, C. N. Dendritic and mitochondrial changes during glutamate excitotoxicity. *Neuropharmacology*, *53*(8), 891-8. doi: 10.1016/j.neuropharm.2007.10.003

Gröschel, M., Basta, D., Ernst, A., Mazurek, B., & Szczepek, A. J. (2018). Acute noise exposure is associated with intrinsic apoptosis in murine central auditory pathway. *Frontiers in Neuroscience*, *12*, 312. doi: 10.3389/fnins.2018.00312

Gröschel, M., Götze, R., Ernst, A., & Basta, D. (2010). Differential impact of temporary and permanent noise-induced hearing loss on neuronal cell density in the mouse central auditory pathway. *Journal of Neurotrauma*, *27*(8), 1499–1507. doi: 10.1089/neu.2009.1246

Gröschel, M., Müller, S., Götze, R., Ernst, A., & Basta, D. (2011). The possible impact of noise-induced Ca2+-dependent activity in the central auditory pathway: A manganese-enhanced MRI study. *NeuroImage*, *57*(1), 190–197. doi: 10.1016/j.neuroimage.2011.04.022

Gröschel, M., Ryll, J., Götze, R., Ernst, A., & Basta, D. (2014). Acute and long-term effects of noise exposure on the neuronal spontaneous activity in cochlear nucleus and inferior colliculus brain slices. *BioMed Research International*, *2014*, 909260. doi: 10.1155/2014/909260

Gunes, C. M., Gunes, M. S., Vural, A., Aybuga, F., Bayram, A., Bayram, K. K., Sahin, M. I., Dogan, M. E., Ozdemir, S. Y., & Ozkul, Y. (2021). Change in gene expression levels of GABA, glutamate and neurosteroid pathways due to acoustic trauma in the cochlea. *Journal of Neurogenetics*, *35*(1), 45–57. doi: 10.1080/01677063.2021.1904922

Gusel'nikova, V. V., & Korzhevskiy, D. E. (2015). NeuN as a neuronal nuclear antigen and neuron differentiation marker. *Acta Naturae*, *7*(2), 42–47. doi: 10.32607/20758251-2015-7-2-42-47

Habib, S. H., & Habib, S. S. (2021). Auditory brainstem response: An overview of neurophysiological implications and clinical applications -A Narrative Review. *Journal of the Pakistan Medical Association*, *71*(9), 2230–2236. doi: 10.47391/JPMA.03-432

Hackett, T. A. (2011). VGLUT1 and VGLUT2 mRNA expression in the primate auditory pathway. *Hear Res.*, *274 (1-2)*, 129–141. doi: 10.1016/j.heares.2010.11.001.VGLUT1

Hakuba, N., Koga, K., Gyo, K., Usami, S. I., & Tanaka, K. (2000). Exacerbation of noise-induced hearing loss in mice lacking the glutamate transporter GLAST. *Journal of Neuroscience*, *20*(23), 8750–8753. doi: 10.1523/jneurosci.20-23-08750.2000

Heeringa, A. N., & van Dijk, P. (2014). The dissimilar time course of temporary threshold shifts and reduction of inhibition in the inferior colliculus following intense sound exposure. *Hearing Research*, *312*, 38–47. doi: 10.1016/j.heares.2014.03.004

Heeringa, A. N., Amarins, N., Wu, C., Chung, C., West, M., Martel, D., Liberman, L., Liberman, M. C., & Shore, S. E. (2018). Glutamatergic Projections to the Cochlear Nucleus are Redistributed in Tinnitus. *Neuroscience*, *391*, 91–103. doi: 10.1016/j.neuroscience.2018.09.008.Glutamatergic

Heeringa, A. N., Stefanescu RA, Raphael Y, Shore SE. Altered vesicular glutamate transporter distributions in the mouse cochlear nucleus following cochlear insult (2016). *Neuroscience*, 315, 114-24. doi: 10.1016/j.neuroscience.2015.12.009.

Henderson, E., Testa, M.A., Hartnick, C. (2017). Prevalence of noise-induced hearing-threshold shifts and hearing loss among US youths. *Pediatrics*, *127*(1), 39-46. doi: 10.1542/peds.2010-0926

Henderson, D., Bielefeld, E. C., Harris, K. C., & Hu, B. H. (2006). The role of oxidative stress in noise-induced hearing loss. *Ear and Hearing*, *27*(1), 1–19. doi: 10.1097/01.aud.0000191942.36672.f3

Henderson, D., Subramaniam, M., & Boettcher, F. A. (1993). Individual susceptibility to noise-induced hearing loss: An old topic revisited. *Ear and Hearing*, *14*(3), 152–168. doi: 10.1097/00003446-199306000-00002

Henry, J. (2013). Springer Handbook of Auditory Research, *International Journal of Audiology*, *52*(3), 207, doi: 10.3109/14992027.2012.754109

Hesse, G., Kastellis, G.. (2019). Hidden hearing loss-damage to hearing processing even with low-threshold noise exposure?. *Hno*, *67*(6), 417-424. doi: 10.1007/s00106-019-0640-8

Hickman, T. T., Hashimoto, K., Liberman, L. D., & Liberman, M. C. (2020). Synaptic migration and reorganization after noise exposure suggests regeneration in a mature mammalian cochlea. *Scientific Reports*, *10*(1), 1–14. doi: 10.1038/s41598-020-76553-w

Hickox, A. E., & Liberman, M. C. (2014). Is noise-induced cochlear neuropathy key to the generation of hyperacusis or tinnitus? *Journal of Neurophysiology*, *111*(3), 552–564. doi: 10.1152/jn.00184.2013

Hildebrandt, H., Hoffmann, N. A., & Illing, R. B. (2011). Synaptic reorganization in the adult rat's ventral cochlear nucleus following its total sensory deafferentation. *PLoS ONE*, *6*(8). doi: 10.1371/journal.pone.0023686

Hong, O. S., Kerr, M. J., Poling, G. L., & Dhar, S. (2013). Understanding and preventing noise-induced hearing loss. *Disease-a-Month*, *59*(4), 110–118. doi: 10.1016/j.disamonth.2013.01.002

Hong, Y., Shao, A. W., Wang, J., Chen, S., Wu, H. J., McBride, D. W., Wu, Q., Sun, X. J., & Zhang, J. M. (2014). Neuroprotective effect of hydrogen-rich saline against neurologic damage and apoptosis in early brain injury following subarachnoid hemorrhage: Possible role of the Akt/GSK3β signaling pathway. *PLoS ONE*, *9*(4). doi: 10.1371/journal.pone.0096212

Honkura, Y., Matsuo, H., Murakami, S., Sakiyama, M., Mizutari, K., Shiotani, A., Yamamoto, M., Morita, I., Shinomiya, N., Kawase, T., Katori, Y., & Motohashi, H. (2016). NRF2 is a key target for prevention of noise-induced hearing loss by reducing oxidative damage of cochlea. *Scientific Reports*, *6*(9), 1–2. doi: 10.1038/srep19329

Hu, N., Rutherford, M. A., & Green, S. H. (2020). Protection of cochlear synapses from noise-induced excitotoxic trauma by blockade of Ca2+-permeable AMPA receptors. *Proceedings of the National Academy of Sciences of the United States of America*, *117*(7), 3828–3838. doi: 10.1073/pnas.1914247117

Huffman, R. F., & Henson, O. W. (1990). The descending auditory pathway and acousticomotor systems: connections with the inferior colliculus. *Brain Research Reviews*, *15*(3), 295–323. doi: 10.1016/0165-0173(90)90005-9

Husain, F. T., Medina, R. E., Davis, C. W., Szymko-bennett, Y., Simonyan, K., Pajor, N. M., & Horwitz, B. (2011). Neuroanatomical Changes due to Hearing Loss and Chronic Tinnitus: A Combined VBM and DTI Study. *Brain Res,* 74–88. doi: 10.1016/j.brainres.2010.10.095.

Ibrahim, B. A., & Llano, D. A. (2019). Aging and central auditory disinhibition: Is it a reflection of homeostatic downregulation or metabolic vulnerability? *Brain Sciences*, *9*(12). doi: 10.3390/brainsci9120351

Illing, R. B., Horváth, M. (1995). Re-emergence of GAP-43 in cochlear nucleus and superior olive following cochlear ablation in the rat. *Neurosci Lett, 194*(1-2), 9-12. doi: 10.1016/0304-3940(95)11706-3

Illing, R. B., Horváth, M., & Laszig, R. (1997). Plasticity of the auditory brainstem: Effects of cochlear ablation on GAP-43 immunoreactivity in the rat. *Journal of Comparative Neurology*, *382*(1), 116–138. doi: 10.1002/(SICI)1096-9861(19970526)382:1<116::AID-CNE8>3.0.CO;2-4

Illing, R. B., Kraus, K. S., & Meidinger, M. A. (2005). Reconnecting neuronal networks in the auditory brainstem following unilateral deafening. *Hearing Research*, *206*(1–2), 185–199. doi: 10.1016/j.heares.2005.01.016

Imam, L., & Alam Hannan, S. (2017). Noise-induced hearing loss: A modern epidemic? *British Journal of Hospital Medicine*, *78*(5), 286–290. doi: 10.12968/hmed.2017.78.5.286

Isler, B., von Burg, N., Kleinjung, T., Meyer, M., Stämpfli, P., Zölch, N., & Neff, P. (2022). Lower glutamate and GABA levels in auditory cortex of tinnitus patients: a 2D-JPRESS MR spectroscopy study. *Scientific Reports*, *12*(1), 1–14. doi: 10.1038/s41598-022-07835-8

Ito, T., & Oliver, D. L. (2010). Origins of glutamatergic terminals in the inferior colliculus identified by retrograde transport and expression of VGLUT1 and VGLUT2 genes. *Frontiers in Neuroanatomy*, *4*(9), 1–11. doi: 10.3389/fnana.2010.00135

Ito, T., Bishop, D. C., & Oliver, D. L. (2009). Two classes of GABAergic neurons in the inferior colliculus. *Journal of Neuroscience*, *29*(44), 13860–13869. doi: 10.1523/JNEUROSCI.3454-09.2009

Ito, T., Bishop, D. C., Oliver, D. L. (2011). Expression of Glutamate and Inhibitory Amino Acid Vesicular Transporters in the Rodent Auditory Brainstem. *J Comp. Neurol.*, *519*(2), 316–340. doi: 10.1002/cne.22521.

Ito, T., Bishop, D. C., Oliver, D. L. (2016). Functional organization of the local circuit in the inferior colliculus. *Anat Sci Int.*, *91*(1), 22–34. doi: 10.1007/s12565-015-0308-8

Ito, T., Oliver D. L. (2012). The basic circuit of the IC: tectothalamic neurons with different patterns of synaptic organization send different messages to the thalamus. *Front Neural Circuits*. 26, *6*(48). doi: 10.3389/fncir.2012.00048.

Izquierdo, M. A., Gutiérrez-Conde, P. M., Merchán, M. A., & Malmierca, M. S. (2008). Non-plastic reorganization of frequency coding in the inferior colliculus of the rat following noise-induced hearing loss. *Neuroscience*, *154*(1), 355–369. doi: 10.1016/j.neuroscience.2008.01.057

Jafari, Z., Kolb, B. E., & Mohajerani, M. H. (2019). Age-related hearing loss and tinnitus, dementia risk, and auditory amplification outcomes. *Ageing Research Reviews*, *56*(March), 100963. doi: 10.1016/j.arr.2019.100963

Janke, L. J., Ward, J. M., & Vogel, P. (2019). Classification, Scoring, and Quantification of Cell Death in Tissue Sections. *Veterinary Pathology*, *56*(1), 33–38. doi: 10.1177/0300985818800026

Janssen, M. L. F., & Jahanshahi, A. (2022). *The Effect of Noise Trauma and Deep Brain Stimulation of the Medial Geniculate Body on Tissue Activity in the Auditory Pathway*.

Jean-Baptiste, M., & Morest, D. K. (1975). Transneuronal changes of synaptic endings and nuclear chromatin in the trapezoid body following cochlear ablations in cats. *Journal of Comparative Neurology*, *162*(1), 111–133. doi: 10.1002/cne.901620107

Jerger, J. (1978). Prediction of Sensorineural Hearing Level From the Brain Stem Evoked Response. *Archives of Otolaryngology*, *104*(8), 456–461. doi: 10.1001/archotol.1978.00790080038010

Jewett, D. L., & Williston, J. S. (1971). Auditory-evoked far fields averaged from the scalp of humans. *Brain*, *94*(4), 681–696. doi: 10.1093/brain/94.4.681

Jiang, M. Q., Zhao, Y. Y., Cao, W., Wei, Z. Z., Gu, X., Wei, L., & Yu, S. P. (2017). Long-term survival and regeneration of neuronal and vasculature cells inside the core region after ischemic stroke in adult mice. *Brain Pathology*, *27*(4), 480–498. doi: 10.1111/bpa.12425

Kalappa, B. I., Brozoski, T. J., Turner, J. G., & Caspary, D. M. (2014). Single unit hyperactivity and bursting in the auditory thalamus of awake rats directly correlates with behavioural evidence of tinnitus. *Journal of Physiology*, *592*(22), 5065–5078. doi: 10.1113/jphysiol.2014.278572

Kaltenbach, J. A., & Afman, C. E. (2000). Hyperactivity in the dorsal cochlear nucleus after intense sound exposure and its resemblance to tone-evoked activity: A physiological model for tinnitus. *Hearing Research*, *140*(1–2), 165–172. doi: 10.1016/S0378-5955(99)00197-5

Kaltenbach, J. A., Czaja, J. M., & Kaplan, C. R. (1992). Changes in the tonotopic map of the dorsal cochlear nucleus following induction of cochlear lesions by exposure to intense sound. *Hearing Research*, *59*(2), 213–223. doi: 10.1016/0378-5955(92)90118-7

Kaltenbach, J. A., Godfrey, D. A., Neumann, J. B., McCaslin, D. L., Afman, C. E., & Zhang, J. (1998). Changes in spontaneous neural activity in the dorsal cochlear nucleus following exposure to intense sound: Relation to threshold shift. *Hearing Research*, *124*(1–2), 78–84. doi: 10.1016/S0378-5955(98)00119-1

Kamke, M. R., Brown, M., & Irvine, D. R. F. (2003). Plasticity in the tonotopic organization of the medial geniculate body in adult cats following restricted unilateral cochlear lesions. *Journal of Comparative Neurology*, *459*(4), 355–367. doi: 10.1002/cne.10586

Kapolowicz, M. R., & Thompson, L. T. (2016). Acute high-intensity noise induces rapid Arc protein expression but fails to rapidly change GAD expression in amygdala and hippocampus of rats: Effects of treatment with D-cycloserine. *Hearing Research*, *342*, 69–79. doi: 10.1016/j.heares.2016.09.010

Karnes, H. E., Kaiser, C. L., & Durham, D. (2009). Deafferentiation-induced caspase-3 activation and DNA

fragmentation in chick cochlear nucleus neurons. *NSC*, *159*(2), 804–818. doi: 10.1016/j.neuroscience.2008.12.031

Karuppagounder, S. S., Qingli Shi, Xu, H., & Gibson, G. E. (2007). Changes in Inflammatory Processes Associated With Selective Vulnerability Following Mild Impairment of Oxidative Metabolism. *Neurobiol Dis.*, *26*(2), 353–362. doi: 10.1016/j.nbd.2007.01.011.

Keifer, O. P. Jr, Gutman, D. A., Hecht, E. E., Keilholz, S. D., Ressler, K. J. (2015) A comparative analysis of mouse and human medial geniculate nucleus connectivity: a DTI and anterograde tracing study. *Neuroimage*, *105*, 53-66. doi: 10.1016/j.neuroimage.2014.10.047.

Kiefer, L., Koch, L., Merdan-Desik, M., Gaese, B. H., & Nowotny, M. (2022). Comparing the electrophysiological effects of traumatic noise exposure between rodents. *Journal of Neurophysiology*, *127*(2), 452–462. doi: 10.1152/jn.00081.2021

Kilicarslan, R., Alkan, A., Aralasmak, A., Aksoy, F., Toprak, H., Yetis, H., & Ozturan, O. (2014). Magnetic resonance spectroscopy features of heschl's gyri in patients with unilateral acoustic neuroma: Preliminary study. *Academic Radiology*, *21*(12), 1501–1505. doi: 10.1016/j.acra.2014.07.007

Kim, J. J., Gross, J., Morest, D. K., & Potashner, S. J. (2004). Quantitative study of degeneration and new growth of axons and synaptic endings in the chinchilla cochlear nucleus after acoustic overstimulation. *Journal of Neuroscience Research*, *77*(6), 829–842. doi: 10.1002/jnr.20211

Kim, K. X., Payne, S., Yang-Hood, A., Li, S. Z., Davis, B., Carlquist, J., Ghaffari, B. V., Gantz, J. A., Kallogjeri, D., Fitzpatrick, J. A. J., Ohlemiller, K. K., Hirose, K., & Rutherford, M. A. (2019). Vesicular glutamatergic transmission in noise-induced loss and repair of cochlear ribbon synapses. *Journal of Neuroscience*, *39*(23), 4434–4447. doi: 10.1523/JNEUROSCI.2228-18.2019

Knipper, M., Singer, W., Schwabe, K., Hagberg, G. E., Li Hegner, Y., Rüttiger, L., Braun, C., & Land, R. (2022). Disturbed Balance of Inhibitory Signaling Links Hearing Loss and Cognition. *Frontiers in Neural Circuits*, *15*, 1–25. doi: 10.3389/fncir.2021.785603

Knipper, M., Van Dijk, P., Nunes, I., Rüttiger, L., & Zimmermann, U. (2013). Advances in the neurobiology of hearing disorders: Recent developments regarding the basis of tinnitus and hyperacusis. *Progress in Neurobiology*, *111*, 17–33. doi: 10.1016/j.pneurobio.2013.08.002

Kohrman, D. C., Wan, G., Cassinotti, L., & Corfas, G. (2020). Hidden hearing loss: A disorder with multiple etiologies and mechanisms. *Cold Spring Harbor Perspectives in Medicine*, *10*(1), 1–20. doi: 10.1101/cshperspect.a035493

Koops, E. A., de Kleine, E., & van Dijk, P. (2020). Gray matter declines with age and hearing loss, but is partially maintained in tinnitus. *Scientific Reports*, *10*(1), 1–12. doi: 10.1038/s41598-020-78571-0

Kou, Z. Z., Qu, J., Zhang, D. L., Li, H., & Li, Y. Q. (2013). Noise-induced hearing loss is correlated with alterations in the expression of GABAB receptors and PKC gamma in the murine cochlear nucleus complex. *Frontiers in Neuroanatomy*, *7*, 1–11. doi: 10.3389/fnana.2013.00025

Kraus, K. S., & Canlon, B. (2012). Neuronal connectivity and interactions between the auditory and limbic systems. Effects of noise and tinnitus. *Hearing Research*, *288*(1–2), 34–46. doi: 10.1016/j.heares.2012.02.009

Kraus, K. S., & Illing, R. B. (2004). Superior olivary contributions to auditory system plasticity: Medial but not lateral olivocochlear neurons are the source of cochleotomy-induced GAP-43 expression in the ventral cochlear nucleus. *Journal of Comparative Neurology*, *475*(3), 374–390. doi: 10.1002/cne.20180

Kraus, K. S., Ding, D., Jiang, H., Lobarinas, E., Sun, W., Salvi, R.J. (2011). Relationship between noise-induced hearing-loss, persistent tinnitus and growth-associated protein-43 expression in the rat cochlear nucleus: does synaptic plasticity in ventral cochlear nucleus suppress tinnitus? *Neuroscience*, 194, 309-25. doi: 10.1016/j.neuroscience.2011.07.056

Kraus, K. S., Ding, D., Zhou, Y., & Salvi, R. J. (2009). Central auditory plasticity after carboplatin-induced unilateral inner ear damage in the chinchilla: Up-regulation of GAP-43 in the ventral cochlear nucleus. *Hearing Research*, *255*(1–2), 33–43. doi: 10.1016/j.heares.2009.05.001

Krizman, J., Rotondo, E. K., Nicol, T., Kraus, N., & Bieszczad, K. (2021). Sex differences in auditory processing vary across estrous cycle. *Scientific Reports*, *11*(1), 1–7. doi: 10.1038/s41598-021-02272-5

Kuan, L., Li, Y., Lau, C., Feng, D., Bernard, A., Sunkin, S. M., Zeng, H., Dang, C., Hawrylycz, M., & Ng, L. (2015). Neuroinformatics of the Allen Mouse Brain Connectivity Atlas. *Methods (San Diego, Calif.)*, *73*, 4–17. doi: 10.1016/J.YMETH.2014.12.013

Kujawa, S. G., & Liberman, M. C. (2009). Adding insult to injury: Cochlear nerve degeneration after "temporary" noise-induced hearing loss. *Journal of Neuroscience*, *29*(45), 14077–14085. doi: 10.1523/JNEUROSCI.2845-09.2009

Kujawa, S. G., & Liberman, M. C. (2015). Synaptopathy in the noise-exposed and aging cochlea: Primary neural degeneration in acquired sensorineural hearing loss. *Hearing Research*, *330*, 191–199. doi: 10.1016/j.heares.2015.02.009

Kujawa, S. G., & Liberman, M. C. (2017). Cochlear synaptopathy in acquired sensorineural hearing loss: Manifestations and mechanisms. *Hear Res.*, *349*, 138–147. doi: 10.1016/j.heares.2017.01.003.

Kurabi, A., Keithley, E. M., Housley, G. D., Ryan, A. F., & Wong, A. C. Y. (2017). Cellular mechanisms of noise-induced hearing loss. *Hearing Research*, *349*, 129–137. doi: 10.1016/j.heares.2016.11.013

Kurioka, T., Lee, M. Y., Heeringa, A. N., Beyer, L. A., Swiderski, D. L., Kanicki, A. C., Kabara, L. L., Dolan, D. F., Shore, S. E., & Raphael, Y. (2016). Selective hair cell ablation and noise exposure lead to different patterns of changes in the cochlea and the cochlear nucleus. *Neuroscience*, *332*, 242–257. doi: 10.1016/j.neuroscience.2016.07.001

Kyrylkova, K., Kyryachenko, S., Leid, M., & Kioussi, C. (2012). Detection of Apoptosis by TUNEL Assay. *Odontogenesis: Methods and Protocols*, *887*, 41–47. doi: 10.1007/978-1-61779-860-3

Landgrebe, M., Langguth, B., Rosengarth, K., Braun, S., Koch, A., Kleinjung, T., May, A., de Ridder, D., & Hajak, G. (2009). Structural brain changes in tinnitus: Grey matter decrease in auditory and non-auditory brain areas. *NeuroImage*, *46*(1), 213–218. doi: 10.1016/j.neuroimage.2009.01.069

Lauer, Amanda M., El-Sharkawy, A. M. M., Kraitchman, D. L., & Edelstein, W. A. (2012). MRI acoustic noise can harm experimental and companion animals. *Journal of Magnetic Resonance Imaging*, *36*(3), 743–747. doi: 10.1002/jmri.23653

Lauer, Amanda Marie, & Schrode, K. M. (2017). Sex Bias in Basic and Preclinical Noise-Induced Hearing Loss Research. *Noise & Health*, *19*(90), 207. doi: 10.4103/NAH.NAH_12_17

Le Prell, C. G., Hackett, T. A., & Ramachandran, R. (2020). Noise-induced hearing loss and its prevention: current issues in mammalian hearing. *Current Opinion in Physiology*, *18*, 32–36. doi: 10.1016/j.cophys.2020.07.004

Le, T. N., Straatman, L. V., Lea, J., & Westerberg, B. (2017). Current insights in noise-induced hearing loss: a literature review of the underlying mechanism, pathophysiology, asymmetry, and management options. *Journal of Otolaryngology - Head and Neck Surgery*, *46*(1), 1–15. doi: 10.1186/s40463-017-0219-x

Leaver, A. M., Renier, L., Chevillet, M. A., Morgan, S., Kim, H. J., & Rauschecker, J. P. (2011). Dysregulation of Limbic and Auditory Networks in Tinnitus. *Neuron*, *69*(1), 33–43. doi: 10.1016/j.neuron.2010.12.002

Leaver, A. M., Seydell-Greenwald, A., Rauschecker, J. P. (2016) Auditory-limbic interactions in chronic tinnitus: Challenges for neuroimaging research. *Hear Res.* 334, 49-57. doi:

10.1016/j.heares.2015.08.005.

Lee, A. C., & Godfrey, D. A. (2014). Cochlear Damage Affects Neurotransmitter Chemistry in the Central Auditory System. *Frontiers in Neurology*, *5*(11), 1–16. doi: 10.3389/fneur.2014.00227

Lein, E. S., Hawrylycz, M. J., Ao, N., Ayres, M., Bensinger, A., Bernard, A., Boe, A. F., Boguski, M. S., Brockway, K. S., Byrnes, E. J., Chen, L., Chen, L., Chen, T. M., Chin, M. C., Chong, J., Crook, B. E., Czaplinska, A., Dang, C. N., Datta, S., … Jones, A. R. (2007). Genome-wide atlas of gene expression in the adult mouse brain. *Nature*, *445*(7124), 168–176. doi: 10.1038/nature05453

Lewis-Wambi, J. S., & Jordan, V. C. (2009). Estrogen regulation of apoptosis: How can one hormone stimulate and inhibit? *Breast Cancer Research*, *11*(3), 1–12. doi: 10.1186/bcr2255

Liberman, M. C. (2016). Noise-Induced Hearing Loss: Permanent Versus Temporary Threshold Shifts and the Effects of Hair Cell Versus Neuronal Degeneration. *Adv Exp Med Biol, 875*, 1–7. doi: 10.1007/978-1-4939-2981-8

Liberman, M. C. (2017). Noise-induced and age-related hearing loss: New perspectives and potential therapies. *F1000Research*, *6*(0), 1–11. doi: 10.12688/f1000research.11310.1

Lin, H. W., Furman, A. C., Kujawa, S. G., & Liberman, M. C. (2011). Primary neural degeneration in the guinea pig cochlea after reversible noise-induced threshold shift. *JARO - Journal of the Association for Research in Otolaryngology*, *12*(5), 605–616. doi: 10.1007/s10162-011-0277-0

Llano, D. A., Turner, J., & Caspary, D. M. (2012). Diminished cortical inhibition in an aging mouse model of chronic tinnitus. *Journal of Neuroscience*, *32*(46), 16141–16148. doi: 10.1523/JNEUROSCI.2499-12.2012

Lockwood, A. H., Salvi, R. J., Coad, M. L., Towsley, M. L., Wack, D. S., & Murphy, B. W. (1998). The functional neuroanatomy of tinnitus: Evidence for limbic system links and neural plasticity. *Neurology*, *50*(1), 114–120. doi: 10.1212/WNL.50.1.114

Loughrey, D. G., Kelly, M. E., Kelley, G. A., Brennan, S., & Lawlor, B. A. (2018). Association of age-related hearing loss with cognitive function, cognitive impairment, and dementia a systematic review and meta-analysis. *Otolaryngology, Head and Neck Surgery*, *144*(2), 115–126. doi: 10.1001/jamaoto.2017.2513

Luan, Y., Salvi, R., Liu, L., Lu, C., Jiao, Y., Tang, T., Liu, H., & Teng, G. J. (2021). High-frequency Noise-induced Hearing Loss Disrupts Functional Connectivity in Non-auditory Areas with Cognitive Disturbances. *Neuroscience Bulletin*, *37*(5), 720–724. doi: 10.1007/s12264-021-00663-2

Ma, K., Zhang, A., She, X., Yang, H., Wang, K., Zhu, Y., Gao, X., & Cui, B. (2021). Disruption of Glutamate Release and Uptake-Related Protein Expression After Noise-Induced Synaptopathy in the Cochlea. *Frontiers in Cell and Developmental Biology*, *9*(8), 1–11. doi: 10.3389/fcell.2021.720902

Ma, L., Ono, M., Qin, L., & Kato, N. (2020). Acoustic trauma induced the alteration of the activity balance of excitatory and inhibitory neurons in the inferior colliculus of mice. *Hearing Research*, *391*, 107957. doi: 10.1016/j.heares.2020.107957

Ma, W. L. D., Hidaka, H., & May, B. J. (2006). Spontaneous activity in the inferior colliculus of CBA/J mice after manipulations that induce tinnitus. *Hearing Research*, *212*(1–2), 9–21. doi: 10.1016/j.heares.2005.10.003

Manohar, S., Chen, G. D., Ding, D., Liu, L., Wang, J., Chen, Y. C., Chen, L., & Salvi, R. (2022). Unexpected Consequences of Noise-Induced Hearing Loss: Impaired Hippocampal Neurogenesis, Memory, and Stress. *Frontiers in Integrative Neuroscience*, *16*(4), 1–17. doi: 10.3389/fnint.2022.871223

Manohar, S., Ramchander, P. V., Salvi, R., & Seigel, G. M. (2019). Synaptic Reorganization Response in the Cochlear Nucleus Following Intense Noise Exposure. *Neuroscience*, *399*(1), 184–198. doi:

10.1016/j.neuroscience.2018.12.023

Manohar, Senthivelan, Russo, F. Y., Seigel, G. M., & Richard Salvi. (2020). Dynamic Changes in Synaptic Plasticity Genes in Ipsilateral and Contralateral Inferior Colliculus Following Unilateral Noise-induced Hearing Loss. *Neuroscience*, *436*, 136–153. doi: 10.1016/j.neuroscience.2020.04.010

Manzoor, N. F., Licari, F. G., Klapchar, M., Elkin, R. L., Gao, Y., Chen, G., & Kaltenbach, J. A. (2012a). Noise-induced hyperactivity in the inferior colliculus: Its relationship with hyperactivity in the dorsal cochlear nucleus. *Journal of Neurophysiology*, *108*(4), 976–988. doi: 10.1152/jn.00833.2011

Manzoor, N. F., Licari, F. G., Klapchar, M., Elkin, R. L., Gao, Y., Chen, G., & Kaltenbach, J. A. (2012b). Noise-induced hyperactivity in the inferior colliculus: Its relationship with hyperactivity in the dorsal cochlear nucleus. *Journal of Neurophysiology*, *108*(4), 976–988. doi: 10.1152/jn.00833.2011

Mao H, Chen Y. Noise-Induced Hearing Loss: Updates on Molecular Targets and Potential Interventions. *Neural Plast*, 6, 2021, 4784385. doi: 10.1155/2021/4784385.

McJury, M., & Shellock, F. G. (2000). Auditory noise associated with MR procedures: A review. *Journal of Magnetic Resonance Imaging*, *12*(1), 37–45. doi: 10.1002/1522-2586(200007)12:1<37::AID-JMRI5>3.0.CO;2-I

McPherson, D. R. (2018). Sensory hair cells: An introduction to structure and physiology. *Integrative and Comparative Biology*, *58*(2), 282–300. doi: 10.1093/icb/icy064

Mellott, J. G., Foster, N. L., Ohl, A. P., & Schofield, B. R. (2014). Excitatory and inhibitory projections in parallel pathways from the inferior colliculus to the auditory thalamus. *Frontiers in Neuroanatomy*, *8*(November), 1–11. doi: 10.3389/fnana.2014.00124

Meltser, I., Cederroth, C. R., Basinou, V., Savelyev, S., Lundkvist, G. S., & Canlon, B. (2013). TrkB mediated protection against circadian sensitivity to noise trauma in the murine cochlea. *Curr. Biol.*, *24*(6), 658–663. doi: 10.1016/j.cub.2014.01.047.TrkB

Miao, L., Zhang, J., Yin, L., Pu, Y. (2023) Hearing loss and hypertension among noise-exposed workers: a pilot study based on baseline data. *Int J Environ Health Res*. *33*(8), 783-795. doi: 10.1080/09603123.2022.2050681

Milbrandt, J. C., Holder, T. M., Wilson, M. C., Salvi, R. J., & Caspary, D. M. (2000). GAD levels and muscimol binding in rat inferior colliculus following acoustic trauma. *Hearing Research*, *147*(1–2), 251–260. doi: 10.1016/S0378-5955(00)00135-0

Milloy, V., Fournier, P., Benoit, D., Noreña, A., & Koravand, A. (2017). Auditory brainstem responses in tinnitus: A review of who, how, and what? *Frontiers in Aging Neuroscience*, *9*(JUL). doi: 10.3389/fnagi.2017.00237

Milon, B., Mitra, S., Song, Y., Margulies, Z., Casserly, R., Drake, V., Mong, J. A., Depireux, D. A., & Hertzano, R. (2018). The impact of biological sex on the response to noise and otoprotective therapies against acoustic injury in mice. *Biology of Sex Differences*, *9*(1), 1–14. doi: 10.1186/s13293-018-0171-0

Morest, D. K., Kim, J., Potashner, S. J., & Bohne, B. A. (1998). Long-term degeneration in the cochlear nerve and cochlear nucleus of the adult chinchilla following acoustic overstimulation. *Microscopy Research and Technique*, *41*(3), 205–216. doi: 10.1002/(SICI)1097-0029(19980501)41:3<205::AID-JEMT4>3.0.CO;2-S

Morest, D. K., & Bohne, B. A. (1983). Noise-induced degeneration in the brain and representation of inner and outer hair cells. *Hearing Research*, *9*(2), 145–151. doi: 10.1016/0378-5955(83)90024-2

Mossop, J. E., Wilson, M. J., Caspary, D. M., & Moore, D. R. (2000). Down-regulation of inhibition following unilateral deafening. *Hearing Research*, *147*(1–2), 183–187. doi: 10.1016/S0378-5955(00)00054-X

Mostafapour, S. P., Cochran, S. L., Del Puerto, N. M., Rubel E. W. (200). Patterns of cell death in mouse anteroventral cochlear nucleus neurons after unilateral cochlea removal. *J Comp Neurol*, *426*(4), 561-71. doi: 10.1002/1096-9861(20001030)426:4<561::aid-cne5>3.0.co;2-g

Muca, A., Standafer, E., Apawu, A. K., Ahmad, F., Ghoddoussi, F., Hali, M., Warila, J., Berkowitz, B. A., Holt, A. G (2018). Tinnitus and temporary hearing loss result in differential noise-induced spatial reorganization of brain activity. *Brain Struct Funct*, *223*(5), 2343-2360. doi: 10.1007/s00429-018-1635-z

Mulders, W., & Robertson, D. (2009). Hyperactivity in the auditory midbrain after acoustic trauma: dependence on cochlear activity. *Neuroscience*, *164*(2), 733–746. doi: 10.1016/j.neuroscience.2009.08.036

Mulders, W., & Robertson, D. (2013). Development of hyperactivity after acoustic trauma in the guinea pig inferior colliculus. *Hearing Research*, *298*, 104–108. doi: 10.1016/j.heares.2012.12.008

Mulders, W., Wilhelmina Henrica A. M., Seluakumaran, K., & Robertson, D. (2010). Efferent pathways modulate hyperactivity in inferior colliculus. *Journal of Neuroscience*, *30*(28), 9578–9587. doi: 10.1523/JNEUROSCI.2289-10.2010

Mullen, R. J., Buck, C. R., & Smith, A. M. (1992). NeuN, a neuronal specific nuclear protein in vertebrates. *Development*, *116*(1), 201–211. doi: 10.1242/dev.116.1.201

Muly, S. M., Gross, J. S., & Potashner, S. J. (2004). Noise Trauma Alters D-[3H]Aspartate Release and AMPA Binding in Chinchilla Cochlear Nucleus. *Journal of Neuroscience Research*, *75*(4), 585–596. doi: 10.1002/jnr.20011

Muly, S. M., Gross, J. S., Morest, D. K., & Potashner, S. J. (2002). Synaptophysin in the cochlear nucleus following acoustic trauma. *Experimental Neurology*, *177*(1), 202–221. doi: 10.1006/exnr.2002.7963

Nakai, T., Kamiya, N., Sone, M., Muranaka, H., Tsuchihashi, T., Yamada, N., & Yamaguchi, S. (2012). A survey analysis of acoustic trauma related to MR scans. *Magnetic Resonance in Medical Sciences*, *11*(4), 253–264. doi: 10.2463/mrms.11.253

Natarajan, N., Batts, S., & Stankovic, K. M. (2023). Noise-Induced Hearing Loss. *Journal of Clinical Medicine*, *12*(6). doi: 10.3390/jcm12062347

Neitzel, R. L., & Fligor, B. J. (2019). Risk of noise-induced hearing loss due to recreational sound: Review and recommendations. *The Journal of the Acoustical Society of America*, *146*(5), 3911–3921. doi: 10.1121/1.5132287

Newcomb, J. K., Zhao, X., Pike, B. R., & Hayes, R. L. (1999). Temporal profile of apoptotic-like changes in neurons and astrocytes following controlled cortical impact injury in the rat. *Experimental Neurology*, *158*(1), 76–88. doi: 10.1006/exnr.1999.7071

Niu, Y., Kumaraguru, A., Wang, R., & Sun, W. (2013). Hyperexcitability of inferior colliculus neurons caused by acute noise exposure. *Journal of Neuroscience Research*, *91*(2), 292–299. doi: 10.1002/jnr.23152

Nolan, L. S. (2020). Age-related hearing loss: Why we need to think about sex as a biological variable. *Journal of Neuroscience Research*, *98*(9), 1705–1720. doi: 10.1002/jnr.24647

Nordmann, A. S., Bohne, B. A., & Harding, G. W. (2000). Histopathological differences between temporary and permanent threshold shift. *Hearing Research*, *139*(1–2), 13–30. doi: 10.1016/S0378-5955(99)00163-X

Noreña, A. J., & Eggermont, J. J. (2003). Changes in spontaneous neural activity immediately after an acoustic trauma: Implications for neural correlates of tinnitus. *Hearing Research*, *183*(1–2), 137–153. doi: 10.1016/S0378-5955(03)00225-9

Oishi, N., Schacht, J. (2011). Emerging treatments for noise-induced hearing loss. *Expert Opin Emerg*

Drugs. *16*(2), 235-45. doi: 10.1517/14728214.2011.552427.

Oluwole, O. G., James, K., Yalcouye, A., & Wonkam, A. (2022). Hearing loss and brain disorders: A review of multiple pathologies. *Open Medicine*, *17*(1), 61–69. doi: 10.1515/med-2021-0402

Orrenius, S., Zhivotovsky, B., & Nicotera, P. (2003). Regulation of cell death: The calcium-apoptosis link. *Nature Reviews Molecular Cell Biology*, *4*(7), 552–565. doi: 10.1038/nrm1150

Oxenham, A. J. (2016). Predicting the Perceptual Consequences of Hidden Hearing Loss. *Trends in Hearing*, *20*, 1–6. doi: 10.1177/2331216516686768

Palmer, A. R., & Berger, J. I. (2018). Changes in the inferior colliculus associated with hearing loss: Noise-induced hearing loss, age-related hearing loss, tinnitus and hyperacusis. *The Oxford Handbook of the Auditory Brainstem*, *December*, 527–547. doi: 10.1093/oxfordhb/9780190849061.013.20

Park, S., Han, S. H., Kim, B. G., Suh, M. W., Lee, J. H., Oh, S. H., & Park, M. K. (2020). Changes in microrna expression in the cochlear nucleus and inferior colliculus after acute noise-induced hearing loss. *International Journal of Molecular Sciences*, *21*(22), 1–20. doi: 10.3390/ijms21228792

Park, S., Lee, D. H., Lee, S. M., Lee, C. H., & Kim, S. Y. (2020). Noise exposure alters MMP9 and brevican expression in the rat primary auditory cortex. *BMC Neuroscience*, *21*(1), 1–10. doi: 10.1186/s12868-020-00567-3

Paxinos, George. & Franklin, Keith B. J. (2001). *The mouse brain in stereotaxic coordinates*.

Persic, D., Thomas, M. E., Pelekanos, V., Ryugo, D. K., Takesian, A. E., Krumbholz, K., & Pyott, S. J. (2020). Regulation of auditory plasticity during critical periods and following hearing loss. *Hearing Research*, *397*, 107976. doi: 10.1016/j.heares.2020.107976

Peters, R. (2006). Ageing and the brain. *Postgraduate Medical Journal*, *82*(964), 84–88. doi: 10.1136/pgmj.2005.036665

Peterson, D. C., Reddy, V., & Hamel, R. N. (2022). Neuroanatomy, Auditory Pathway. *StatPearls*. https://www.ncbi.nlm.nih.gov/books/NBK532311/

Pickles, J. O. Auditory pathways: anatomy and physiology. *Handb Clin Neurol*, *129*, 3-25. doi: 10.1016/B978-0-444-62630-1.00001-9

Pienkowski, M. (2021). Loud music and leisure noise is a common cause of chronic hearing loss, tinnitus and hyperacusis. *International Journal of Environmental Research and Public Health*, *18*(8). doi: 10.3390/ijerph18084236

Plack, C. J., Barker, D., & Prendergast, G. (2014). Perceptual consequences of “hidden” hearing loss. *Trends in Hearing*, *18*, 1–11. doi: 10.1177/2331216514550621

Profant, O., Balogová, Z., Dezortová, M., Wagnerová, D., Hájek, M., & Syka, J. (2013). Metabolic changes in the auditory cortex in presbycusis demonstrated by MR spectroscopy. *Experimental Gerontology*, *48*(8), 795–800. doi: 10.1016/j.exger.2013.04.012

Puel, J. (1999). Excitotoxicity, Synaptic Repair, and Functional Recovery in the Mammalian Cochlea: **A** Review of Recent Findings. *Annals New York Academy of Sciences*, 249–254

Qiu, C. X., Salvi, R., Ding, D., & Burkard, R. (2000). Inner hair cell loss leads to enhanced response amplitudes in auditory cortex of unanesthetized chinchillas: evidence for increased system gain. *Hearing Research*, *139*(1–2), 153–171. doi: 10.1016/S0378-5955(99)00171-9

Radeloff, A., Cebulla, M., & Shehata-Dieler, W. (2014). Akustisch evozierte Potenziale: Grundlagen und klinische Anwendung. *Laryngo- Rhino- Otologie*, *93*(9), 625–637. doi: 10.1055/s-0034-1385868

Resnik J, Polley DB. Cochlear neural degeneration disrupts hearing in background noise by increasing auditory cortex internal noise. *Neuron*, *109*(6), 984-996. doi: 10.1016/j.neuron.2021.01.015

Reuss S. (2000). Introduction to the superior olivary complex. *Microsc Res Tech*, *51*(4), 303-6. doi: 10.1002/1097-0029(20001115)51:4<303::AID-JEMT1>3.0.CO;2-B.

Reuss, S., Closhen, C., Riemann, R., Jaumann, M., Knipper, M., Rüttiger, L., & Wolpert, S. (2016). Absence of Early Neuronal Death in the Olivocochlear System Following Acoustic Overstimulation. *Anatomical Record*, *299*(1), 103–110. doi: 10.1002/ar.23277

Ryan, A. F. (2000). Protection of auditory receptors and neurons: Evidence for interactive damage. *Proceedings of the National Academy of Sciences of the United States of America*, *97*(13), 6939–6940. doi: 10.1073/pnas.97.13.6939

Säljö, A., Bao, F., Jingshan, S., Hamberger, A., Hansson, H. A., & Haglid, K. G. (2002). Exposure to short-lasting impulse noise causes neuronal c-Jun expression and induction of apoptosis in the adult rat brain. *Journal of Neurotrauma*, *19*(8), 985–991. doi: 10.1089/089771502320317131

Salvi, R. J., Saunders, S. S., Gratton, M. A., Arehole, S., & Powers, N. (1990). Enhanced evoked response amplitudes in the inferior colliculus of the chinchilla following acoustic trauma. *Hearing Research*, *50*(1–2), 245–257. doi: 10.1016/0378-5955(90)90049-U

Salvi, Richard J., Wang, J., & Ding, D. (2000). Auditory plasticity and hyperactivity following cochlear damage. *Hearing Research*, *147*(1–2), 261–274. doi: 10.1016/S0378-5955(00)00136-2

Sametsky, E. A., Turner, J. G., Larsen, D., Ling, L., Caspary, D. M. (2015). Enhanced GABAA-Mediated Tonic Inhibition in Auditory Thalamus of Rats with Behavioral Evidence of Tinnitus. *J Neurosci*, *35*(25), 9369-80. doi: 10.1523/JNEUROSCI.5054-14.2015.

Sanford C. Bledsoe, Jr., Shigeyo Nagase, J. M. M. and R. A. A. (1995). *Deafness-induced plasticity in the mature central auditory system* (pp. 225–229).

Sato, M. P., Higuchi, T., Nin, F., Ogata, G., Sawamura, S., Yoshida, T., Ota, T., Hori, K., Komune, S., Uetsuka, S., Choi, S., Masuda, M., Watabe, T., Kanzaki, S., Ogawa, K., Inohara, H., Sakamoto, S., Takebayashi, H., Doi, K., Tanaka, K. F., Hibino, H. (2017). Hearing Loss Controlled by Optogenetic Stimulation of Nonexcitable Nonglial Cells in the Cochlea of the Inner Ear. *Front Mol Neurosci*, 10, 300. doi: 10.3389/fnmol.2017.00300.

Saunders, J. C., Cohen, Y. E., & Szvmko, Y. M. (1991). The structural and functional consequences of acoustic injury in the cochlea and peripheral auditory system: A five year update. *Journal of the Acoustical Society of America*, *90*(1), 136–146. doi: 10.1121/1.401307

Scholl, B., & Wehr, M. (2008). Disruption of balanced cortical excitation and inhibition by acoustic trauma. *Journal of Neurophysiology*, *100*(2), 646–656. doi: 10.1152/jn.90406.2008

Schormans, A. L., Typlt, M., & Allman, B. L. (2017). Crossmodal plasticity in auditory, visual and multisensory cortical areas following noise-induced hearing loss in adulthood. *Hearing Research*, *343*, 92–107. doi: 10.1016/j.heares.2016.06.017

Schrode, K. M., Muniak, M. A., Kim, Y. H., & Lauer, A. M. (2018). Central compensation in auditory brainstem after damaging noise exposure. *ENeuro*, *5*(4). doi: 10.1523/ENEURO.0250-18.2018

Sears, S. M. S., & Hewett, S. J. (2021). Influence of glutamate and GABA transport on brain excitatory/inhibitory balance. *Experimental Biology and Medicine*, *246*(9), 1069–1083. doi: 10.1177/1535370221989263

Sedley, W., Parikh, J., Edden, R. A. E., Tait, V., Blamire, A., & Griffiths, T. D. (2015). Human auditory cortex neurochemistry reflects the presence and severity of tinnitus. *Journal of Neuroscience*, *35*(44), 14822–14828. doi: 10.1523/JNEUROSCI.2695-15.2015

Seki, S., & Eggermont, J. J. (2003). Changes in spontaneous firing rate and neural synchrony in cat primary auditory cortex after localized tone-induced hearing loss. *Hearing Research*, *180*(1–2), 28–38. doi: 10.1016/S0378-5955(03)00074-1

Shi, L., Liu, K., Wang, H., Zhang, Y., Hong, Z., Wang, M., Wang, X., Jiang, X., & Yang, S. (2015). Noise induced reversible changes of cochlear ribbon synapses contribute to temporary hearing loss in mice. *Acta Oto-Laryngologica*, *135*(11), 1093–1102. doi: 10.3109/00016489.2015.1061699

Shore, S.E., Koehler, S., Oldakowski, M., Hughes, L. F., & Syed, S. (2008). Dorsal cochlear nucleus responses to somatosensory stimulation are enhanced after noise-induced hearing loss. *Eur J Neurosci.*, *27*(1), 155–168. doi: 10.1111/j.1460-9568.2007.05983

Shore, Susan E., & Wu, C. (2019). Mechanisms of Noise-Induced Tinnitus: Insights from Cellular Studies. *Neuron*, *103*(1), 8–20. doi: 10.1016/j.neuron.2019.05.008

Shuster, B., Casserly, R., Lipford, E., Olszewski, R., Milon, B., Viechweg, S., Davidson, K., Enoch, J., McMurray, M., Rutherford, M. A., Ohlemiller, K. K., Hoa, M., Depireux, D. A., Mong, J. A., & Hertzano, R. (2021). Estradiol protects against noise-induced hearing loss and modulates auditory physiology in female mice. *International Journal of Molecular Sciences*, *22*(22). doi: 10.3390/ijms222212208

Simonoska, R., Stenberg, A. E., Duan, M., Yakimchuk, K., Fridberger, A., Sahlin, L., Gustafsson, J. Å., & Hultcrantz, M. (2009). Inner ear pathology and loss of hearing in estrogen receptor-β deficient mice. *Journal of Endocrinology*, *201*(3), 397–406. doi: 10.1677/JOE-09-006

Singer, W., Gröschel, M., Zuccotti, A., Mueller, S., Ernst, A., Basta, D., Knipper, M., & Rüttiger, L. (2020). The aftermath of tinnitus-inducing inner ear damage for auditory brainstem responses and MEMR imaging of central brain activity in the rat. *Hearing, Balance and Communication*, *18*(4), 225–233. doi: 10.1080/21695717.2020.1816116

Sliwinska-Kowalska M, Davis A. (2012). Noise-induced hearing loss. *Noise Health, 14*(61), 274-80. doi: 10.4103/1463-1741.104893

Sliwinska-Kowalska, M., & Zaborowski, K. (2017). WHO environmental noise guidelines for the European region: A systematic review on environmental noise and permanent hearing loss and tinnitus. *International Journal of Environmental Research and Public Health*, *14*(10). doi: 10.3390/ijerph14101139

Sturm, J. J., Zhang-Hooks, Y. X., Roos, H., Nguyen, T., & Kandler, K. (2017). Noise trauma-induced behavioral gap detection deficits correlate with reorganization of excitatory and inhibitory local circuits in the inferior colliculus and are prevented by acoustic enrichment. *Journal of Neuroscience*, *37*(26), 6314–6330. doi: 10.1523/JNEUROSCI.0602-17.2017

Sułkowski, W., Owczarek, K., & Olszewski, J. (2017). Contemporary noise-induced hearing loss (NIHL) prevention. *Otolaryngologia Polska*, *71*(4), 1–7. doi: 10.5604/01.3001.0010.2241

Sun, W., Deng, A., Jayaram, A., & Gibson, B. (2012). Noise exposure enhances auditory cortex responses related to hyperacusis behavior. *Brain Research*, *1485*, 108–116. doi: 10.1016/j.brainres.2012.02.008

Suneja SK, Yan L, Potashner SJ. Regulation of NT-3 and BDNF levels in guinea pig auditory brain stem nuclei after unilateral cochlear ablation (2005). *J Neurosci Res*, *80*(3), 381-90. doi: 10.1002/jnr.20457

Syka, J. (2002). Plastic changes in the central auditory system after hearing loss, restoration of function, and during learning. *Physiological Reviews*, *82*(3), 601–636. doi: 10.1152/physrev.00002.2002

Szczepaniak, W. S., & Moller, A. R. (1995). Evidence of decreased GABAergic influence on temporal integration in the inferior colliculus following acute noise exposure: a study of evoked potentials in the rat. *Neuroscience Letters*, *196*, 77–80.

Szczepaniak, W. S., & Møller, A. R. (1996). Evidence of neuronal plasticity within the inferior colliculus after noise exposure: A study of evoked potentials in the rat. *Electroencephalography and Clinical Neurophysiology*, *100*(2), 158–164. doi: 10.1016/0013-4694(95)00234-0

Tagoe, T., Deeping, D., & Hamann, M. (2017). Saturation of long-term potentiation in the dorsal cochlear

nucleus and its pharmacological reversal in an experimental model of tinnitus. *Experimental Neurology*, *292*, 1–10. doi: 10.1016/j.expneurol.2017.02.011

Talavage, T. M., Gonzalez-Castillo, J., & K. Scott, S. (2014). Auditory Neuroimaging with fMRI and PET. *Hear Res.*, *307*(1), 4–15. doi: 10.1016/j.heares.2013.09.009.Auditory

Themann, C. L., & Masterson, E. A. (2019). Occupational noise exposure: A review of its effects, epidemiology, and impact with recommendations for reducing its burden. *The Journal of the Acoustical Society of America*, *146*(5), 3879–3905. doi: 10.1121/1.5134465

Theodoroff, S. M., Lewis, M. S., Folmer, R. L., Henry, J. A., & Carlson, K. F. (2015). Hearing impairment and tinnitus: Prevalence, risk factors, and outcomes in us service members and veterans deployed to the Iraq and Afghanistan Wars. *Epidemiologic Reviews*, *37*(1), 71–85. doi: 10.1093/epirev/mxu00

Tuerdi, A., Kinoshita, M., Kamogashira, T., Fujimoto, C., Iwasaki, S., Shimizu, T., & Yamasoba, T. (2017). Manganese superoxide dismutase influences the extent of noise-induced hearing loss in mice. *Neuroscience Letters*, *642*, 123–128. doi: 10.1016/j.neulet.2017.02.003

Valderrama, J. T., de la Torre, A., & McAlpine, D. (2022). The hunt for hidden hearing loss in humans: From preclinical studies to effective interventions. *Frontiers in Neuroscience*, *16*(9), 1–13. doi: 10.3389/fnins.2022.1000304

Vale, C., & Sanes, D. H. (2002). The effect of bilateral deafness on excitatory and inhibitory synaptic strength in the inferior colliculus. *European Journal of Neuroscience*, *16*(12), 2394–2404. doi: 10.1046/j.1460-9568.2002.02302

Verdaasdonk, J. S., Lawrimore, J., & Kerry Bloom. (2014). Determining absolute protein numbers by quantitative fluorescence microscopy Jolien. *Methods Cell Biol.*, 347–365. doi: 10.1002/9783527687732

Villavisanis, D. F., Elisa, R. B., Lauer, A. M., Cosetti, M. K., & Schrode, K. M. (2020). Sex-Based Differences in Hearing Loss: Perspectives from Non- Clinical Research to Clinical Outcomes. *Otol Neurotol.*, *41*(3), 290–298. doi: 10.1053/j.gastro.2016.08.014.CagY

Wang, J., Ding, D., & Salvi, R. J. (2002). Functional reorganization in chinchilla inferior colliculus associated with chronic and acute cochlear damage. *Hearing Research*, *168*(1–2), 238–249. doi: 10.1016/S0378-5955(02)00360

Wang, J., Salvi, R. J., & Powers, N. (1996). Plasticity of response properties of inferior colliculus neurons following acute cochlear damage. *Journal of Neurophysiology*, *75*(1), 171–183. doi: 10.1152/jn.1996.75.1.171

Wang, Q., Wang, X., Yang, L., Han, K., Huang, Z., & Wu, H. (2021). Sex differences in noise-induced hearing loss: a cross-sectional study in China. *Biology of Sex Differences*, *12*(1), 1–10. doi: 10.1186/s13293-021-00369-0

Wang, T. C., Chang, T. Y., Tyler, R., Lin, Y. J., Liang, W. M., Shau, Y. W., Lin, W. Y., Chen, Y. W., Lin, C. Der, & Tsai, M. H. (2020). Noise induced hearing loss and tinnitus - new research developments and remaining gaps in disease assessment, treatment, and prevention. *Brain Sciences*, *10*(10), 1–11. doi: 10.3390/brainsci10100732

Wang, W., Zhang, L. S., Zinsmaier, A. K., Patterson, G., Leptich, E. J., Shoemaker, S. L., Yatskievych, T. A., Gibboni, R., Pace, E., Luo, H., Zhang, J., Yang, S., & Bao, S. (2019). Neuroinflammation mediates noise-induced synaptic imbalance and tinnitus in rodent models. *PLoS Biology*, *17*(6), 1–25. doi: 10.1371/journal.pbio.3000307

Wang, Y., Hirose, K., & Liberman, M. C. (2002). Dynamics of noise-induced cellular injury and repair in the mouse cochlea. *Journal of the Association for Research in Otolaryngology*, *3*(3), 248–268. doi: 10.1007/s101620020028

Waters, J. C. (2009). Accuracy and precision in quantitative fluorescence microscopy. *Journal of Cell Biology*, *185*(7), 1135–1148. doi: 10.1083/jcb.200903097

Waters, J. C., & Wittmann, T. (2014). Concepts in quantitative fluorescence microscopy. In *Methods in Cell Biology* (1st ed., Vol. 123). Elsevier Inc. doi: 10.1016/B978-0-12-420138-5.00001-X

Webster, J. D., Solon, M., & Gibson-Corley, K. N. (2021). Validating Immunohistochemistry Assay Specificity in Investigative Studies: Considerations for a Weight of Evidence Approach. *Veterinary Pathology*, *58*(5), 829–840. doi: 10.1177/0300985820960l3

Wieczerzak, K. B., Patel, S. V., MacNeil, H., Scott, K. E., Schormans, A. L., Hayes, S. H., Herrmann, B., & Allman, B. L. (2021). Differential Plasticity in Auditory and Prefrontal Cortices, and Cognitive-Behavioral Deficits Following Noise-Induced Hearing Loss. *Neuroscience*, *455*(November), 1–18. doi: 10.1016/j.neuroscience.2020.11.019

Willott, J. F., & Lu, S. M. (1982). Noise-induced hearing loss can alter neural coding and increase excitability in the central nervous system. *Science*, *216*(4552), 1331–1332. doi: 10.1126/science.7079767

Willott, J. F., & Turner, J. G. (2000). Neural plasticity in the mouse inferior colliculus: Relationship to hearing loss, augmented acoustic stimulation, and prepulse inhibition. *Hearing Research*, *147*(1–2), 275–281. doi: 10.1016/S0378-5955(00)00137-4

Winer, J. A., Miller, L. M., Lee, C. C., & Schreiner, C. E. (2005). Auditory thalamocortical transformation: Structure and function. *Trends in Neurosciences, 28*(5), 255–263. doi: 10.1016/j.tins.2005.03.009

Winer, J. A., Saint Marie, R. L., Larue, D. T., Oliver, D. L. (1996) GABAergic feedforward projections from the inferior colliculus to the medial geniculate body. *Proc Natl Acad Sci USA*, *93*(15), 8005-10. doi: 10.1073/pnas.93.15.8005

Wolak, T., Cieśla, K., Rusiniak, M., Piłka, A., Lewandowska, M., Pluta, A., Skarżyński, H., & Skarżyński, P. H. (2016). Influence of acoustic overstimulation on the central auditory system: An functional magnetic resonance imaging (fMRI) study. *Medical Science Monitor*, *22*, 4623–4635. doi: 10.12659/MSM.897929

World Health Organization. (2011). Burden of disease from environmental noise: quantification of healthy life years lost in Europe. *Regional Office for Europe*. https://apps.who.int/iris/handle/10665/326424

World Health Organization. (WHO). (2021). Deafness and hearing loss. Accessed 15 February 2022, <https://www.who.int/news-room/fact-sheets/detail/deafness-and-hearing-loss>

Xia, C., Yin, M., Pan, P., Fang, F., Zhou, Y., & Ji, Y. (2019). Long-term exposure to moderate noise induces neural plasticity in the infant rat primary auditory cortex. *Animal Cells and Systems*, *23*(4), 260–269. doi: 10.1080/19768354.2019.1643782

Xie, L., Wang, M., Liao, T., Tan, S., Sun, K., Li, H., Fang, Q., & Tang, A. (2018). The characterization of auditory brainstem response (ABR) waveforms: A study in tree shrews (Tupaia belangeri). *Journal of Otology*, *13*(3), 85–91. doi: 10.1016/j.joto.2018.05.004

Yang, S., Cai, Q., Bard, J., Jamison, J., Wang, J., Yang, W., & Hu, B. H. (2015). Variation analysis of transcriptome changes reveals cochlear genes and their associated functions in cochlear susceptibility to acoustic overstimulation. *Hearing Research*, *330*(0), 78–89. doi: 10.1016/j.heares.2015.04.010

Yang, Z. M., Yang, M. F., Yu, W., & Tao, H. M. (2019). Molecular mechanisms of estrogen receptor β-induced apoptosis and autophagy in tumors: implication for treating osteosarcoma. *Journal of International Medical Research*, *47*(10), 4644–4655. doi: 10.1177/0300060519871373

Yin, S. K., Feng, Y. M., Chen, Z. N., & Wang, J. (2008). The effect of noise-induced sloping high-frequency hearing loss on the gap-response in the inferior colliculus and auditory cortex of guinea pigs. *Hearing Research*, *239*(1–2), 126–140. doi: 10.1016/j.heares.2008.02.002

Yousef, A., Robinson, J. L., Irwin, D. J., Byrne, M. D., Kwong, L. K., Lee, E. B., Xu, Y., Xie, S. X., Rennert, L., Suh, E. R., Van Deerlin, V. M., Grossman, M., Lee, V. M. Y., & Trojanowski, J. Q. (2017). Neuron loss and degeneration in the progression of TDP-43 in frontotemporal lobar degeneration. *Acta Neuropathologica Communications*, *5*(1), 68. doi: 10.1186/s40478-017-0471-3

Zeng, C., Nannapaneni, N., Zhou, J., Hughes, L. F., & Shore, S. (2009). Cochlear damage changes the distribution of vesicular glutamate transporters associated with auditory and nonauditory inputs to the cochlear nucleus. *Journal of Neuroscience*, *29*(13), 4210–4217. doi: 10.1523/JNEUROSCI.0208-09.2009

Zeng, C., Shroff, H., & Shore, S. (2011). Cuneate and Spinal Trigeminal Nucleus Projections to the Cochlear Nucleus are Differentially Associated with Vesicular Glutamate Transporter-2. *Neuroscience*, *176*, 142–151. doi: 10.1016/j.neuroscience.2010.12.010

Zeng, C., Yang, Z., Shreve, L., Bledsoe, S., & Shore, S. (2012). Somatosensory projections to cochlear nucleus are upregulated after unilateral deafness. *Journal of Neuroscience*, *32*(45), 15791–15801. doi: 10.1523/JNEUROSCI.2598-12.2012

Zhang, G., Xu, L. C., Zhang, M. F., Zou, Y., He, L. M., Cheng, Y. F., Zhang, D. S., Zhao, W. B., Wang, X. Y., Wang, P. C., & Zhang, G. Y. (2021). Changes of the Brain Causal Connectivity Networks in Patients With Long-Term Bilateral Hearing Loss. *Frontiers in Neuroscience*, *15*(7), 1–15. doi: 10.3389/fnins.2021.628866

Zhang, Li, Chen, S., & Sun, Y. (2022). Mechanism and Prevention of Spiral Ganglion Neuron Degeneration in the Cochlea. *Frontiers in Cellular Neuroscience*, *15*(1), 1–13. doi: 10.3389/fncel.2021.814891

Zhang, Liqin, Wu, C., Martel, D. T., West, M., Sutton, M. A., & Shore, S. E. (2021). Noise Exposure Alters Glutamatergic and GABAergic Synaptic Connectivity in the Hippocampus and Its Relevance to Tinnitus. *Neural Plasticity*, *2021*, 8833087, doi: 10.1155/2021/8833087

Zhang, W., Peng, Z., Yu, S., Song, Q. L., Qu, T. F., Liu, K., & Gong, S. S. (2020). Exposure to sodium salicylate disrupts VGLUT3 expression in cochlear inner hair cells and contributes to tinnitus. *Physiological Research*, *69*(1), 181–190. doi: 10.33549/physiolres.934180

Zhao, Y., Song, Q., Li, X., & Li, C. (2016) Neural Hyperactivity of the Central Auditory System in Response to Peripheral Damage. *Neural Plasticity*, *2016,* 2162105. doi: 10.1155/2016/2162105

Zhou, J., Nannapaneni, N., Shore, S. (2007). Vesicular Glutamate Transporters 1 and 2 Are Differentially Associated With Auditory Nerve and Spinal Trigeminal Inputs to the Cochlear Nucleus. *Journal of Comparative Neurology*, *500*, 777–787. doi: 10.1002/cne

07 AFFIDAVIT

Eidesstattliche Versicherung

„Ich, **Víctor Giménez Esbrí**, versichere an Eides statt durch meine eigenhändige Unterschrift, dass ich die vorgelegte Dissertation mit dem Thema: **Dynamik der lärminduzierten neurodegeneration und neuroplastizität im zentralen nervensystem / Dynamics of noise-induced neurodegeneration and neuroplasticity in the central nervous system** selbstständig und ohne nicht offengelegte Hilfe Dritter verfasst und keine anderen als die angegebenen Quellen und Hilfsmittel genutzt habe.

Alle Stellen, die wörtlich oder dem Sinne nach auf Publikationen oder Vorträgen anderer Autoren/innen beruhen, sind als solche in korrekter Zitierung kenntlich gemacht. Die Abschnitte zu Methodik (insbesondere praktische Arbeiten, Laborbestimmungen, statistische Aufarbeitung) und Resultaten (insbesondere Abbildungen, Graphiken und Tabellen) werden von mir verantwortet.

Ich versichere ferner, dass ich die in Zusammenarbeit mit anderen Personen generierten Daten, Datenauswertungen und Schlussfolgerungen korrekt gekennzeichnet und meinen eigenen Beitrag sowie die Beiträge anderer Personen korrekt kenntlich gemacht habe (siehe Anteilserklärung). Texte oder Textteile, die gemeinsam mit anderen erstellt oder verwendet wurden, habe ich korrekt kenntlich gemacht.

Meine Anteile an etwaigen Publikationen zu dieser Dissertation entsprechen denen, die in der untenstehenden gemeinsamen Erklärung mit dem/der Erstbetreuer/in, angegeben sind. Für sämtliche im Rahmen der Dissertation entstandenen Publikationen wurden die Richtlinien des ICMJE (International Committee of Medical Journal Editors; www.icmje.og) zur Autorenschaft eingehalten. Ich erkläre ferner, dass ich mich zur Einhaltung der Satzung der Charité – Universitätsmedizin Berlin zur Sicherung Guter Wissenschaftlicher Praxis verpflichte.

Weiterhin versichere ich, dass ich diese Dissertation weder in gleicher noch in ähnlicher Form bereits an einer anderen Fakultät eingereicht habe.

Die Bedeutung dieser eidesstattlichen Versicherung und die strafrechtlichen Folgen einer unwahren eidesstattlichen Versicherung (§§156, 161 des Strafgesetzbuches) sind mir bekannt und bewusst.“

Datum Unterschrift

08 CURRICULUM VITAE

"My curriculum vitae does not appear in the electronic version of my paper for reasons of data protection."

09 ACKNOWLEDGEMENTS

Thanks to the unconditional support of Susanne Schwitzer and Dr. Max Meuser from the Center for Medicine Technology of the Unfallkrankenhaus Berlin. Words cannot express the value of their patience and feedback during the entire process. I would also like to thank Dr. Stefan Paul Koch, Susanne Mueller and Marco Foddis from the Experimental MRI group of the Charité Universitätsmedizin Berlin, for their invaluable help in the data acquisition and data analysis process. I am also extremely grateful to Dr. Niclas Gimber from the Advanced Biomedical Imaging Core Facility (AMBIO) of the Charité Universitätsmedizin Berlin, who was able to develop robust and potent image analysis macros that made the analysis of the present data possible. Following, I would like to remark the contribution of Dr. Stefan Donat, Jutta Schüler and Dr. Jan Schmoranzer from the AMBIO, due to the wise advises received from them during the establishment of all imaging processes. Moreover, I would also like to thank Dr. Anja Kühl from the Institute of Pathology of the Charité Universitätsmedizin Berlin, who gave extremely important advises in order to refine the current fluorescence immunohistochemistry protocols. Furthermore, I would like to thank the contributions of my supervisors, Dietmar Basta, Moritz Gröschel and Philipp Boehm-Sturm, for the trust they placed in me throughout the entire project, and for all their helpful discussions, feedbacks, patience and moral support shared.

Last but not least, I would be remiss in not mentioning all my friends and all my family. Especially, I would like to mention my parents Jose Manuel Giménez Navarro and Eva Maria Esbrí Martínez; my sister Marta Giménez Esbrí; my aunt Xaro Giménez Navarro; my uncles José Vicente Esbrí Martinez and Fulgencio Giménez Navarro; and my grandfathers José Esbrí Aymimir and Fulgencio Giménez Soriano, due to all the critical love and support received from them during my entire life. In addition, it is especially important to mention the decisive contribution of my partner Andrea Monfort Querol. Because undoubtedly, her unconditional love, support, strength, persistence and courage made this work possible. Finally, it is a pleasure for me to dedicate the entire work and my entire career to my grandmothers Maria Cruz Martínez García, who left us fighting Alzheimer's disease during the course of this work; and Rosario Navarro Arnau, whose brain injuries prevented her from seeing this project become a reality.

Berlin, 20.10.23

Víctor Giménez Esbrí

10 CERTIFICATE OF ACCREDITED STATISTICIAN

CHARITÉ

CharitéCentrum für Human- und Gesundheitswissenschaften

Charité | Campus Charité Mitte | 10117 Berlin

Institut für Biometrie und klinische Epidemiologie (iBikE)

Direktor: Prof. Dr. Frank Konietschke

Postanschrift:
Charitéplatz 1 | 10117 Berlin
Besucheranschrift:
Reinhardtstr. 58 | 10117 Berlin

Tel. +49 (0)30 450 562171
frank.konietschke@charite.de
https://biometrie.charite.de/

Name, Vorname: Víctor Giménez Esbrí
Emailadresse: victor.gimenez-esbri@charite.de
Matrikelnummer: 4001269
PromotionsbetreuerIn: PD Dr. Dietmar Basta
Promotionsinstitution / Klinik: Unfallkrankenhaus Berlin /Charité Universitätsmedizin Berlin

Bescheinigung

Hiermit bescheinige ich, dass Herr Víctor Giménez Esbrí innerhalb der Service Unit Biometrie des Instituts für Biometrie und klinische Epidemiologie (iBikE) bei mir eine statistische Beratung zu einem Promotionsvorhaben wahrgenommen hat. Folgende Beratungstermine wurden wahrgenommen:

- Termin: 12.04.2023

Folgende wesentliche Ratschläge hinsichtlich einer sinnvollen Auswertung und Interpretation der Daten wurden während der Beratung erteilt:

- Gruppenvergleiche mit ANOVA und Post-Hoc Tests
- Methodenvergleich durch Bland-Altman Plots
- Pearson und Spearman Korrelationsanalyse

Diese Bescheinigung garantiert nicht die richtige Umsetzung der in der Beratung gemachten Vorschläge, die korrekte Durchführung der empfohlenen statistischen Verfahren und die richtige Darstellung und Interpretation der Ergebnisse. Die Verantwortung hierfür obliegt allein dem Promovierenden. Das Institut für Biometrie und klinische Epidemiologie übernimmt hierfür keine Haftung.

Datum: 12.04.2023 Name des Beraters: Dr. Konrad Neumann

DR. Konrad Neumann

Digital unterschrieben von DR. Konrad Neumann
Datum: 2023.04.12 16:44:08 +02'00'

Unterschrift BeraterIn, Institutsstempel

CHARITÉ
UNIVERSITÄTSMEDIZIN BERLIN
Institut für Biometrie und Klinische Epidemiologie
Campus Charité Mitte
Charitéplatz 1 | D-10117 Berlin
Sitz: Reinhardtstr. 58